MERCURY TRANSPORT THROUGH A CAPPED SEDIMENT

A Dissertation

Submitted to the Graduate Faculty of the
Louisiana State University and
Agricultural and Mechanical College
In partial fulfillment of the
requirements for the degree of
Doctor of Philosophy

in

The Department of Chemical Engineering

By
Jianrong Liu
B.S., China University of Petroleum, 1992
M.S., China University of Petroleum, 1997
M.S., Louisiana State University, 2007
August 2008

Acknowledgements

I would like to thank Dr. Kalliat T. Valsaraj and Dr. Danny D. Reible for their guidance during my research.

I am grateful to Nathan Johnson for his assistance with analysis of low level mercury for the effluent water samples in chapter 6 of this document. Nathan Johnson is currently a graduate student of Dr. Reible at the University of Texas at Austin. I am grateful to Dr. Delaune for the offering of analysis of methylmercury and of unlimited usage of the instrument for analysis of total mercury. Dr. Delaune is a professor of Department of Oceanography and Sciences, Wetland Biogeochemistry Institute, Louisiana State University. I am also grateful to my husband, Xiaobao Li, who is always there for me when I need help. He overcame nausea on the boat and helped me collecting sediment from Henderson Lake.

The conventional capping part of this research which is summarized in chapter 3 of this document was supported by the DuPont Company.

I also want to express my appreciation to all of the committee members, Dr. Louis J. Thibodeaux, Dr. James J. Spivey in the department and Mr. John Hull from AquaBlok, Ltd., for their time and advice.

Table of Contents

Abstract

Laboratory simulation cells were employed to evaluate the effectiveness of a sand cap for containing highly mercury-contaminated lake sediments and the resultant impacts on the mercury fate beneath the cap. Sand cap can delay and reduce the migration of mercury into the overlying water; however, due to the small partition coefficient of mercury between sand and water, a capping material with higher partition coefficient is better for the long-term containment of mercury. In the following study, efforts were made to identify and investigate an active capping material which works effectively at containing and inhibiting the methylation of mercury. Based on information from literature and our primary experimental results, iron sulfide (FeS) was selected for the following study.

By amendment of laboratory synthesized iron sulfide (Syn-FeS) into sediment slurries spiked with Hg(II) under anoxic conditions, the inhibition effects of FeS on the methylation of mercury were investigated. A commercial iron sulfide (CIS), which was a mixture of several iron-sulfide species, was also investigated in the experiment. Experimental results showed that both Syn-FeS and CIS were good inhibitors of Hg(II) methylation. It was found that MeHg production was not correlated to total dissolved mercury in pore water.

Via batch sorption experiment, the interaction between aqueous Hg(II) and Syn-FeS was studied under anaerobic conditions. The study included effects of the pH of both initial Hg(II) solution and equilibrium suspension on sorption, mechanism of interactions between Hg(II) and FeS, and the stability of immobilized mercury regarding oxidation. Experimental results showed

that FeS works effectively at immobilizing aqueous Hg(II) via mostly precipitation reaction and also some adsorption on the solid surface.

Finally, in the simulation cells, Syn-FeS and CIS were amended into uncapped sediment or sand cap to investigate their effectiveness at containing mercury and inhibiting the transformation of mercury to MeHg. Results show that, with the addition of iron sulfides, the release of mercury into overlying water was reduced and the methylation of mercury was inhibited.

Chapter 1 Introduction

Mercury is a widely distributed and persistent pollutant in the environment. The ecological and human health effects of mercury are generally related to the environmental transformations of inorganic mercury to the more toxic monomethylmercury (MeHg). Studies have shown that biomagnification of MeHg in the aquatic food web and consumption of fish and shellfish contaminated with MeHg is the primary route of human exposure to Hg(II) (Wheatley and Paradis, 1995). MeHg is toxic to fish and humans. Almost all mercury in fish is MeHg (Bloom, 1992).

MeHg is formed largely in anoxic sediments (Ekstrom et al., 2003) from inorganic mercury methylation mediated primarily by sulfate reducing bacteria (Compeau and Bartha, 1985; Gilmour and Henry, 1991). The bottom sediments are the main reservoirs of mercury and to the extent that this mercury is available to overlying water is a sensitive indicator of risk to the aquatic ecosystem. Effective remediation of such sediments to reduce the release of mercury is essential to minimize the contamination of fish and shellfish with MeHg.

Capping can be an effective means of isolating contaminated sediment from the overlying water. In-situ capping (ISC) is the process of placing a layer of proper isolating material between the contaminated sediment and overlying water. A number of ISC field operations have been performed worldwide under varying site conditions by using sand, sandy sediment, plastic liner, gravel or geotextiles (Azcue et al., 1998; Palermo et al., 1998). In general, relatively low energy aquatic environments, such as lakes and bays, are good candidates for ISC (Thoma et al., 1993).

1.1 Capping Using Sand Cap

Historical mercury releases associated with mercury fulminate production have led to contamination of the delta at the entrance to Pompton Lake in northern New Jersey. Remedial plans for the delta include management of upland delta soil, removal of mercury mass, and capping of the remaining sediments. While capping can effectively isolate contaminated sediments, there is uncertainty as to its effectiveness of containing mercury. Effective isolation of a particular containment depends upon the degree to which that contaminant is effectively adsorbed by a cap and its motion through a cap retarded. In the case of mercury, a cap may also influence redox conditions in the underlying sediment and rates of mercury methylation, thus modifying the fraction of mercury that is in bioavailable and toxic forms. In efforts to evaluate these potential effects, experimental assessments of the effectiveness of capping mercury contaminated sediment were undertaken using laboratory scale capping simulator cells. The first phase of these experiments is to evaluate the effect of a conventional sand cap on the potential release of mercury from sediment to overlying water. Chapter 3 includes the results of the investigation using sand cap to the mercury contaminated sediments from Pompton Lake.

1.2 Capping Using Sand Amended with Iron Sulfides

Methylation processes occurring at the sediment/water interface play a major role in determining the extent of the MeHg flux to the water column (Mason et al., 2006). MeHg depth profiles show that MeHg production occurs most actively in the surface layer of sediments, 0-2.5 cm in the Venice Lagoon sediments, Italy (Han et al., 2007), 0-3 cm in the Lavaca Bay, Texas (Bloom et al., 1999), 0-15cm with a maximum at 2 cm in one sediment core at the head of St.

Croix River Estuary (Sunderland et al., 2004). Considering the rates of mercury methylation is higher in the surface sediments, a layer of a methylation-inhibiting matearial placed over the contaminated sediments should greatly reduce MeHg production and the flux of MeHg into the overlying water column.

A negative correlation between MeHg in sediments and sulfides in pore water has been observed (Benoit et al., 1998; Benoit et al., 1999), which suggests that sulfides limit production and accumulation of MeHg in the system. Iron sulfides are one of the major sinks of mercury in sediments because of their affinity for mercury (Wolfenden et al., 2005). Based on the observations of the negative correlation between MeHg in sediment and sulfide in pore water, the amendment of iron sulfides into anoxic sediments should be able to inhibit the methylation of mercury, by producing a sulfidic environment in the sediments.

The first stage of the study has showed that release of mercury from contaminated sediments can be reduced by placing a layer of sand cap over the sediments (Liu et al., 2007). However, due to the small partition coefficient of mercury between sand and water, a capping material with higher partition coefficient is better for the long-term containment of mercury. This could be improved by amending the sand cap to increase its adsorption capacity and adding a methylation inhibitor. Thus, by binding and inhibiting the methylation of mercury in the sediment and cap, the release of mercury and MeHg into the overlying water body can be greatly reduced. Brown has showed that naturally occurring sulfide minerals are excellent adsorbents for aqueous solutions of Hg^0 and Hg^{2+} and industral wastes containing mercury (Brown et al., 1979). In chapter 5 of this document, a study was designed to test the potential of synthetic FeS to

immobilize mercury in batch sorption experiments. It includes the results of the investigation of the immobilization of Hg(II) (added as $HgCl_2$) with FeS in aqueous solutions, effects of pH of both initial Hg(II) solution and equilibrium suspension on sorption, mechanism of interactions between Hg(II) and FeS, and the stability of immobilized mercury regarding oxidation. Experimental results showed that Mackniwite (FeS) is excellent at immobilizing aqueous Hg(II) via mostly precipitation reaction and also some adsorption on the solid surface (Liu et al., 2008).

As the most toxic form of mercury, the accumulation of MeHg in the aquatic food web is a major concern in sediments in many Louisiana water bodies. Fish advisories have been posted for several lakes in Louisiana by the Department of Environmental Quality of Louisiana (LA-DEQ, 2004). Henderson Lake in the Atchafalaya basin of Louisiana is one such area and fish advisories have been posted in 2004. Therefore, sediment from Henderson Lake was selected for the inhibition experiments. In Chapter 4, the hypothesis that MeHg production will decrease if iron sulfides are amended into the Hg(II) spiked sediment slurries was tested. Both the synthetic FeS (Syn-FeS) and commercial iron sulfide (CIS) were investigated. The inhibition effects of molybdate, Fe^{2+}, and elemental sulfur, the intermediate product of the oxidation of iron sulfide, were also investigated for comparison purpose.

Based on the previous experimental results on inhibition effects of sulfides on mercury methylation and the affinity of sulfides for mercury, the placement of a layer of sand cap amended with iron sulfides over the contaminated sediments should effectively reduce releases of both mercury and MeHg under field conditions. Though many other factors should be considered and investigated before practical application, iron sulfides are good candidates as

components of an active capping material. As the last part of the experiments, simulation cells were set up to investigate the effectiveness of iron sulfides on inhibition of mercury methylation in system simulating on-site conditions. In uncapped cells, CIS and Syn-FeS were respectively amended into mercury spiked sediment collected from Henderson Lake, to test the inhibition effects of iron sulfides. In capped cells, CIS were used directly as the cap, and Syn-FeS was amended into sand, acting as the active component in the cap. Experimental results are summarized in Chapter 6.

In Chapter 7, significant conclusions based on the research are summarized and recommendations are made for further investigations.

Chapter 2 Literature Review

2.1 Mercury Speciation and Cycle

2.1.1 Mercury Speciation

Mercury (Hg) can exist in three oxidation states: 0, +1, and +2. Hg (I) and Hg(II) readily form inorganic complexes, but only Hg(II) can form covalent bonds with carbon to produce methyl-Hg species, the most toxic form of Hg (Kaplan et al., 2002). Mercury released into the atmosphere from natural and anthropogenic sources deposits mainly as Hg(II), from either direct deposition of emitted Hg(II) or from conversion of emitted elemental Hg(0) to Hg(II) through ozone-mediated reduction (U.S.EPA, 1997). Hg(0) can be formed by reduction of Hg(II) compounds/complexes mediated by humic substances (Nriagu, 1979) and by light (Carpi and Lindberg, 1997). This Hg(0) will re-enter the atmosphere via diffusion.

Most of the mercury encountered in water/soil/sediments/biota (all environmental media except the atmosphere) is in the form of inorganic mercuric salts and organomercurics. The compounds of mercury most likely to be found under environmental conditions are these: the mercuric salts $HgCl_2$, $Hg(OH)_2$ and HgS; the MeHg compounds, such as methylmercuric chloride (CH_3HgCl) and methylmercuric hydroxide (CH_3HgOH); and, in small fractions, other organomercurics (i.e., diMeHg and phenylmercury) (U.S.EPA, 1997; Ganguli et al., 2000; Martian-Doimeadios et al., 2000). Hg(II)-CH_3 is a Lewis acid and can accept a lone pair of electrons from a Lewis base to form a coordinate covalent bond. In a complex environment like sediment, there are many kinds of Lewis bases, such as nitrogenous base and chloride base, which can react with Hg(II)-CH_3 to form MeHg compounds (CSD database, Version 5.28).

DiMeHg is very volatile and hardly water-soluble. Thus, it easily evaporates and becomes unavailable for water organisms. Moreover, diMeHg is unstable and undergoes fast degradation to the MeHg group (Boszke et al., 2003). Most of the mercury encountered in the atmosphere is elemental Mercury vapor (Slemr et al., 1985; U.S.EPA, 1997).

The properties and chemical behavior of mercury strongly depend on the oxidation state. As the oxidation state of mercury increases, the solubility of mercury generally increases; elemental Hg(0) and Hg(I) are sparingly soluble, whereas $HgCl_2$ is readily soluble in water (Kaplan et al., 2002). Cinnabar (HgS) is an extremely insoluble solid with a solubility product of 10-36.8 for the reaction (Ravichandran et al., 1998)

$$HgS + H^+ \leftrightarrow Hg^{2+} + HS^-$$ (at 20 ºC and ionic strength I = 1.0 M)

Toxicology studies proved that mercury, especially MeHg, is very toxic to the human embryo and fetus (Bakir et al., 1973; Aminzaki et al., 1976; Harada, 1995). MeHg is the most toxic form of mercury. In aquatic systems, bioaccumulation through food chain may cause high levels of mercury contamination in fish from even very low concentrations of MeHg in water.

2.1.2 Mercury Cycle

Mercury is emitted by both anthropogenic and natural processes. Natural processes include volatilization of mercury in marine and aquatic environments, volatilization from vegetation, degassing of geologic materials (e.g., soils) and volcanic emissions. The natural emissions are thought to be primarily in the elemental mercury form. Anthropogenic mercury releases are thought to be dominated on the national scale by industrial processes and combustion sources that release mercury into the atmosphere. Stack emissions include both

gaseous and particulate forms of mercury. Gaseous mercury emissions include both elemental and oxidized chemical forms, while particulate mercury emissions are thought to be composed primarily of oxidized compounds due to the relatively high vapor pressure of elemental mercury (U.S.EPA, 1997). According to one estimate, about half of total anthropogenic mercury emissions eventually enter the global atmospheric cycle (Mason et al., 1994); the remainder is removed through local or regional cycles. Some anthropogenic processes no longer used still result in significant environmental releases from historically contaminated areas which continue to release mercury to surface water runoff, groundwater and the atmosphere.

There are a number of pathways by which mercury can enter the freshwater environment: Hg(II) and MeHg from atmospheric deposition (wet and dry) can enter water bodies directly; Hg(II) and MeHg can be transported to water bodies in runoff (bound to suspended soil/humus or attached to dissolved organic carbon); or Hg(II) and MeHg can leach into the water body from groundwater flow in the upper soil layers. But the majority of the mercury entering lakes from these sources is Hg(II), the direct deposition of MeHg is even rare. Rather, it is formed within the lake or in the lake catchment by the methylation of Hg(II) (Winfrey and Rudd, 1990). Once entering a water body, mercury can remain in the water column, be lost from the lake through drainage water, revolatilize into the atmosphere, settle into the sediment or be taken up by aquatic biota. After entry, the movements of mercury through any specific water body may be unique.

With all the uncertainties of the global cycle, a focused study at a small scale can provide useful insights about mercury biogeochemistry. The mercury cycling model (MCM) is a

deterministic simulation model that incorporates the major processes that transport mercury across lake boundaries-atmospheric deposition, gas exchange, inflow and outflow of water, and burial in sediments; chemically transform it-reduction, methylation and demethylation; and lead to its accumulation in aquatic biota-uptake, depuration, and trophic level transfer (Watras and Huckabee, 1994). The processes occurring in sediment is shown in Fig. 2.1, which is modified from the MCM model and the mercury cycling schematic reported (Winfrey and Rudd, 1990).

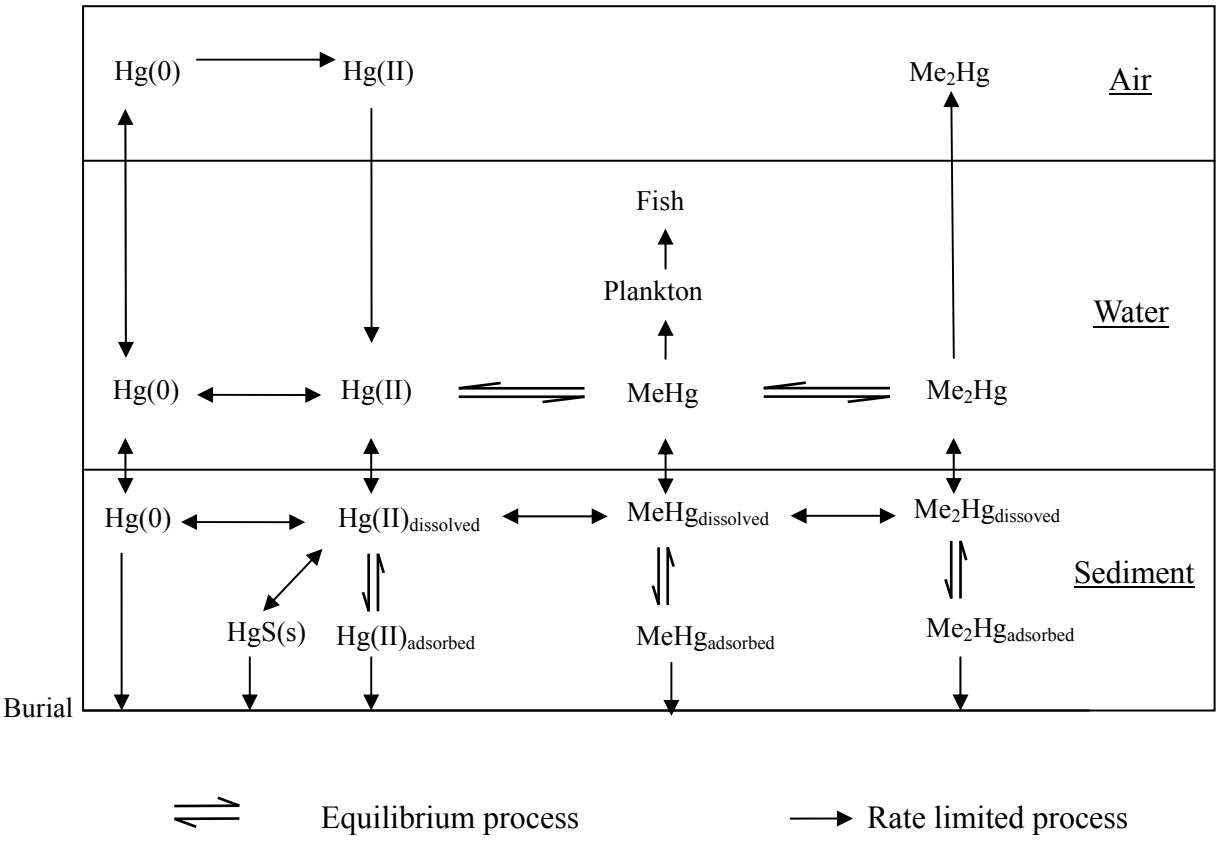

Figure 2.1 The biogeochemical cycling of mercury in freshwater lakes. Modified from (Watras and Huckabee, 1994) and (Winfrey and Rudd, 1990).

MeHg is very bioavailable and accumulates in fish through the aquatic food web; nearly 100% of the mercury found in fish muscle tissue is methylated (Bloom et al., 1991). Because

diMeHg is unstable and undergoes fast degradation to the MeHg group (Boszke et al., 2003), it is not an important species in the sediment. MeHg appears to be primarily passed to planktivorous and piscivorous fish via their diets. Larger, longer-lived fish species at the upper end of the food web typically have the highest concentrations of MeHg in a given water body. In fact, bio-concentration factors for accumulation of MeHg in fish (dry weight basis, compared with the water MeHg concentration) are on the order of 10^5 - 10^6 (Bloom, 1992).

2.1.3 Concentrations of Mercury and Methylmercury in Sediments

The natural total concentration of mercury in the bottom sediments can vary from 10 to 200 ng g^{-1} of dry mass (Ullrich et al., 2001). Very high concentrations of mercury are found in the sediments from highly polluted areas and often from estuaries of some rivers. For example, the mercury concentrations reported for extremely polluted Minamata Bay (Japan) were up to 908 μg g^{-1} dry mass (Fujiki and Tajima, 1992).

At the sediment surface, the fraction of MeHg was narrowly constrained to the range of 0.3-1.6% (at the spring maximum) of the total mercury concentration. MeHg showed much greater variation with depth in the cores, ranging from a maximum of 1.6% of the total in the surface layer of near-shore sediments to less than 0.02% at depth in the long cores (Bloom et al., 1999).

2.2 Transformation of Mercury and Affecting Factors

The transformation of Mercury into MeHg is a dynamic process of methylation and demethylation (Pak and Bartha, 1998). On the basis of some laboratory and in-situ experiments on mercury, it has been shown that the main factors controlling the behavior of this element are

micro-organisms, inorganic sulfides, organic matter, iron and manganese hydroxides, redox potential, chlorides, pH and temperature in the bottom sediments (Boszke et al., 2003).

2.2.1 Mercury Methylation

MeHg is formed largely in anoxic sediment from inorganic Hg(II) methylation mediated primarily by sulfate reducing bacteria (SRB) (Compeau and Bartha, 1984; Gilmour and Henry, 1992). Methylation activity is much less in the water column (Berman and Bartha, 1986; Callister and Winfrey, 1986). The low rate of MeHg production in the water column was likely due to the small number of microorganisms and low nutrient concentrations.

Evidence for the involvement of SRB is that MeHg production is significantly reduced when molybdate, a sulfate reduction inhibitor, is added into sediment samples (Compeau and Bartha, 1985; Kerry et al., 1991; Gilmour et al., 1992; Chen et al., 1997). However, recent research suggests that iron-reducing bacteria (IRB) may play a role in mercury methylation in iron-rich freshwater sediments, where iron was the dominant terminal electron acceptor (Warner et al., 2003; Fleming et al., 2006; Kerin et al., 2006). Besides the biotic methylation, a growing body of evidence suggests that abiotic reactions represent another possible pathway for Hg(II) methylation in the aquatic environment (Chen et al., 1996; Celo et al., 2006). Abiotic Hg(II) methylation in natural environments appears to be of minor importance. In contrast, microbial mercury methylation has been shown to occur in a variety of marine, estuarine, and lacustrine environments. Microorganisms from diverse taxonomic groups have been shown to methylate mercury in laboratory studies (Macalady et al., 2000). Thus, though Hg(II) can be methylated abiotically or microbiologically, abiological methylation is insignificant in sediments, and

abiological methylation may play a more important role in lake water and in streams of the lake watershed, especially at low pH (Lee et al., 1985).

It has been suggested that lipid soluble species such as $HgCl_2$ or dissolved neutral HgS^0 may diffuse passively through biological membranes and thus be available for methylation (Jay et al., 2000). But it was also suggested that HgS^0 is the dominant neutral dissolved complex in sulfidic sediments and that the concentration of this complex affects microbial uptake and methylation. The hypothesis is consistent with the extremely low Hg^{2+} concentration in pore waters, and it describes a situation where dissolved complexes rather than free ions are most readily accumulated by microorganisms (Benoit et al., 1999).

Uptake of Hg(II) by both V. Anguillarum and by E. coli very likely occurs by a facilitated mechanism rather than by passive diffusion of neutrally charged Hg(II) species across the cell membrane (Golding et al., 2002). Evidence for this mechanism was further provided by using *Vibrio anguillarum* and *V. Anguillarum* (Kelly et al., 2003). In these studies, the uptake of Hg(II) under anaerobic conditions was not proportional to the abundance of neutrally charged mercury species but was dependent on the total concentration of mercury in the samples.

2.2.2 Sulfur and Methylation

Sulfur exists as a variety of species in sediments (sulfates, sulfides, elemental sulfur, organic sulfur compounds), which are involved to various degrees in the biogeochemistry of toxic metals (Fabbri et al., 2001). All these sulfur species play a role in the transformation of mercury in aquatic environments.

2.2.2.1 Elemental Sulfur (S^0)

Elemental sulfur (S^0) is another relevant sulfur species in aquatic sediments. Elemental sulfur can exist in a variety of different forms. The stable solid form in environmental conditions is orthorhombic a-sulfur consisting of cycloocta-S molecules. The solubility of S^0 in water is low owing to its hydrophobic character (2×10^{-8} mol L^{-1} as S_8) (Fabbri et al., 2001).

Elemental sulfur can increase the solubility of cinnabar in sulfidic water (Paquette and Helz, 1997; Benoit et al., 1999; Jay et al., 2000; Fabbri et al., 2001). This effect has been attributed to the formation of complexes between mercury and polysulfides, the latter in turn formed by the reaction of S^0 with sulfides. At high sulfide concentrations and alkaline pH, mercury can be mobilized from the solid to the aqueous phase in the form of sulfide complexes. In the presence of S^0, the solubility of solid HgS is increased through the formation of polysulfide complexes (Paquette and Helz, 1997):

$$(n-1)S + xH^+ + yHS^- + HgS \leftrightarrow \text{Hg polysulfides}$$

Detailed reactions are listed in Appendix A.

2.2.2.2 Sulfate

The methylation of inorganic-mercury can be attributed to both abiotic and biotic processes, although sulfate-reducing bacteria (SRB) are shown to be the primary mercury-methylators in aquatic ecosystems. Sulfate both stimulates MeHg production and enhances the activity of SRB in sediments, except under conditions where other conditions limit MeHg production (Benoit et al., 1999; Hammerschmidt and Fitzgerald, 2004). Perhaps the best evidence for the link between sulfate reduction and mercury methylation in sediments was

provided by studies in which the researchers used molybdate, a metabolic inhibitor of sulfate reduction (King et al., 2000); the results of these studies indicated that mercury methylation was almost completely inhibited in the presence of molybdate (Gilmour et al., 1992; Gilmour et al., 1998). Other studies have shown that in pure cultures SRB grown in the absence of sulfate do not generate CH_3Hg from available inorganic mercury (Pak and Bartha, 1998).

2.2.2.3 Sulfides

The solubility of HgS can be augmented by high sulfide concentrations through the formation of dissolved Hg(II) sulfur species, such as the neutral complex HgS^0 and ions such as HgS_2^{2-} (Paquette and Helz, 1997; Benoit et al., 1999; Jay et al., 2000; Fabbri et al., 2001). A characteristic feature of mercury is its strong affinity to sulfur, which is of great importance for biogeochemistry of this element. It also controls the chemistry of mercury in anaerobic sites. The dominant mercury species in the anaerobic conditions are mono- and bi-sulfide complexes such as HgS, HgS_2H_2, HgS_2H^- and HgS_2^{2-}. From among the organic sulfur-mercury compounds, the most important is CH_3HgS (Paquette and Helz, 1997).

An inverse relationship between pore-water sulfide concentration and bulk sediments MeHg concentration has been observed in aquatic ecosystems (Benoit et al., 1998; Benoit et al., 1999; Benoit et al., 1999). Furthermore, sulfide has been shown to have an inhibitory effect on mercury methylation by SRB, which can be explained by a decrease in neutral dissolved mercury species with increasing sulfide (Benoit et al., 1999; Regnell et al., 2001). The negative correlation between pore water sulfide and sediment MeHg, suggest that sulfide decreases bioavailability of mercury to methylating bacteria in sediments with sulfidic pore waters and thus limits production and accumulation of MeHg in this system.

2.2.3 Inorganic Metallic Chemicals and Inhibition of Methylation of Mercury

Field study has showed that the distribution coefficient for MeHg is lowest at the point of the Fe maximum, whereas the dissolved Hg(II) concentrations appear to be unrelated to changes in dissolved Fe and Mn (Bloom et al., 1999)**.** Laboratory experiments conducted by adding Hg(II) and Fe(II) ($FeCl_2.4H_2O$) to sediments collected from estuarine wetlands showed that addition of 3.9 $mg.g^{-1}$ Fe(II) decreased net mercury methylation relative to that of unamended controls by a factor of 2.1-6.6 (Mehrotra and Sedlak, 2005). When iron was added to one of the sediment samples at doses that were small relative to the concentration of sulfide present, net mercury methylation either increased slightly or was unaffected. Using pure cultures of the sulfate-reducing bacterium Desulfobulbus propionicus (1pr3), it was also showed that adding Fe(II) ($FeCl_2.4H_2O$) to sulfidic wetland sediments decreases net methylation (Mehrotra et al., 2003).

Adsorption and co-precipitation of mercury on pyrite (FeS_2) and acid volatile sulfides ("AVS", e.g. FeS, MnS) can limit the amount of mercury dissolved in the pore water in anaerobic conditions. Examined using radiolabled mercury compounds in San Francisco Bay-Delta surface sediments, MeHg production decreased sharply with depth at two of three sites, both of which exhibited a corresponding increase in reduced sulfur compounds with depth (Marvin-DiPasquale and Agee, 2003). Iron monosulfides represent a pool of solid sulfur available for the precipitation of mercury, as they have higher solubility than mercury sulfides (Fabbri et al., 2001):

$$FeS(s) + Hg^{2+} \leftrightarrow HgS(s) + Fe^{2+}$$

However, mercury bound with these minerals can be released to the pore water as a result of gradual oxidation of the sediment (Regnell et al., 2001). The presence of ions competing for bonding sites in the humus matter such as Cl^- can significantly lower the reduction rate. The rate of mercury methylation decreases with increasing concentration of salt, which is most probably a result of the inhibitory effect of chlorine-complexes (Barkay et al., 1997; Boszke et al., 2003).

Study results indicated that mercury methylation was almost completely inhibited in the presence of molybdate (Gilmour et al., 1992; Gilmour et al., 1998; Pak and Bartha, 1998, 1998; King et al., 2000), a metabolic inhibitor of sulfate reduction (Rothermich et al., 2002).

It is reported that the methylation of Hg(II) was suppressed under iron-reducing conditions (Warner et al., 2003). Elemental sulfur forms Hg(II)-polysulfides with Hg(II) and thus enhance the solubility of Hg(II) (Marvin-Dipasquale and Oremland, 1998), but to our knowledge, its effects on Hg(II) methylation has not been reported. If HgS^0 is the dominant neutral mercury complex available for methylation in sulfidic sediments (Benoit et al., 2001), the formation of charged Hg-disulfide complexes may inhibit the Hg(II) methylation.

2.2.4 Organic Matter and Mercury Speciation

Organic matter is one of the most important components of bottom sediments and it is mostly responsible for binding metals (Boszke et al., 2003). It has been estimated that organic matter can bind up to 95% of the divalent mercury species (Ravichandran et al., 1998). Adsorption on the clay minerals and bindings in their structure as well as by the iron and manganese hydroxides is less important for the speciation of mercury than for the other metals, since the most effective species in mercury binding are organic matter and sulfides (Boszke et al.,

2003). Microbial activities that produce and decompose MeHg are dependent on the availability of biodegradable organic carbon. Studies have demonstrated that mercury methylation is enhanced by increased availability of organic carbon (Shin and Krenkel, 1976; Furutani and Rudd, 1980; Wright and Hamilton, 1982), and increased decomposition of organic matter is a major cause of increased methylation in newly flooded reservoirs (Bodaly et al., 1984; Morrison and Therien, 1991; Hall et al., 2005). However, recent study has shown that potential rates of microbial mercury methylation are related inversely with sedimentary organic content, which governs the partitioning of Hg(II) between dissolved and sediment phases (Hammerschmidt and Fitzgerald, 2004).

2.2.5 Redox Potential

2.2.5.1 Definition

Redox potential (Eh) is defined as the reduction potential (Patric et al., 1996). Redox reactions of soil oxdidants are represented by the following half-cell reduction equation:

$$Ox + mH^{+} + ne^{-} \rightarrow \mathrm{Re}d$$

Ox is the oxidized component or electron acceptor, Red is the reduced component or electron donor, m is the number of hydrogen ions involved in the reaction, and n is the number of electrons involved in the reaction. At 298K, the redox potential can be expressed as,

$$Eh(mv) = E^{o} - \frac{59}{n}\log\frac{(\mathrm{Re}d)}{(Ox)} - 59\frac{m}{n}pH$$

E^0: Redox potential at standard state referring to hydrogen electrode.

2.2.5.2 Measurement

For redox potential measurements in biological-chemical systems such as sediments, a platinum electrode is usually employed. A saturated calomel or silver/silver-chloride reference electrode and a millivolt meter are also needed. By convention, electrochemists consider all electrode potential measurements to be made using a standard hydrogen electrode as the reference electrode (Patric et al., 1996; Drever, 1997). The readings of the meter should be corrected by adding 245mv if a calomel reference electrode is employed and by adding 199mv if a silver/silver-chloride electrode is employed instead.

2.2.5.3 Redox Conditions in Sediments

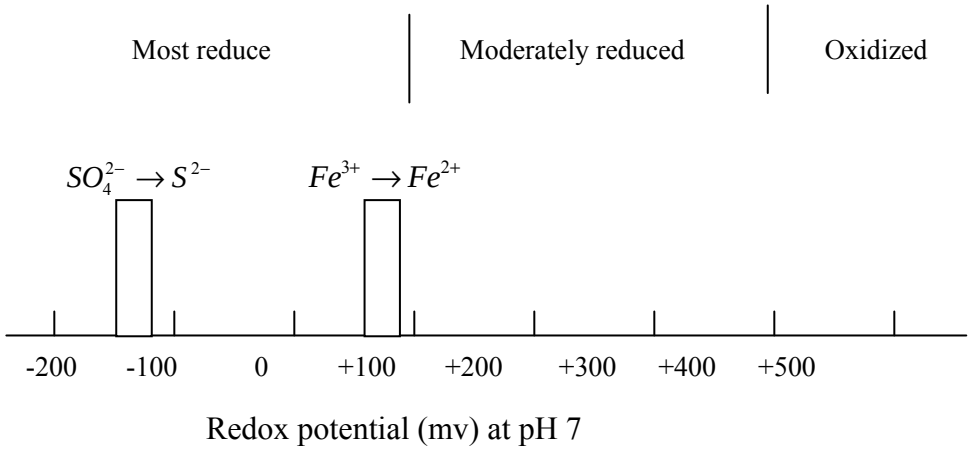

Figure 2.2 Oxidation-reduction potential at which reducible inorganic substances in flooded soils and sediments are reduced. Modified from (Masscheleyn and Patrick, 1993).

Wetland soils and sediments can experience redox potentials ranging from –300 to +600 mv (Masscheleyn and Patrick, 1993). In most reduced submerged soils, the Eh ranges from -300 to +100 mv. Moderately reduced wetland soild are characterized by an Eh between +100 and + 400 mv (Fig. 2.2). The Eh is a small range around -130 mv for the transition of SO_4^{2-} and S^{2-} to

occur. Below this Eh, S^{2-} is more stable, and above this Eh, SO_4^{2-} is more stable. The Eh for the transition reaction between Fe^{3+} and Fe^{2+} is about + 80 mv.

Oxygen penetration depth varies in sediments. A sharp decrease and restriction of oxygen to 1 and 3 mm depth at two stations of Skagerrak sediments, while oxygen penetrates deeper (up to 15 mm) with a less gradient at another station (Rajendran et al., 1992). The penetration depth is 50 mm in one core in eastern Mediterranean sediments (Van Der Zee et al., 2005)

2.2.5.4 Redox and Methylation of Mercury

It has been wildly accepted that MeHg is formed largely in anoxic sediment from inorganic mercury methylation mediated primarily by SRB (Compeau and Bartha, 1984; Gilmour and Henry, 1992). However, recent study using bacteria strains *V. Anguillarum* and by *E. coli* under anaerobic conditions has shown that Hg(II) uptake was greatly decreased compared with aerobic conditions, even though the chemical composition of the medium was identical except for the lack of oxygen.

Methylation of mercury in lakes occurs at the anoxic boundary, which is often present just below the sediment surface except in low oxygen bottom waters (Matilainen, 1995). Oxygenation of sediments has been shown to inhibit microbial methylation (Matilainen et al., 1991).

2.2.5.5 Spatial Variation of MeHg in Sediment

In a laboratory system without macro-organisms, formation and release of MeHg occurs almost entirely in the upper 1cm of the sediment (Jernelov, 1970). In simultaneous measurement of methylation and demethylation in incubation experiments, methylation of mercury was

highest in the flocculent sediment at surface, and decreased with depth in the profundal sediment core (Korthals and Winfrey, 1987). The peak in net MeHg production did not appear to be due to decreased demethylation activity, but rather to an increase in methylation relative to demethylation. The greatest potential for mercury methylation in sediments occurs where microbial activity is high and newly sedimented highly degradable organic carbon is concentrated.

Under field conditions, MeHg depth profiles also show that MeHg production occurs most actively in the surface layer of sediments, 0-2.5 cm in the Venice Lagoon sediments, Italy (Han et al., 2007), 0-3 cm in the Lavaca Bay, Texas (Bloom et al., 1999), 0-15cm with a maximum at 2 cm in one sediment core of at the head of St. Croix River Estuary (Sunderland et al., 2004). In marine sediments, net methylation rates are highest in the transition zone between oxic and anoxic conditions because these conditions are most conducive to the activity of SRB (Hintelmann et al., 2000; King et al., 2001). In addition, these microbes require organic matter as a substrate for microbial activity (Mason and Lawrence, 1999).

2.2.6 pH

At low pH, heavy metals are usually released from bottom sediments. As far as mercury is concerned, the data on the mobility of this element at different pH are variable (Boszke et al., 2003). The desorption, adsorption and transformation of mercury in sediments is a complicated process and depends on many factors, so the effect of pH may depend on the specificity of soils or sediments. But many studies show that lower pH favors the formation of MeHg.

In fresh water lakes, fish in low pH lakes has higher mercury concentration than fish in high pH lakes (Wren and Maccrimmon, 1983; Richman et al., 1988; Grieb et al., 1990; Wiener and Stokes, 1990; Parkman and Meili, 1993). Because fish tissues and organs do not methylate mercury, the elevated level of mercury in low pH lakes must be results of accumulation of MeHg. Mercury concentrations in fish of Sweden Lakes were higher when the pH was at levels of 5 and lower levels were observed both in lakes which were more acidified and in those which were less acidified (Andersson et al., 1995). The effect of increasing hydrogen ion (H^+) concentration on the uptake of Hg(II) by an aquatic bacterium was studied in defined media in laboratory (Kelly et al., 2003). Even small decreases in pH resulted in large increases in Hg(II) uptake. Uptake could have been stimulated by changes in chemical speciation of Hg(II) or by an effect on the bacterial uptake process itself.

Thus, the increased concentration of mercury in fish in low pH lakes could be due to direct effects on fish, such as gill permeability (Rodgers and Beamish, 1983), and the decreased growth rate which results in the decreased biomass. Alternatively, the elevated MeHg concentrations in fish could be due to higher concentrations of bioavailable MeHg in the ecosystems caused by altered chemical partitioning of MeHg across the sediment-water interface or increased production of MeHg in lakes (Ramlal et al., 1985; Hamasaki et al., 1991; Miskimmin et al., 1992).

2.2.7 Temperature

The transformation of mercury in the bottom sediments, including methylation and dimethylation, is temperature dependent. The methylation process is inhibited at either low or

high temperature. In freshwater sediments, methylation was inhibited at low temperature (Wright and Hamilton, 1982), and has a optimal temperature of 35 ˚C (Callister and Winfrey, 1986; Steffan et al., 1988), which is consistent with observations in one study that methylation increased from 10 to 35 ˚C, and decreased thereafter. The process was completely inhibited at 90 ˚C (Mauro et al., 1999). The optimum temperature of mercury methylation is between 33-45 ˚C, and with further temperature increase the rate of methylation decreased and the process ceased at 55 ˚C (Guimaraes et al., 1998). Temperature also affects the process of demethylation. The rate of demethylation increases at higher temperatures (Matilainen and Verta, 1995). In lakes, temperature plays an important role in the seasonality of mercury methylation which often peaks in late summer and is low throughout the remainder of the year (Korthals and Winfrey, 1987).

2.2.8 Sanity

Probably as a result of inhibition effect of chlorine-complexes, the rate of mercury methylation usually decreases with the increase of salt concentrations (Compeau and Bartha, 1983; Barkay et al., 1997). Therefore, in the marine and estuary sediments, the ratio of MeHg to total mercury concentration is smaller than that in freshwater sediment. The ratio is ~ 0.5% in marine sediment and reaches 1-1.5% in fresh water sediments. The divalent mercury in compounds endowed with negative charge (e.g. $HgCl_3^-$ or $HgCl_4^{2-}$) is hardly available for the biotic methylation in comparison with the neutral species of Hg(II) (Compeau and Bartha, 1983). It is supposed that the processes of mercury demethylation are more effective in the marine ecosystems with relatively high salinity than in the fresh waters (Compeau and Bartha, 1984).

2.3 Iron Sulfide (FeS)

2.3.1 Species of Iron Sulfides

There is a variety of binary compounds formed from iron and sulfur. The common forms existing in anoxic sediments include mackinawite (FeS), greigite (Fe_3S_4), pyrite (FeS_2) and pyhhorite ($Fe_{1-x}S$). Greigite and pyhhorite have been shown to contain mixed Fe (II) and Fe (III) valence states (Vaughan and Tossell, 1981; Pratt et al., 1994), formed from the oxidation of mackinawite. Pyhhorite is an excellent scavenger for aqueous Hg(II) complexes (Jean and Bancroft, 1986) and so is pyrite (Ehrhardt et al., 2000; Behra et al., 2001). Mackinawite together with greigite has been accepted to be the major mineral constituents of Acid Volatile Sulfide (AVS) in anoxic sediments and are involved in the formation of more stable pyrite (Berner, 1970; Canfield et al., 1992). The composition of mackinawite is not well constrained. From previous reported analyses, synthetic mackinawite has a chemical composition varying from $Fe_{0.87}S$ to $Fe_{1.15}S$ (Berner, 1964; Sweeney and Kaplan, 1973; Lennie et al., 1997). Presently available evidence suggests that it closely approximates stoichiometric FeS in composition (Rickard et al., 2006).

2.3.2 Structure of FeS

Iron(II) monosulfide (FeS) has been presumed to be a major mineral constituent of AVS. It was demonstrated that the synthetic black iron(II) monosulfide phase produced by precipitation of Fe(II) salts with S(-II) in ambient aqueous systems had a tetragonal structure (Berner, 1964). This phase was identified as mackinawite and showed that it was a major constituent of the black iron sulfide material of sediments (Berner, 1962).

Neutron scattering analysis of a synthetic mixture of greigite and mackinawite showed the presence of 2 nm nanoparticles (Watson et al., 2000). By XRPD analysis, mackinawite is nanocrystalline, with an average primary particle size equivalent to a crystallite size of 4 nm and a corresponding specific surface area of 350 m^2/g. It can be described in terms of a mixture of two end-member phases with different long-range ordering. The first formed phase has an average particle size of 2.2 ×1.7 nm and the second phase has an average primary particle size of 7.4 × 2.9 nm (Wolthers et al., 2003). At present, it appears that the composition of pure mackinawite is close to stoichiometric FeS (Rickard and Morse, 2005).

2.3.3 Solubility of FeS

2.3.3.1 Solubility of FeS in Natural Waters

In natural waters, the concentration of S^{2-} is not significant, the solubility of FeS cannot be calculated from $FeS = Fe^{2+} + S^{2-}$. Instead, the solubility product is calculated from equation, $FeS + 2H^+ = Fe^{2+} + H_2S$

The equilibrium constant is designed

$$\log K^*_{sp,FeS} = \log \alpha_{Fe^{2+}} + \log \alpha_{H_2S} + 2\,pH$$

Benning obtained a value of 3.1 for this equilibrium constant at 25˚C (Benning et al., 2000). The equilibrium constant is 3.0 for amorphous FeS and 3.6 for mackniwite (Davison, 1991; Davison et al., 1999). The solubility of FeS can be described by a pH-dependent reaction and a pH-independent reaction. The pH-dependent dissolution reaction which is presented by equation $FeS + 2H^+ = Fe^{2+} + H_2S$ tends to occur in acidic water. The pH-independent dissolution reaction involves the formation of the aqueous FeS cluster complex and can be

represented by $FeS = FeS^0$, with $\log K_0(FeS) = -5.7$. The pH-independent dissolution tends to occur in natural to alkaline environments (Rickard, 2006).

2.3.3.2 Solubility of FeS in HCl

It was found that only 81% of FeS was recovered in hot 6 M HCl digestion over 1 hour and 104% recovered in cold 6 M HCl digestion over 1 hour. Using hot HCl, the recovery efficiency of FeS from dried FeS was less than that of wet FeS. The reasons are unknown. Dried FeS has a strong static charge and it may be that this contributes to a difficulty in wetting the sample. Dried FeS also tends to flocculate into hard cakes with limited pore space (Watson et al., 2000) and this may reduce the surface area to such a degree that dissolution is less efficient.

2.3.4 Sorption of Mercury onto FeS

FeS has a high adsorptive capacity for various divalent metals (Arakaki and Morse, 1993; Morse and Arakaki, 1993; Morse and Luther, 1999; Coles et al., 2000; Wharton et al., 2000), but in-depth studies of Hg(II) sorption to FeS are rare. Metals whose sulfide phases are less soluble than FeS exhibit an increasing surface affinity with decreasing solubility (Morse and Arakaki, 1993). At 25˚C and low to moderate ionic strength, the solubility constant for FeS is about -3.6 (Davison, 1991), and it is -45.7 and -45.1 for metacinnabar and cinnabar respectively (Dyrssen and Kremling, 1990). This explains the affinity of mercury to FeS.

2.4 Remediation of Contaminated Sediments

2.4.1 Remediation Methods

Contaminants can be transported into the overlying water column by advective and diffusive mechanisms. Mixing and reworking of the upper layer of contaminated sediment by

benthic organisms continually exposes contaminated sediment to the sediment-water interface where it can be released to the water column (Reible et al., 1993).

Table 2.1 Remedial approaches for contaminated sediments

In-situ approches	Ex-situ approches
In-situ capping • Single-layer granular caps • Multi-layer granular caps, • Combination granular/geotextile caps Monitored natural recovery • Physical isolation or other processes • Chemical transformation/sequestration • Biological transformation/sequestration Hybrid approaches • Thin layer of sand or other material to enhance recovery via natural deposition. Institutional controls • Fish consumption advisories • Commercial fishing bans • Waterway or land use restrictions (e.g., no anchor or no wake zones, limitations on navigational dredging • Dam or other structure maintenance agreements. In-situ treatment • Reactive caps • Additives/enhanced biodegradation.	Dredging • Hydraulic, mechanical, or combination/hybrid dredging and transport to shore • Treatment of dredged sediment and/or removed water • Disposal of dredged sediment or treatment residuals in upland landfill, confined disposal facility, or other placement • Backfill or dredged area, as needed or appropriate. Excavation • Water diversion or dewatering • Excavation of sediment and transport to staging or processing • Treatment of excavated sediment • Disposal of excavated sediment or treatment residuals in upland landfills, confined disposal facility, or other placement • Backfill of excavated area, as needed or appropriate.

Thus, proper environmental management procedures should be applied to lower contaminant levels in contaminated water systems. Source control, contaminated sediment remediation, or their combination, are the usual options for cleaning up contaminated sites (Wang et al., 2004). In-situ and ex-situ are the two basic options for remediation of contaminated

sediments. There are several approaches for each of these two options (Table2.1) (U.S.EPA, 2005). Capping and dredging are two widely used active remedial solutions for contaminated sediment in aquatic systems.

2.4.2 In-situ Capping

In-situ capping (ISC), is the process of placing a layer of proper isolating materials (e.g., sand) between the layer of contaminated sediment and overlying water. ISC is a form of containment in-place. Generally speaking, capping is a promising economical method for treating contaminated aquatic systems (Palermo et al., 1998). Conventional capping usually involves placement of sand or clean dredged material. Specialized materials may be used to enhance the chemical isolation capacity or otherwise decrease the thickness of caps compared to sand caps. Examples include engineered clay aggregate materials (e.g., AquaBlok™), and reactive/adsorptive materials such as activated carbon, apatite, coke, organoclay, zero-valent iron and zeolite.

Depending on the contaminants and sediment environment, a cap is designed to reduce risk through the following primary functions: (1) Physical isolation of the contaminated sediment sufficient to reduce exposure due to direct contact and to reduce the ability of burrowing organisms to move contaminants to the surface; (2) Stabilization of contaminated sediment and erosion protection of sediment and cap, sufficient to reduce resuspension and transport to other sites; (3) Chemical isolation of contaminated sediment sufficient to reduce exposure from dissolved and colloidally bound contaminants transported into the water column.

One of the major advantages of in-situ capping is that it can quickly reduce exposure to contaminants and that, unlike dredging or excavation, it requires less infrastructure in terms of material handling, dewatering, treatment, and disposal. A well-designed and well-placed cap should more quickly reduce the exposure of fish and other biota to contaminated sediments as compared to dredging, as there should be no or very little contaminant residual on the surface of the cap. Another advantage is that the potential for contaminant resuspension and the risks associated with dispersion and volatilization of contaminated materials during construction are typically lower for ISC than for dredging operations and risks associated with transport and disposal of contaminated sediment are avoided.

The major limitation of ISC is the contaminated sediment remains in the aquatic environment where contaminants could become exposed or be dispersed if the cap is significantly disturbed or if contaminants move through the cap in significant amounts. In addition, in some environments, it can be difficult to place a cap without significant contaminant losses from compaction and disruption of the underlying sediment. If the water body is shallow, it may be necessary to develop institutional controls, which can be limited in terms of effectiveness and reliability, to protect the cap from disturbances such as boat anchoring and keel drag (U.S.EPA, 2005).

2.4.3 Remediation of Mercury Contaminated Sediments

Mercury concentrations in fish in lakes are elevated due to increased global cycling of mercury. Effective remedial methods need to be applied to lower mercury levels in heavily mercury-polluted aquatic systems. Source control, contaminated sediment remediation, or their

combination, is the usual options for cleaning up mercury-contaminated sites. Capping, dredging and natural attenuation are promising remedial methods for mercury-contaminated sediments. In natural attenuation, no containment or treatment measures are implemented to contaminated systems.

2.4.3.1 In-situ Capping

ISC field studies were conducted in Hamilton Harbour, Canada, which suffered significant contamination from zinc, copper, mercury, and other metals. A cap, approximately 35 cm thick and composed mostly of sand, was placed in the system to contain polluted sediment (Azcue et al., 1998). After one year of in situ capping, a field study investigated the effectiveness of ISC. Except for a few cases in some sampling cores, mercury concentrations were less than 0.005 μg g^{-1} in the capping layer, which was much less than 430-960 μg g^{-1} in the original sediment (Azcue et al., 1998). It should be noted that mercury in the capping layer may be caused by deposition from the overlying water.

There are two major concerns about ISC (Wang et al., 2004): First, buried mercury may pass through the capping layer and enter into the overlying water by hydrodynamic flows, bioturbation, consolidation, transformation, diffusion, etc.. For example, laboratory experiments suggest that subaqueous groundwater flow reduces the efficiency of capping significantly. The movement of benthic organisms may also facilitate the remobilization of buried mercury. Sediment consolidation, due to gravity, moves mercury from buried sediment into the capping layer. The second major concern is that the placing of the capping layer can cause resuspension of originally settled sediment. However, a pilot test conducted in a Canadian harbor suggests that

no significant sediment was resuspended by the placement of the capping layer (Hamblin et al., 2000).

2.4.3.2 Dredging

Dredging appears to be an effective remedy for systems heavily polluted by mercury. Dredging of the heavily mercury-contaminated sediments in Minamata Bay in Japan is a successful example. Minamata Disease, methylmercury poisoning, was recognized late in 1953 among the inhabitants living around Minamata Bay. Highest mercury concentration in muds reached 908 μg g^{-1} (dry weight) in 1969 (Fujiki and Tajima, 1992). Since 1977, dredging work had been carried out to remove mercury-contaminated mud and all of the work had finished at March 1990. Monitoring data shows that careful implementation of dredging did not cause significant adverse impact on the environment from sediment resuspension. At most sampling points, mercury concentrations were below 5 μg g^{-1} after dredging (Hosokawa, 1993). The concentration of mercury in fishes from the bay was very high in 1959: shellfishes approximately 178 μg g^{-1} (dry weight) and fish 15 μg g^{-1} (wet weight). Mercury concentration in fishes has decreased markedly since 1966. Total mercury concentration in fishes (87 species) were approximately 1.74 μg g^{-1} (wet weight) and fishes containing over 0.4 μg g^{-1} of total mercury were 16 species in 1989 (Fujiki and Tajima, 1992).

2.4.3.3 Natural Attenuation

Natural attenuation is the process that contamination decreases by naturally occurring processes, with adequate source control. Two important ways to naturally reduce Hg(II) in surface waters are photoreduction and microbial reduction (Wang et al., 2004). Relying on

natural attenuation alone, no aggressive remedial methods would be applied, and contaminated aquatic systems would be expected to recover naturally. If no serious adverse environmental effects would occur, natural attenuation may be a choice for less contaminated sites. However, contaminated systems in natural attenuation should be regularly monitored to ensure environmental safety.

Field experiments in natural attenuation of mercury-contaminated aquatic systems were performed in the state of Washington. In Whatcom Waterway at Bellingham, mercury concentration in the surface sediment was about 4.5 μg g^{-1} in the 1960s. After source control and natural attenuation, mercury concentration in the surface sediment was reduced to about 0.5 μg g^{-1} (Garbaciak et al., 1998).

2.4.3.4 Possible Ways to Lower MeHg Concentrations in Aquatic System

A review summarizes several possible ways to lower MeHg concentrations in fresh water reservoirs and lakes (Mailman et al., 2006), which includes intensive fishing, adding selenium, adding lime to acidified systems, controlled burning before flooding, removing standing trees, adding phosphorous, demethylating MeHg by photodegradation, capping bottom sediment, dredging bottom sediment and aerating anoxic bottom sediments or waters.

Phosphorus addition to aquatic systems has lowered mercury concentrations in fish mainly by increased growth rate of fishes and dilution of MeHg because of overall increases in biomass of the system, which is known as growth dilution (Larsson et al., 1992).

Demethylation of MeHg by ultraviolet irradiation may lower the amount of MeHg present in new reservoirs and decrease MeHg bioaccumulation. Via in-situ incubations of lake

water, it shows that MeHg is decomposed by photo-degradation in surface waters. This process is abiotic and the rate is first-order with respect to MeHg concentration and the intensity of solar radiation. (Sellers et al., 1996). Methylation mostly occurs in anoxic sediments, especially at anoxic boundary. It has been shown oxygenation of sediments can inhibit microbial methylation (Matilainen et al., 1991). Therefore, aeration of anoxic bottom sediments or waters may inhibit the formation of MeHg.

In Swedish Lakes, after treatment with lime to elevate pH values to 6.5-7.0, the fastest and largest decreases of mercury in fish were obtained in the lakes which were moderately acid before liming (mean pH 5.4-5.8). In small perch, the mercury-concentration was markedly reduced in two years and showed an 80% decrease in ten years (Andersson et al., 1995). Another study also showed that addition of lime could lower MeHg concentration in fish (Rask and Verta, 1995). These studies demonstrate that addition of lime could be a useful method to lower MeHg concentrations in low pH reservoirs and lakes for the long-term.

2.5 Incubation Experiments on Evaluating Methylation of Mercury

2.5.1 Hg(II) Spiked for Incubation

Due to the higher bioavailability (Bloom and Preus, 2003), aqueous Hg(II) has been widely used as the spiking form of Hg(II). There are two kind of Hg(II) commonly used in the methylation incubation studies.

2.5.1.1 Trace Isotope Aqueous Hg(II)

The most commonly used is the radiochemical isotope ^{203}Hg(II), which is measured by gamma spectrometry (Gilmour et al., 1998; Guimaraes et al., 2000; Turner et al., 2001). Trace

isotope $^{200}Hg(II)$ was also used for the incubation, with the measurement based on ICP-MS (Hammerschmidt and Fitzgerald, 2004).

2.5.1.2 Natrualy Occurring Aqueous Hg(II)

$HgCl_2$ and $Hg(NO_3)_2$ are commonly used to provide additional Hg(II) for the methylation incubation experiments (Gilmour et al., 1992; King et al., 2000; Macalady et al., 2000; King et al., 2001; Bloom and Preus, 2003; Mehrotra et al., 2003; Hammerschmidt and Fitzgerald, 2004; Harmon et al., 2007). Most of the measurements for total mercury and MeHg are based on traditional cold vapor technique and GC-AFS respectively. Occasionally, ICP-MS was used for the analysis.

2.5.2 Sediments for Incubation

Sediment types affect the fraction of mercury in the methylated form due to the levels of organic carbon and sulfate which sustain the bacteria populations and sulfur- reducing bacteria activity (Gilmour et al., 1992; Bloom et al., 1999). Also, the methylation percentage of total mercury depends on the total mercury concentration in the sediment. Bloom (Bloom and Preus, 2003) showed that the percentage of added Hg(II) methylated was highest at low total Mercury concentration (<5 ug/g) and relatively constant in this concentration range. The percentage of methylation decreased rapidly as the concentration of total mercury increases, even the total MeHg continued to increase.

Chapter 3 Capping of Mercury-Contaminated Sediments with Sand

3.1 Materials and Methods

3.1.1 Sediment Collection and Properties

Sediment samples were collected from four divided areas (labeled Areas 1-4) proposed for capping on the delta at the entrance to the Pompton Lake (Fig. 3.1). Surface sediment samples (0-150 mm) were collected with a Van Veen grab sampler and placed in a 0.0189 m^3 (5-gallon) HDPE bucket. A 5 cm layer of surface water was placed over the sediment in order to maintain anaerobic conditions. These buckets were sealed, shipped to the lab and stored at room temperature. Sediments were withdrawn from the buckets for experiments and the remaining sediments were resealed after covering again by water. Prior to use, the sediments were coarse sieved by using a steel mesh with 11 mm openings to remove large debris. All operations were performed as quickly as possible to minimize the exposure of sediments to the air.

Sediment moisture was measured by weight change upon drying at 110 °C for overnight. Organic matter content was determined as weight loss on ignition (LOI) (550 °C, overnight) of dried (110 °C) sediment samples. The pH value of the collected sediment was represented by that of the sediment slurry prepared by mixing sediment with the overlying water in a 1:1 ratio (weight). The measurement of pH was conducted using an Orion Model 210 pH meter.

The partition coefficient K_d for the sediment-water system was determined using a batch method (U.S. EPA and U.S. DOE 1999). Briefly, the pore water was separated from the solid phase by centrifugation followed by vacuum filtration with 0.7 μm glass filter, and total mercury (THg) concentrations in supernatants were measured.

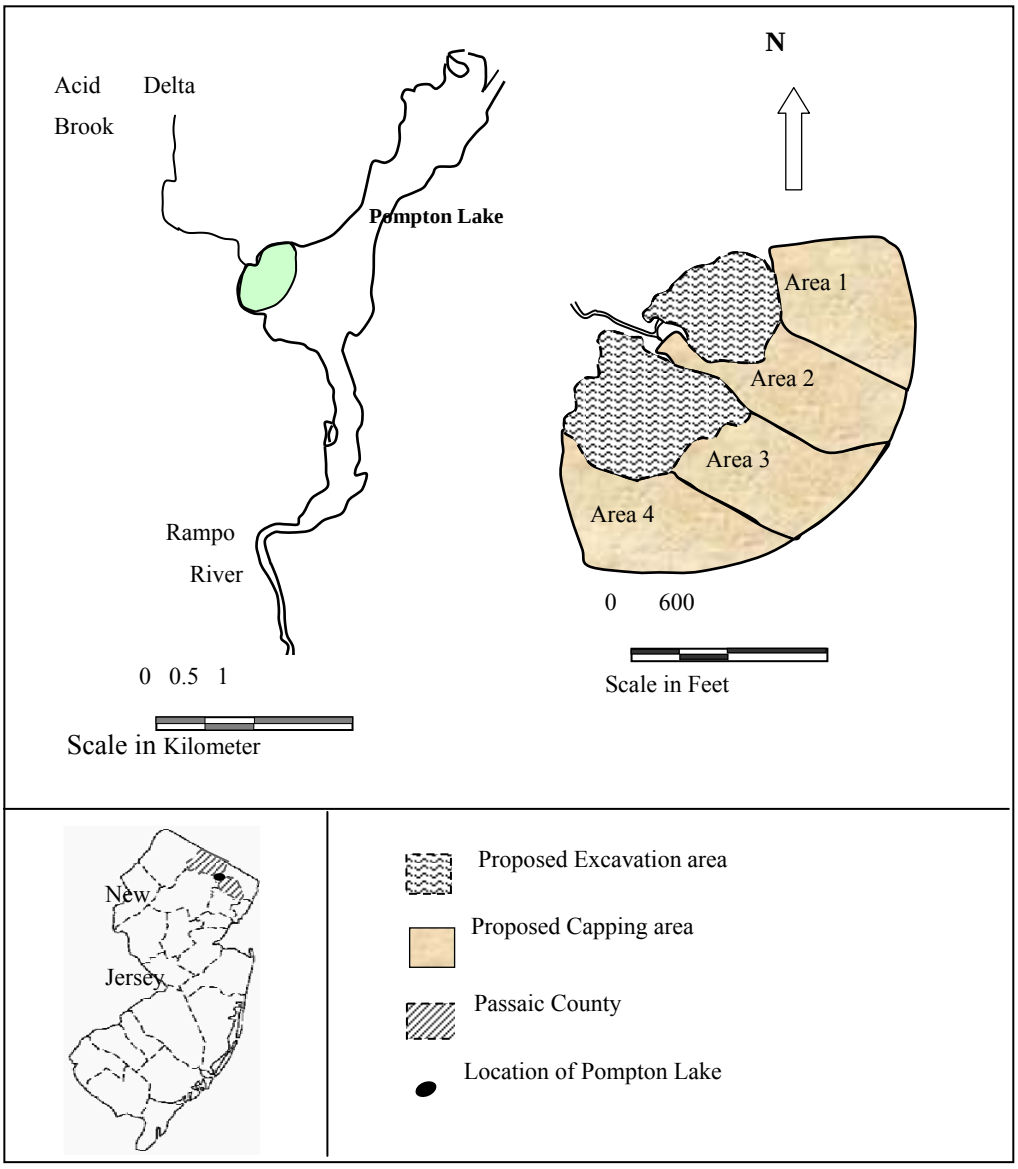

Figure 3.1 Sediment sampling locations
(area 1, area 2, area 3 and area 4) at the entrance of Pompton lake

3.1.2 Experimental Setup

Experiments in acrylic capping simulator cells were conducted to investigate the fate and transport of mercury in capped and uncapped sediments. Six cells were set up. Of the six cells,

two were uncapped using sediments from area 3 and 4, and four were capped using sediments from each of the 4 areas. The size of the sediment-containing part of the cell is 100 mm × 50 mm × 150 mm (L × W × H), and of the water-containing part is 300 mm × 50 mm × 45 mm (L × W × H). The schematic diagrams of the capped and uncapped cells are shown on Fig. 3.2. Sediments were filled to the top for uncapped cells and filled up to 10 mm below the top for capped cells. Then the sediments were allowed to consolidate for 4 days, by which we were trying to minimize the drop of sediment/cap top to below desired level due to consolidation during the experiment. Any water expressed to the surface via consolidation after placement was removed and new sediment was added to fill the cell to the desired height. For capped cells, sand was spread over the sediments to l0 mm thickness. The capping material used for the cells was play-sand from a hardware store. The sand used was the portion selected by two sieves with openings 0.125 and 0.85 mm in diameter, then washed with detergent, rinsed with deionized water and dried at 110 °C before it was used for the experiment. Total mercury concentration of the sand was undetectable by cold vapor atomic absorption spectrometry (CVAAS) analysis after acid digestion.

During the experiment, the top of the cells were covered with acrylic plates to reduce possible evaporation of mercury to the air, and all the cells were wrapped with aluminum foil avoiding direct exposure to light and reduce the potential for algal growth. Deionized water was passed over the sediment or cap during the experiment at a flow rate of 10 ml hr^{-1} for each cell. The depth of the overlaying water was about 12 mm. Teflon tubing was used at the outlet for water sample collection.

(a) Plan view of uncapped and capped cells

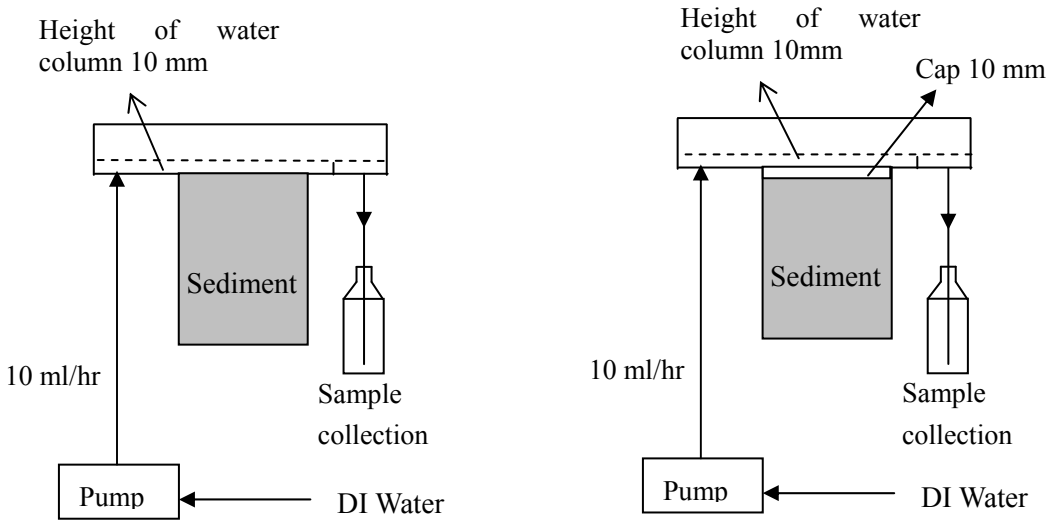

(b) Three dimensional schematic of capped cell (only one electrode is shown here)

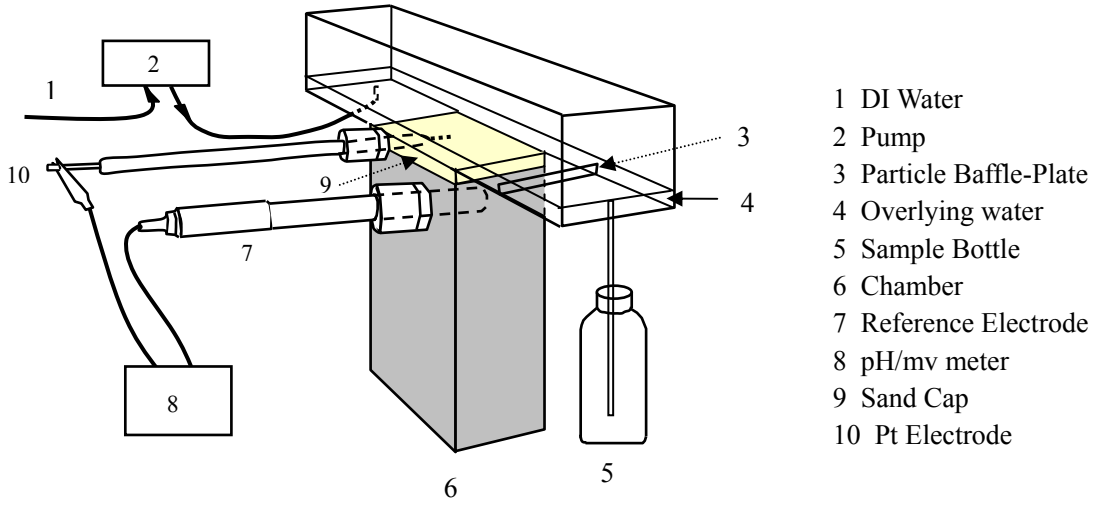

Figure 3.2 Schematic of experimental setups for capping simulations

After approximately 8 months of operation, the cells were cored for analysis to determine THg and MeHg migration in the system. An aluminum scraper with Teflon tip was used to perform slicing. Each 2 mm slice was removed with a scraper, and collected with a piece of Teflon sheet, the leftover on the cell was collected with a spatula coated with Teflon. After each slice, the cell was cleaned with cotton swabs to prevent sample mixing between slices. The

collected samples were placed into glass vials and the spare space in the vials was filled with N_2. These samples were refrigerated at 4 °C before analysis which was performed within 10 days of collection.

To investigate the redox conditions in the simulation system, a reference electrode (Accumet, Fisher Sci.) and platinum electrodes were installed at a certain depth of each cell. The platinum electrodes were made, cleaned and tested following the methods suggested by Patrick (Patric et al., 1996). Briefly, a platinum wire with a length of 12 mm and a diameter of 0.762 mm was fused onto a 180 mm of 2.063-mm diameter copper wire. Then it was inserted into a 160 mm, 6-mm O.D. glass tube and sealed with wax. After cleaning, it was tested in pH 4 and pH 7 buffer solutions of quinhydrone (Alfa Aesar) respectively. The reference electrode was installed 30 mm below the water-sediment/cap interface for each cell. For uncapped cells, three platinum electrodes were installed at 30, 20, 10 mm below the water-sediment interface. For capped cells, of 5 platinum electrodes applied, 2 were in the cap layer (at 5 mm from water-cap interface), 1 was at the cap-sediment interface (at 10 mm from water-cap interface), and the other 2 were in the sediment (at 30 mm and 20 mm from water-cap interface). The redox potentials were measured using a pH/mV meter (Oakton, pH 510 series). The electrodes used in this cell were tested again after removal and the values were in the acceptable range.

Oxygen concentration was measured with a Clark-style oxygen microelectrode (Diamond General Inc.) coupled to a 1201 chemical microsensor (Diamond General Inc.). The outer diameter of the tip of the electrode was 60 μm. The system was calibrated via a 1251 dual calibration cell by using pure N_2 gas (0% O_2) and ambient air (21% O_2) prior to every measurement.

3.1.3 Measurements of Total Hg and MeHg

Total Hg (THg) in sediment was measured by a vapor technique based on U.S. EPA Method 7471A using a Mercury Lab Analyzer Model 254. Total Hg in the sediment was extracted on a 1-2 g sample using hydrochloric–nitric acid and potassium permanganate. The oxidized mercury during digestion was reduced to the volatile elemental form by addition of stannous chloride and quantitatively measured by cold vapor atomic absorption spectrometry (CVAAS) (Gambrell et al., 2001). The qualitative analysis was performed using a 9-point calibration curve ranging from 0.2 to 1.8 μg L^{-1}, a stable and accurate calibration was obtained ($R^2 = 0.998$). The estimated detection limit for the method was 0.5 ng g^{-1} (dry sediment).

Sample preparation for MeHg in sediments was performed based on the method of (Alli et al., 1994) and (Cai et al., 1996). MeHg was measured using a GC separation and AFS detection system. An integrated GC-AFS included a Hewlett-Packard model HP 6890 Series with a gas chromatograph coupled to a PSA Merlin detector via a pyrolysis oven maintained at 810 °C (DeLaune et al., 2004). Quantitative MeHg analysis was obtained using a 5-point (between 0.2 μg L^{-1} and 10 μg L^{-1}) calibration curve forced to zero ($R^2 \geq 0.998$). The calibration curve was checked using a secondary standard solution source (5.0 μg L^{-1}) diluted from a MeHgCl solution (1000 mg L^{-1} Hg) in water. The recovery was 97.7%. The absolute detection limit calculated as three times of the standard deviation of the baseline noise was 0.15 pg Hg for MeHg. The detection limit was determined by analyzing over 300 noise peaks of five separate baseline runs.

Water samples were analyzed by Studio Geochemica in Seattle, WA. Reagents, gases, and DI water are all reagent or ultra-pure grade, and previously analyzed for mercury to ensure

very low blanks. Inorganic Hg standards are prepared by direct dilution of NIST certified NBS-3133 10.00 mg mL^{-1} mercury standard solution, and results independently verified by the analysis of NIST-1641d. MeHg standards were made up from the pure powder, diluted into a mixture of 5% acetic acid and 0.2% HCl, and then accurately calibrated for MeHg (equal to THg minus ionic Hg) against NBS-3133. MeHg results were also cross-verified by daily analysis of NRCC DORM-2. For THg, freshwater samples were oxidized using BrCl, and mercury was quantified using cold vapor atomic fluorescence spectrometry (CVAFS) as a detector (Bloom and Fitzgerald 1988), with dual pen chart recorders as output devices. For MeHg, water samples were distilled to liberate the CH_3Hg (Horvat et al., 1993) using an all Teflon® distillation system. The volatile $CH_3CH_2HgCH_3$ formed was separated from the aqueous matrix by purging onto a Carbotrap™. The trap was then thermally desorbed into an isothermal GC column for peak separation and then quantified by CVAFS (Bloom, 1989). All recoveries were in the range of 95-109%, with precision of results more than 10 times the detection limits typically less than 7% relative percent difference. All blanks and estimated detection limits were low, and typical for the methods employed. The estimated method detection limit was 0.05 ng L^{-1} for THg and 0.011 ng L^{-1} for MeHg.

3.2 Results and Discussion

3.2.1 Sediment Properties

Sediment samples from areas 1, 3 and 4 were fine-grained cohesive soft sediments. A sediment sample from area 2 contained significantly more sand, and also contained gravel and debris. The pH, organic matter content, water fraction, THg and MeHg in sediment, THg in pore

water, and partition coefficients of the four collected sediments are shown in Table 3.1. pH values of these sediments indicated that they were slightly acidic. The properties listed were similar for sediments from areas 1, 3, and 4. Organic matter content was around 10% (weight) of dry sediments by LOI at 550 °C. Sediment from area 2 contained approximately half as much water (37%) and organic carbon (5.33%) as the sediments from the other areas.

Table 3.1 Sediment characteristics

Sample Location	Sediment					Pore Water	K_d[c]
	pH	OM % LOI	Moisture %, w	MeHg[a,b] ng g^{-1}, dw	Total Hg[a,b,c] µg g^{-1}, dw	Total Hg[c] ng L^{-1}	L g^{-1}
#1	6.14	9.75	67.13	3.49 ± 0.15 2.78 ± 0.21	6.31 ± 0.39 5.48 ± 0.17 5.52 ± 0.42	36.9 ± 6.7	145
#2	5.78	5.33	37.27	13.65 ± 0.64 22.4 ± 1.38	40.84 ± 4.31 37.00 ± 1.31 33.19 ± 1.52	420.3 ± 6.1	79
#3	5.66	10.0	70.23	9.57 ± 0.81 12.7 ± 1.19	41.38 ± 3.99 45.00 ± 2.32 39.69 ± 0.46	115.6 ± 4.6	343
#4	6.27	11.5	70.28	3.96 ± 0.23 5.51 ± 0.47	17.37 ± 1.21 14.80 ± 1.23 16.77 ± 0.11	29.3 ± 3.5	573

Note: (a) Performed in Aug. 2004; (b) performed in Dec. 2004; (c) performed in Mar. 2005. Numbers before and after "±" represent average values and standard deviations. Abbreviations: OM = Organic Matter (dry weight); Kd = partition coefficient; dw = dry weight; w = wet weight.

The measurement method of partition coefficient Kd used for sediment-water system was similar to the in-situ batch method (U.S.EPA and U.S.DOE, 1999). Briefly, the pore water was separated from the solid phase by centrifugation followed by filtration with 0.7µm glass filter paper. Then the THg concentrations in both phases were measured. Kd was calculated by using the equation below:

$$Kd = \frac{W_s}{C_{w,Hg}} \quad (3\text{-}1)$$

Where,

W_s : Total Hg in solid phase;

$C_{w,Hg}$: Total Hg in pore water.

MeHg was only a small fraction of THg, ranging from 0.228‰ to 0.55‰. According to Bloom (Bloom and Preus, 2003), the percentage of MeHg decreases rapidly as the concentration of THg increases, though the MeHg concentration continues to increase. Organic matter plays an important role in methylation of mercury by binding mercury (Ravichandran et al., 1998), and an inverse relationship between potential rates of microbial mercury methylation and sedimentary organic content has been observed (Hammerschmidt and Fitzgerald, 2004). Thus the low fraction of MeHg over THg in the sediments was possibly due to high mercury concentrations and organic contents. The THg concentrations in the source sediments did not change significantly over the 7-month period between samples, and neither did the MeHg concentrations change significantly over the 4-month period between samples (sampling times were shown in Table 3.1). This indicates the stability of both of these components in unexposed sediments. The effective sediment-water partition coefficients for these sediments were calculated with THg concentration in dry sediments divided by THg concentration in pore waters (both truly dissolved and associated with fine (< 0.7 μm) particulate matter). This measurement is simply a measure of THg on sediment relative to pore water concentrations and does not account for mercury speciation or chemistry. However, it does provide a relative measure of the mobile

fraction of mercury in the sediments under study, which can be used in preliminary modeling efforts describing metal migration and release from the sediments. Measured partition coefficients varied from 79 to 573 L g^{-1}. These K_d's are in the range observed by other authors (Babiarz et al., 2001; Le Roux et al., 2001; Turner et al., 2001; Hammerschmidt and Fitzgerald, 2004), and U.S. EPA (U.S.EPA, 1997) also reported a range of 0.06-990 L g^{-1} under a variety of conditions. Sediment from area 3 has both the highest organic content and partition coefficient, while sediment from area 2 has the lowest organic content and partition coefficient. A positive relationship between the organic matter content and partition coefficient has been observed previously by Hammerschmidt and Fitzgerald (Hammerschmidt and Fitzgerald, 2004).

The calculated water fraction, dry bulk density, solid phase density, and porosity of the sediments are shown in Table 3.2. These data will be used in the modeling prediction in Section 3.3.

Table 3.2 Sediment parameters used in modeling

	Area 1	Area 2	Area 3	Area 4	Sand
f_w, w%	67.13	37.27	70.23	70.28	18.32
ε_w	0.8	0.575	0.832	0.847	0.348
ρ_b, kg m^{-3}	390.6	967.3	351.9	354.5	1554
ρ_S, kg m^{-3}	1959	2276	2095	2317	2383

Where,

f_w**:** Water fraction in wet sediment, mass of water mass of wet sediment

ρ_b: Dry bulk density, mass of dry sediment / total volume of the sediment.

ρ_S : Solid phase density, mass of dry sediment / (total volume of sediment – water volume).

ε_w : Porosity of wet sediment, volume of water / total volume of wet sediment

Water porosity was calculated by using the equation below,

$$\varepsilon_w = \frac{(1 - f_S)\rho_S}{(1 - f_S)\rho_S + f_S\rho_w} \tag{3.2}$$

f_S : Dry sediment weight fraction of the wet sediment

ρ_w : Water density, about 1 g cm^{-3} at room temperature.

3.2.2 Redox Conditions in Cells

Redox potential was monitored at different depths in each cell throughout the experiment. Fig. 3.3 shows the typical monitored results from an uncapped cell, in which the depth is relative to the water-sediment interface. The monitored results for a typical capped cell are shown on Fig. 3.4, in which the depth is relative to water-cap interface. Cap thickness was 10 mm as stated in the previous text. At depths of 10-30 mm below the water interface in uncapped cells, the redox potential decreased sharply to around –200 mv within a month, and was basically steady thereafter. Similar behavior was noted in the capped cells although attainment of these fully reduced conditions required ~100 days at a depth of 10 mm (i.e. at the original sediment-water interface) and ~ 200 days at a depth of 5 mm below the cap surface (5 mm above the original sediment-water interface). The cap-induced development of reducing conditions in the thin oxidized surface layer of the original sediment may encourage the formation of sulfate reducing bacteria which has been linked to methylation (Compeau and Bartha, 1985; Gilmour et al., 1992).

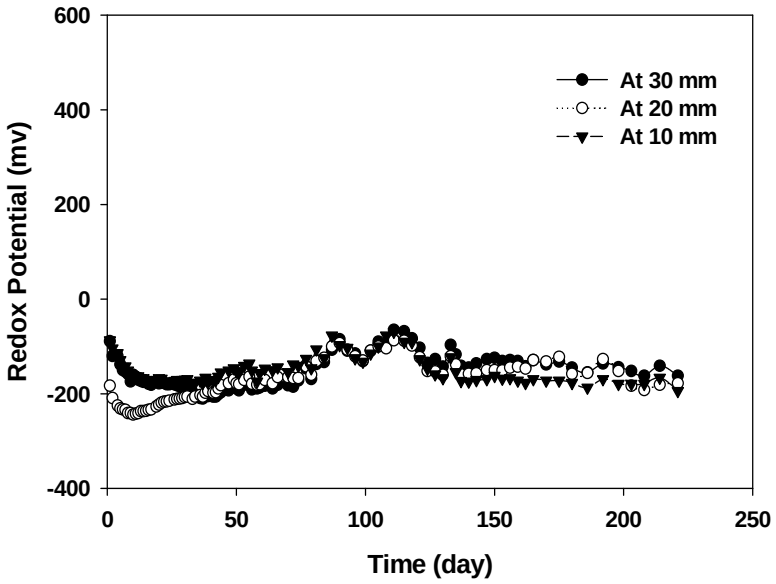

Figure 3.3 Redox potential in an uncapped cell at different depths relative to the water-sediment interface.

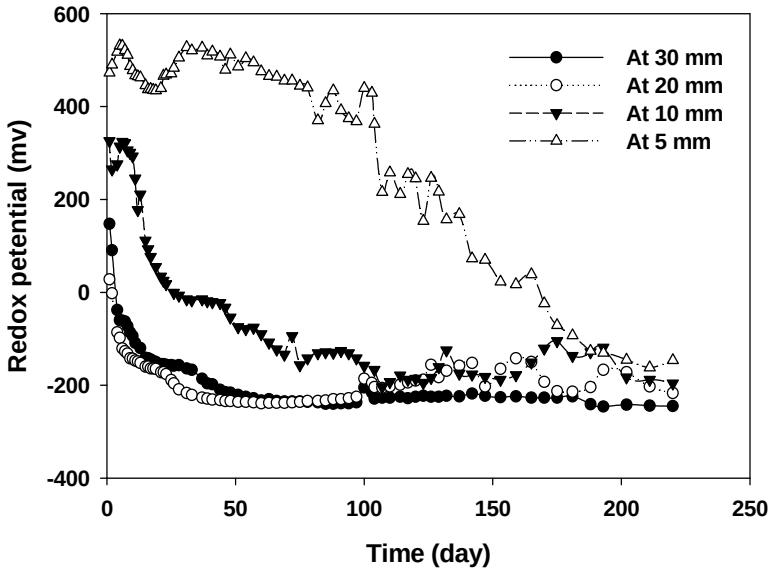

Figure 3.4 Redox potential in a capped cell at different depths relative to the water-cap interface.

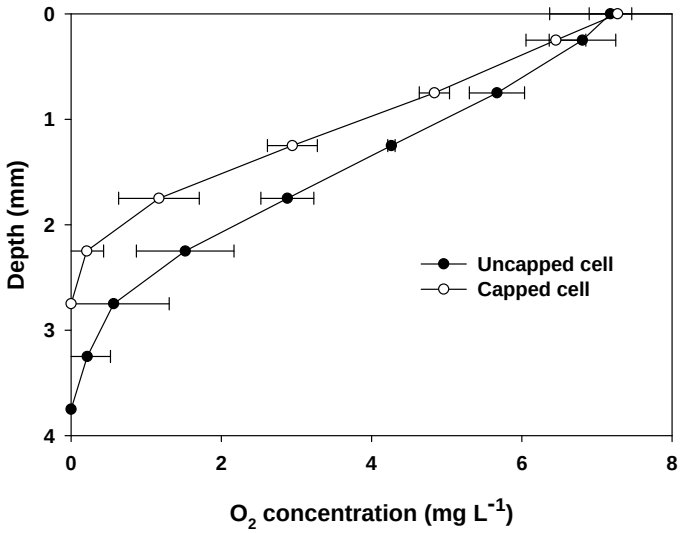

Figure 3.5 Oxygen content in cells at different depths in cap and sediment. "0" represents the water-sediment or water/cap interface.

Oxygen profiles in cells are complimentary to the redox conditions measured by electrodes. Fig. 3.5 shows the profiles measured after 162 days of operation of the cells. At this time, the redox conditions in both capped and uncapped cells had reached an approximately steady state. Zero represents the water interface (water-sediment interface for uncapped cells or water-cap interface for capped cells). Data for two uncapped cells and three capped cells were used to create the profiles. From this Figure, oxygen concentration decreased sharply from ~7 to 0 mg L^{-1} in both the cap and sediment within 3-4 mm of the water interface. Oxygen was essentially uniform and saturated in the overlying water (data not shown). The oxygen and redox levels showed that the originally oxidized layer of sediment underlying the cap would be strongly reduced after a short period of time following cap placement.

Under in-situ conditions in the lake, with much larger heights of water body and cap than those under the simulation conditions in the laboratory, the sediment beneath the cap is also expected to be strongly reduced.

3.2.3 Release of MeHg and Total Hg into the Overlying Water

Because mercury concentrations in the effluent water were too low to obtain reliable results from the available instrument we had (CVAAS), right before the end of the experiment, we collected a 200 ml water sample from each cell and sent to Studio Geochimica (Seattle, WA) for analysis. The bottles for water samples were shipped to our lab in double bags. After the samples were collected, the sample bottles were double bagged, packed with blue ice and shipped back to the lab for analysis via overnight services.

Table 3.4 Total Hg and MeHg in effluent water samples

Sample	THg ng L^{-1}	MeHg ng L^{-1}	Sedi	Capped/ Uncapped	Sedi THg µg g^{-1}
Cell A	2.18	0.016	#4	Uncapped	17.4
Cell B	1.76	BD	#4	Capped	17.4
Dupli B	2.38	BD	#4	Capped	17.4
Cell C	2.22	BD	#2	Capped	40.8
Cell D	1.83	0.017	#1	Capped	6.3
Cell E	6.68	0.019	#3	Uncapped	41.4
Control cell	1.70	BD	No		
Feed water [1]	1.73	BD			
Feed water +1.0ml HCl [2]	2.54	BD			
Freshly exposed sediment cell [3]	15.8	0.035	#4	Uncapped	16.8

Note: DI water in the supply plastic bottle before pump; 12N HCl used for sample preservation;water sample was collected after 24 hours of initiation of water flow; BD means “below detection limit” .

Results showed that MeHg was below detection limit (0.011 ng L^{-1}) for all the capped cells (Table 3.4). For the two uncapped cells, the MeHg concentration was 0.017 and 0.019 ng L^{-1}, which was slightly higher than the detection limit. The concentrations of THg were 1-2 ng L^{-1}

in the effluent from the capped cells, which was indistinguishable from the feed-water. In the uncapped cell using sediment from area 3 (THg was 115.6 ng L^{-1} in the pore water of the source sediment), the effluent THg concentration was 6.68 ng L^{-1}. While in the cell using sediment from area 4 (THg was 29.3 ng L^{-1} in the pore water of the source sediment), the effluent THg was 2.18 ng L^{-1}, which was a little bit higher than THg in the feed water (1.73 ng L^{-1}).

Because the flow rate in the cells was low, we assumed the concentration of total mercury or MeHg in the overlying water was uniform, and used the equation 3.3 to estimate fluxes from sediment to overlying water,

$$N = \frac{Q \cdot C}{A} \tag{3.3}$$

Where,

N: THg or MeHg flux to the overlying water

Q: The flow rate of overlying water. Q =10.0 ml hr^{-1} for all the cells.

C: THg or MeHg concentration in effluent water.

A: Interface area between sediment and overlying water. A=50 cm^2 for all the cells.

Based on the level of mercury in influent water, the minimum detectable total mercury flux from the exposed sediment was estimated to be approximately 1×10^{-3} ng m^{-2} s^{-1}. The calculated flux from cell using sediment from area 3 was 3.7×10^{-3} ng m^{-2} s^{-1}. Due to the length of time between initiation of the experiments and the submission of samples to Studio Geochemical, the measured fluxes had likely decreased over time. Sediment from area 4 was used to investigate the flux of THg and MeHg from freshly exposed uncapped sediment to the

overlying water. The THg profile of the first 5 effluent samples collected during 116 hours was shown in Fig. 3.6. During 116 hours of operation, THg in effluent ranged from 15.8 to 8.3 ng L^{-1}. The measured concentration of THg at 24 hours was 15.8 ng L^{-1} and MeHg was 0.035 ng L^{-1}, corresponding to fluxes of 8.8×10^{-3} ng m^{-2} s^{-1} and 1.9×10^{-5} ng m^{-2} s^{-1}, respectively.

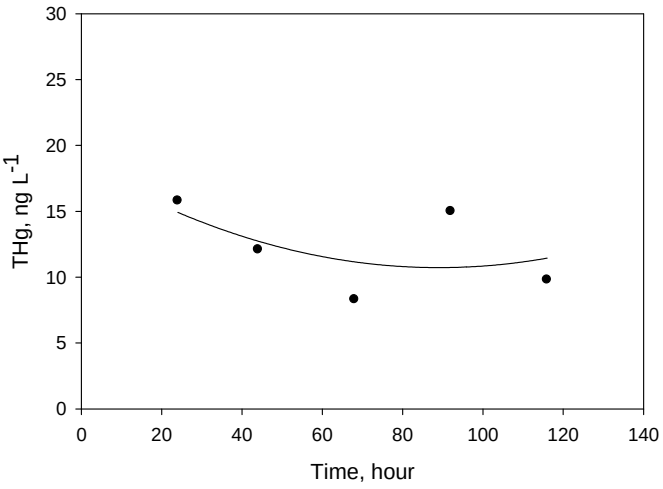

Figure 3.6 Total Hg in the effluent of an uncapped sediment cell using sediment from area 4.

Due to the limitation of available analysis instruments, we could not obtain the whole profiles of effluent samples for the cells, but based on the results from previous and the new uncapped cells, we estimated the fluxes of THg were ~10^{-2} to10^{-3} ng m^{-2} s^{-1} and of MeHg were ~10^{-5} ng m^{-2} s^{-1} in uncapped cells. In capped cells, THg concentrations were about the same as THg concentration in feed water. At least we could conclude that mercury flux was reduced due to the placement of the sand cap.

3.2.4 Migration of MeHg and Total Hg in Sediment and Cap

After approximately 8 months of operation, the cells were cored with 2 mm vertical resolution. The concentration distributions of THg for uncapped and capped cells are shown in

Fig. 3.7 and of MeHg are shown in Fig. 3.8. For purpose of comparison, here we only show data from cells using sediment from area 3 and 4, because we only had capped cells using sediment from area 1 and 2. Zero was at the water interface with the cap (capped cells) or sediment (uncapped cells). The dashed line represents the interface between sand and the underlying sediment.

There was no evidence of migration of THg and MeHg out of the sediment in the capped case. A slight decrease of THg and MeHg was observed at the top layer of the sediment for uncapped case. Even for the uncapped case, the release of mercury from solid phase was a very slow process due to the partitioning of mercury onto solid particles (mercury concentration was small in pore water. see Table 3.1).

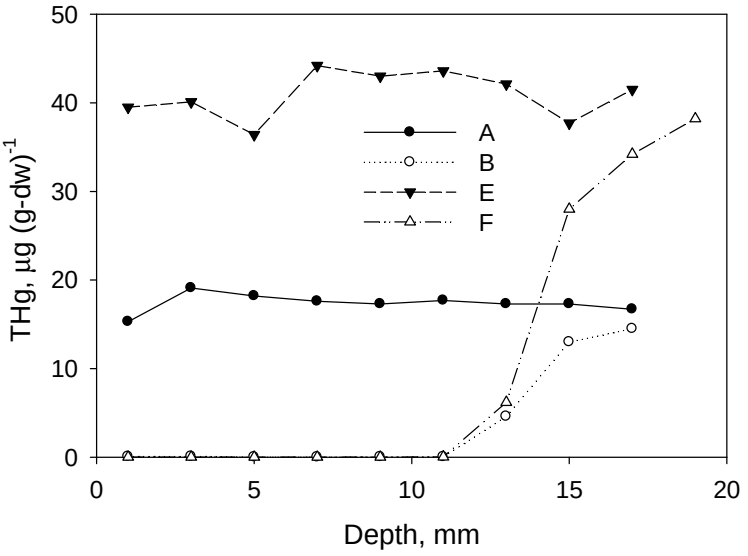

Figure 3.7 Total Hg profiles in capped and uncapped cells
A: uncapped using sediment from area 4; B: capped using sediment from area 4; E: uncapped using sediment from area 3; F: capped using sediment from area 3.

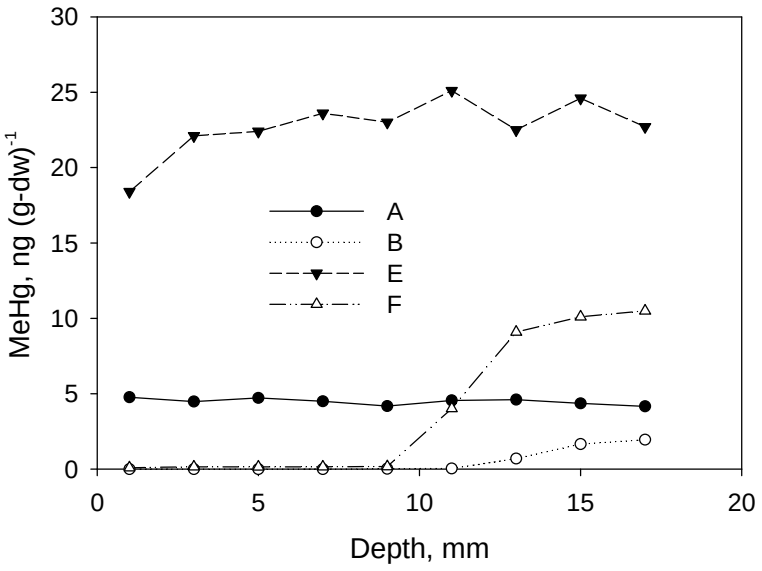

Figure 3.8 MeHg profiles in capped and uncapped cells
A: uncapped using sediment from area 4; B: capped using sediment from area 4; E: uncapped using sediment from area 3; F: capped using sediment from area 3.

Table 3.5 Fractions of MeHg over total Hg in sediment profiles

	Sediment from area 3			Sediment from area 4		
Depth[a] mm	MeHg/THg ($\times 10^{-4}$) Capped	Uncapped	Ratio of capped to uncapped	MeHg/THg ($\times 10^{-4}$) Capped	Uncapped	Ratio of capped to uncapped
1	6.5	4.7	1.4	1.5	3.1	0.48
3	3.3	5.5	0.60	1.3	2.4	0.54
5	3.0	6.2	0.48	1.3	2.6	0.50
7	2.8	5.3	0.53	1.7	2.6	0.65

Note: for capped cells, zero represents the interface of sand cap and sediment; for uncapped cells, zero represents the interface of water and sediment.

A gradual transition to the bulk sediment concentration of THg was observed in the capped case. This likely represented some intermixing of the cap into the sediment causing some dilution of the bulk sediment concentrations. If the mercury concentration profiles were the result of migration, mercury would have been measured in the cap layer and significant mercury would also have been measured in the effluent water for capped case. No significant mercury was

detected in any sand-cap sample that did not also contain fine-grained material from the sediment layer underlying the cap.

Although THg concentrations showed no significant influence of a cap except in the intermixed layer, MeHg showed decreases beneath the cap. In addition to Fig. 3.8, this is shown in Table 3.5, in which the ratio of MeHg to THg concentrations in the capped and uncapped cells are summarized. In particular, no increases in MeHg were noted as a result of the reduction of the surficial sediments.

3.3 Preliminary Model Prediction

3.3.1 Model and Boundary Conditions

3.3.1.1 Model for Uncapped Situation

Analytical models were used to predict concentrations and fluxes in both capped and uncapped sediments to extend the measurements in the laboratory to field conditions and times. The model used for simulation for uncapped cells was the "Finite layer with uniform initial concentration and mass transfer at the surface, and zero flux at the base" (Choy and Reible, 2001). The system was defined by the following dynamics and boundary conditions:

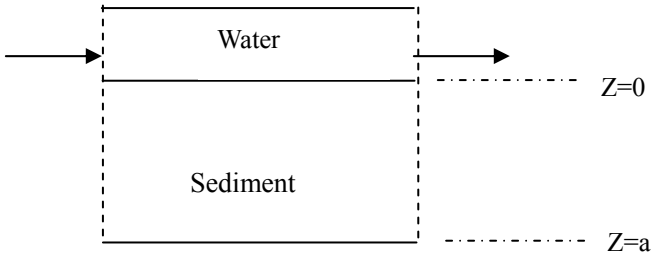

$$\frac{\partial C_A}{\partial t} = \left(\frac{D_{A(eff)}}{R_f} \right) \frac{\partial^2 C_A}{\partial z^2} \tag{3.4}$$

Boundary conditions,

$$D_{A(eff)} \frac{\partial C_A}{\partial z}\Big|_{z=0} + k_a C_A(z,t)\Big|_{z=0} = 0 \qquad t > 0$$

$$\frac{\partial C_A}{\partial z}\Big|_{z=a} = 0 \qquad t > 0$$

Initial conditions,

$$C_A(z, t=0) = C_{A0} \qquad z \in [0, a]$$

Where,

C_A: Concentration of chemical A (Here, it refers to THg) in pore water.

R_f : Retardation factor,

$$R_f = \varepsilon_w + K_d \cdot \rho_b \tag{3.4-1}$$

$D_{THg(eff)}$: Effective diffusivity of mercury in sediment,

$$D_{THg\,(eff)} = D_{w,THg} \cdot \varepsilon_w^{\,4/3} \tag{3.4-2}$$

k_a : Mass transfer coefficient at water side, cm/s.

Convection mass transfer coefficient at the water side is estimated by using the equation for laminar flow (Thibodeaux, 1999),

$$k_a = k_{w,Gypsum} \cdot \left[\frac{D_{w,THg}}{D_{w,Gypsum}} \right]^{1/2} \tag{3.4-3}$$

Where,

$D_{w,\ THg}$: Diffusivity of THg in water, cm^2/s.

$k_{w,Gypsum}$: Convection mass transfer coefficient for gypsum at water side.

$D_{w,Gypsum}$: Diffusivity of gypsum in water.

The measured values at room temperature for $k_{w,Gypsum}$ and $D_{w,Gypsum}$ are 6.26×10^{-8} m s^{-1} and 8.12×10^{-8} m^2 s^{-1} respectively, which were measured in the similar simulation system. Substitute these values into the equation and the calculated convection mass transfer coefficient at the water side k_a equals 5.5×10^{-8} m s^{-1}.

3.3.1.2 Model for Capped Situation

The model used for simulation for capped cells was the "Two layer finite system with arbitrary initial concentrations, mass transfer at the surface, and zero flux at the base" (Choy and Reible, 2001). The system is defined by the following dynamics and boundary conditions:

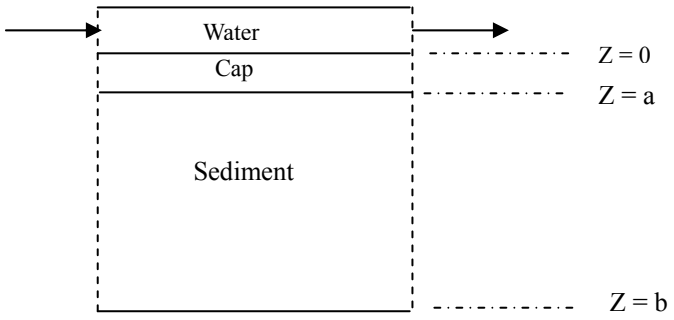

$$\frac{\partial C_{A,1}}{\partial t} = \left(\frac{D_{A(eff),1}}{R_{f,1}} \right) \frac{\partial^2 C_{A,1}}{\partial z^2} \qquad z \in [0, a]$$

$$\frac{\partial C_{A,2}}{\partial t} = \left(\frac{D_{A(eff),2}}{R_{f,2}} \right) \frac{\partial^2 C_{A,2}}{\partial z^2} \qquad z \in [a, b] \qquad (3.5)$$

Boundary conditions,

$$-D_{A(eff),1}\frac{\partial C_{A,1}}{\partial z}\Big|_{z=0} + k_a C_{A,1}(z,t)\Big|_{z=0} = 0 \qquad t>0$$

$$\frac{\partial C_{A,2}}{\partial z}\Big|_{z=b} = 0 \qquad t>0$$

Initial conditions,

$$C_{A,1}(z,t)\Big|_{t=0} = C_{A0,1}(z) \qquad z\in[0,a]$$

$$C_{A,2}(z,t)\Big|_{t=0} = C_{A0,2}(z) \qquad z\in[a,b]$$

3.3.2 Modeling Results under Experimental Period

From section 3.2.1.1, k_a = 5.5×10^{-8} m s^{-1}. Other parameters involved in the model simulation are listed in Table 3.6.

Table **3.6** Parameters for modeling simulation

	Cap/ Uncapped situation	Sedi used	t day	$D_{THg(eff)}$ m^2 s^{-1}	R_f	C_{THg0} ng L^{-1}	Sedi-water Kd L g^{-1}	Sand-water Kd L g^{-1}
Cell A	Uncapped	#4	253	5.5×10^{-10}	203000	29.3	573	
Cell B	Capped	#4	253	5.5×10^{-10}	203000	29.3	573	2.2
Cell C	Capped	#2	253	3.01×10^{-10}	77030	420.3	78.9	2.2
Cell D	Capped	#1	253	4.68×10^{-10}	56638	36.9	145	2.2
Cell E	Uncapped	#3	253	4.93×10^{-10}	121000	115.6	343	
Cell F	Capped	#3	253	4.93×10^{-10}	121000	115.6	343	2.2

The modeling results are very similar for uncapped cells A and E and similar for capped cells B, C, D and F, therefore, only results for uncapped cell E and capped cell F are shown, which both used sediment from area 3.

Fig. 3.9 shows the modeling results of THg profiles in uncapped cell E and capped cell F after 253 days of operation respectively. For cell F, the profile from experimental data is also shown for comparison.

From Fig. 3.9 and modeling data**,** after more than half a year, the penetration depth of THg migration in sediment at the water-sediment interface is less than 2 mm for the uncapped cell, which is consistent with the uniform distribution of THg with depth shown in Fig 3.7; for capped cells, the depth is about 1.6 mm in sediment and 2.5 mm into the cap.

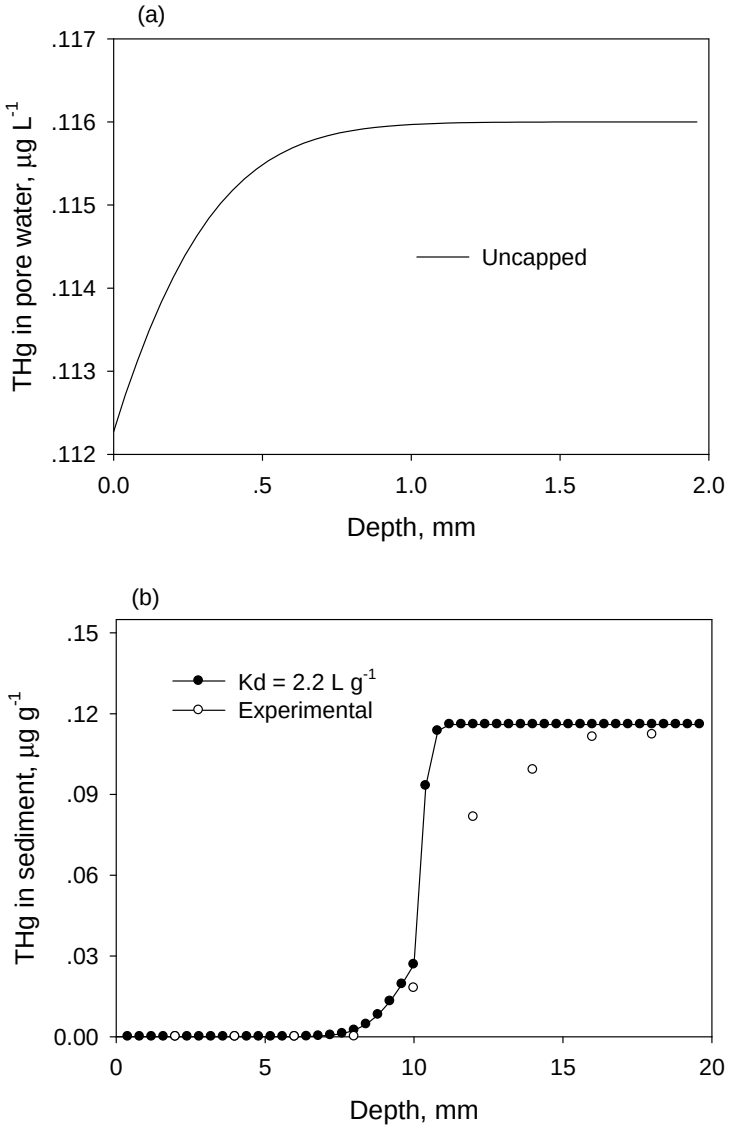

Figure 3.9 Total Hg profiles in cell E and cell F
The x-axis refers to the depth into the sediment from the sediment-water for (a) or into the cap and sediment from cap-water interfaces for (b). The cap-sediment interface is at 10 mm.

For the comparison of experimental and modeling THg migration in pore water, experimental THg concentrations in pore water are calculated by using Eq. 3.1, $Kd = \frac{W_s}{C_{w,Hg}}$. K_d and W_s values used for calculations are shown in Table 3.1. The profile from modeling is consistent with the experimental data, except in a 5 mm zone below the cap-sediment interface. At this zone, the measured THg concentration is lower than the modeling data, which was caused by the intermixing between cap (sand) and the sediment. With a much higher bulk density, sand tended to sink into the softer sediment beneath it and caused intermixing. Both modeling and experiment suggest no significant migration of mercury through the cap to the overlying water for the operational period.

For the uncapped case, the flux from the sediment into the overlying water is at the level of 10^{-3} ng m^{-2} s^{-1} (Fig. 3.10a), leveling slowly from 6.35×10^{-3} to 6.16×10^{-3} ng m^{-2} s^{-1} in 253 days. The predicted flux is in the same order with the experimental flux calculated from the THg concentrations in effluent water samples.

For the capped case, the THg flux from the sand cap into the overlying water rises from 0 to 5×10^{-14} ng m^{-2} s^{-1} in 253 days and is still rising. Comparing the capped and uncapped situations using the same sediment, up to real operating time, the flux into the overlying water through the water-cap interface was negligible compared to that from the sediment into the water directly. This further confirms that there were no significant releases of mercury into the overlying water in the capped cells.

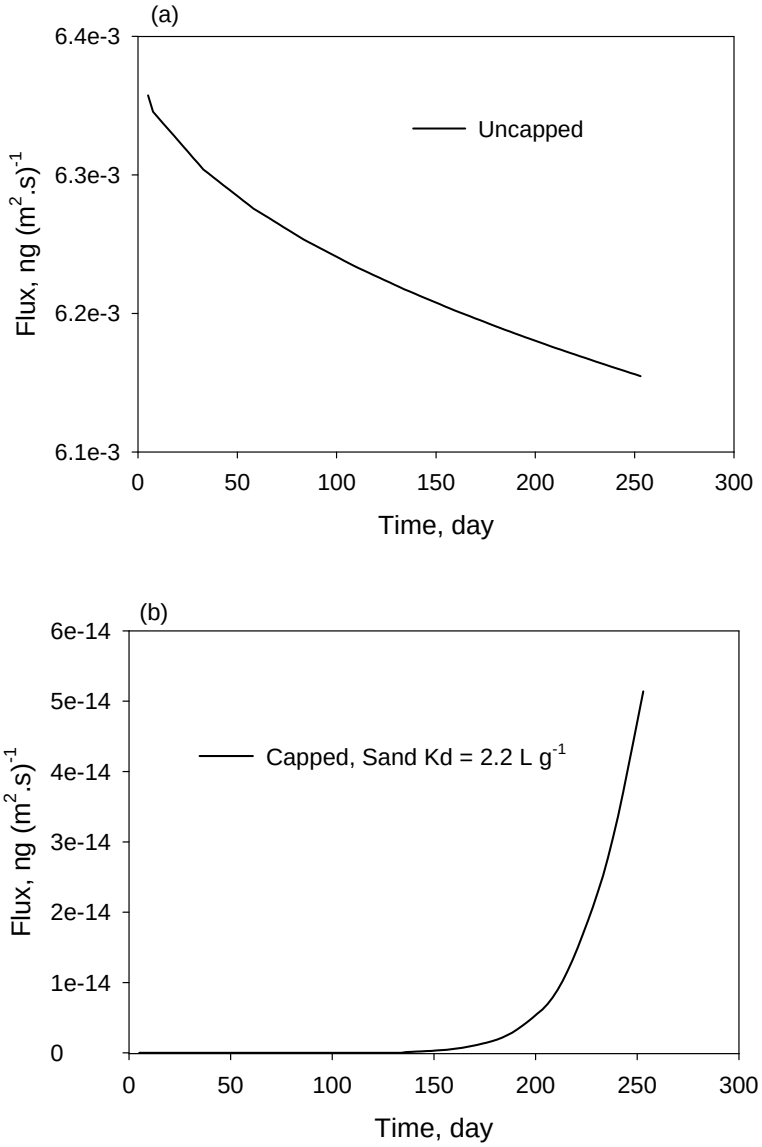

Figure 3.10 Flux into the overlying water for uncapped cell E and capped cell F

3.3.3 Effects of Kd on the Retardation of Mercury Release

Using a sediment with properties same as the sediment from area 3 of Pompton Lake, modeling was conducted when the thickness of the cap was 10 mm with Kd value of 0.038, 2.2 and 343 L g^{-1} respectively (Fig 3.11). The Kd of 0.038 L g^{-1} was the measured value using sand cleaned with detergent. A value of 2.2 L g^{-1} is close to the real condition in the capping

experiment because tiny mixing might exist during the placement of the sand cap. A value of 343 L g^{-1} is the same as that for the sediment, which is the case when clean sediment is applied as the capping material. At 10 years with a 10 mm cap, the penetration depth of diffusion was about 5 mm into sediment for caps with different Kds. However, with the increase of Kd, THg concentration at the same depth in this 5 mm zone increase, which means that less mercury has passed through the cap-sediment interface. With a Kd of 343 L g^{-1}, mercury has diffused about 3.5 mm into the cap. With a Kd of 2.2 L g^{-1}, mercury has diffused through the cap, and significant flux increase has been observed (data not shown). While with a Kd of 0.038 L g^{-1}, the cap holds little mercury and most of the mercury released from the underlying sediment has been released into the overlying water column.

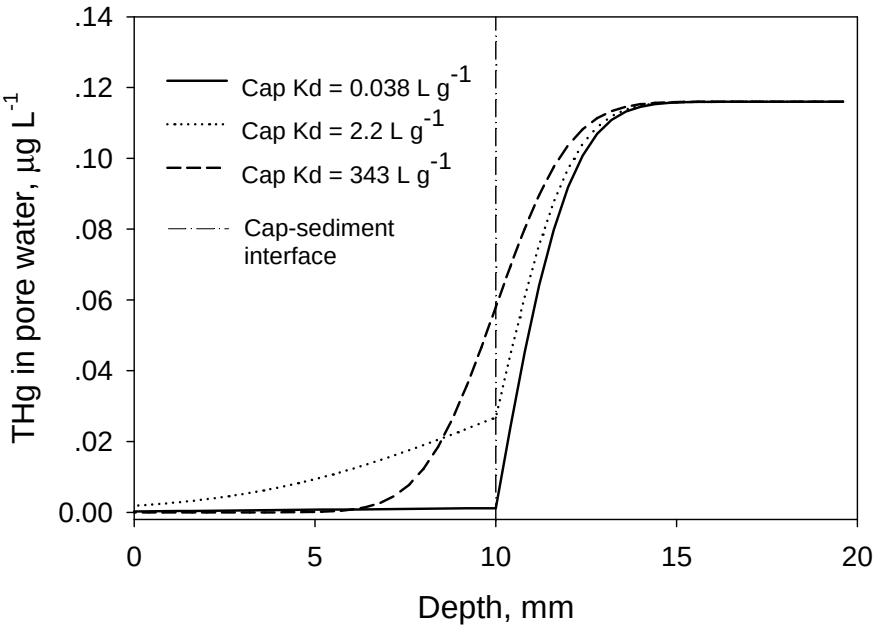

Figure 3.11 Total Hg profiles in cap and sediment with 10 mm cap at 10 years

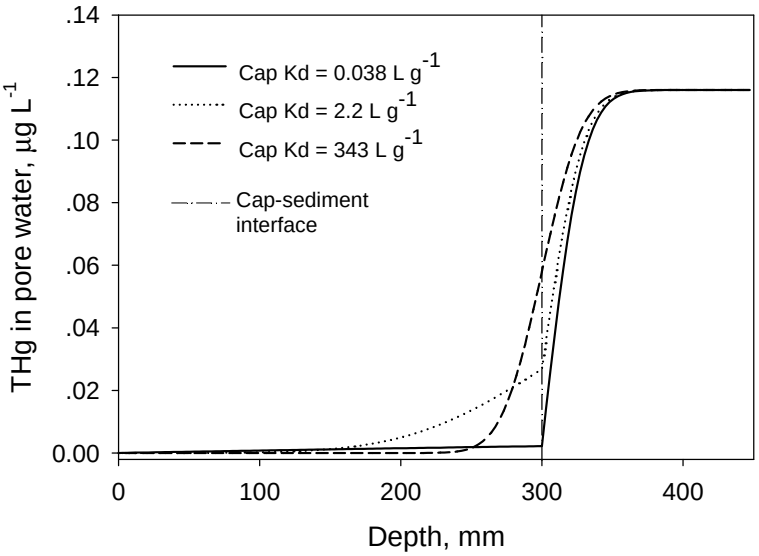

Figure 3.12 Total Hg profiles in cap and sediment with 300 mm cap at 2000 years

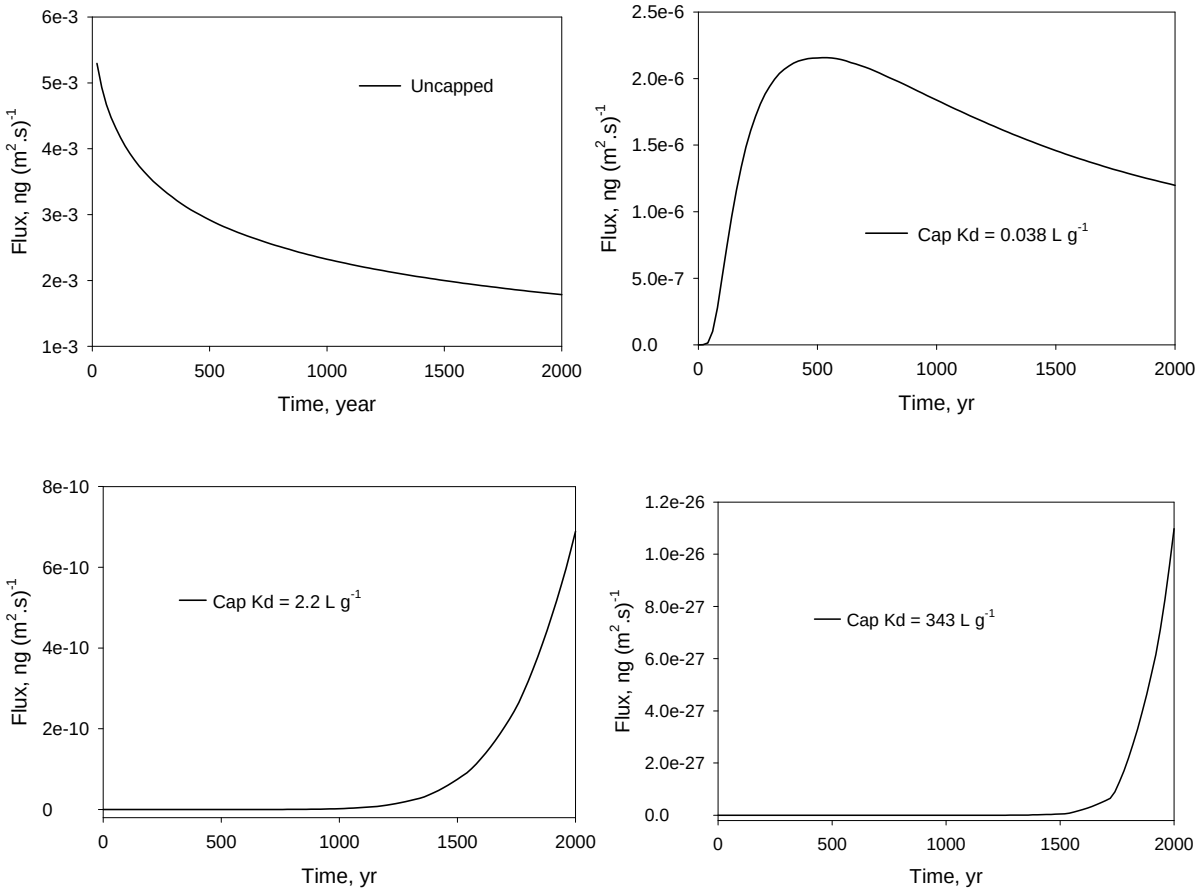

Figure 3.13 Flux of total Hg into the overlying water from sediments uncapped or with 300 mm cap.

For field application, a cap with the thickness of 300 mm is common (Palermo, 1998), therefore, modeling for a cap of thickness of 300 mm was conducted. It was assumed that the conditions at the water-cap interface is the same as those in the experiment conducted in the laboratory. With a 300 mm cap, the penetration depth of diffusion into the sediment is about 80 mm 2000 year after the placement of the cap (Fig. 3.12). With different Kds, same trend is shown as the case with 10 mm cap. With larger Kd, less mercury diffuses passing the cap-sediment interface, and more mercury is contained in the cap. With Kd values of 2.2 L g^{-1} and 343 L g^{-1}, no significant mercury has released into the water. Significant increase of mercury in the cap from the cap-sediment interface is 150 mm for the case with Kd of 2.2 L g^{-1}, and 80 mm for the case with Kd of 343 L g^{-1}. While with a Kd of 0.038 L g^{-1}, significant release of mercury into water has occurred at this time, which can be seen by the smaller area at the cap side than that at the sediment side under the curve. This can be further confirmed by the flux profiles for the uncapped case and the capped case with different Kds.

During 2000 years, the flux from the uncapped sediment decreases slowly and keeps at level of 10^{-3} ng $(m^2\ s)^{-1}$(Fig. 3.13). With a cap of thickness of 300 mm, the flux has decreased significantly, especially for larger Kds. With Kd of 2.2 L g^{-1} or 343 L g^{-1}, the flux of mercury into water is negligible compared to that from the uncapped sediment. For the case with a cap having a Kd vale of 0.038 L g^{-1}, at about 500 years, the flux reaches a maximum and then decreased gradually. With a larger Kd, the appearance of the maximum flux is delayed.

Under field conditions, the mass transfer coefficient ka might be larger due to the larger energy of flowing water. Also, mercury release rate may be significantly increased by the

destruction of the cap layer from the disturbance caused by human activities, ground water flow and burrowing organism, etc.. Thus, the modeling results represent the ideal case.

3.4 Summary

Capping of the mercury contaminated sediments can separate the contamination from the near-surface zone that is colonized by benthic organisms. Due to the low mobility of mercury even in sand caps, this isolation can be relatively long with no mobility observed over the eight month period of the experiment. In addition, MeHg which represents a relatively mobile and toxic form of mercury may be produced in lesser quantities under the fully reduced conditions after cap placement.

Modeling results show that capping material with higher partitioning coefficient of mercury between the solid and pore water has a high capacity to delay mercury release and contain mercury released from sediment. Because of the small Kd of sand for mercury, sand may be not adequate for long-term containment of mercury.

Chapter 4 Inhibition of Mercury Methylation by Iron Sulfides

4.1 Experimental Methods

4.1.1 Sediment Sampling and Preservation

Surface sediment was collected using a Peterson dredge at a water depth of 1.5 m in Henderson Lake, Louisiana. The sediment was placed in HDPE buckets and covered with a layer of surface water before sealing. Surface water was collected using polyethylene bottles at the same site. Upon arrival in the laboratory, the sediment was mixed thoroughly, sieved through 1.68 mm openings, placed into 4 L glass jars and sealed tightly before placed at 4 ˚C. Shortly before each incubation experiment, the sediment from the same glass jar was mechanically homogenized on a roller for 8 hours. Sediment for sulfide measurements was filled to the top of a glass jar and preserved with 2N zinc acetate solution and refrigerated at 4 ˚C prior to analysis.

4.1.2 Commercial and Synthetic Iron Sulfide

Considering availability, applicability and cost for possible capping application, an economical commercial iron sulfide (CIS) was selected as an amendment. X-ray powder diffraction (XRPD) analysis shows that CIS was actually a complicated mixture as the result of the oxidation of FeS. Therefore, high purity FeS (Syn-FeS) was synthesized to investigate the effects of pure FeS on the inhibition of Hg(II) methylation and to theoretically help understand the mechanism of the inhibition effects.

Commercial iron sulfide (CIS) was purchased from Fisher Scientific, Rochester, NY and was ground and sieved to less than 125 μm (mesh size) for use in the inhibition experiments.

Syn-FeS was prepared following a literature method (Rickard, 1995) with some modifications. Because FeS, especially wet FeS, is very reactive to oxidation, the preparation of the reactant solutions, the reaction and filtration were conducted under N_2. FeS was prepared from $FeSO_4.(NH_4)_2(SO_4)_2.6H_2O$ (Mohr's salt) and $Na_2S.9H_2O$ at room temperature (24˚C). Mohr's salt is the preferred reagent with aqueous iron(II) since it is relatively resistant to oxidation. After purged with high purity N_2 for half an hour, 100 ml 0.4 M Mohr's salt prepared in a separation flask was purged into 100 ml 0.4 M $Na_2S.9H_2O$ in a three necks flask and magnetically stirred for 5 minutes. The suspension was then purged in the vacuum filtration system and filtered through a 0.45 μm filter. In order to remove retained ions from FeS, wet FeS was rinsed with deionized water following the procedure: immediately after filtration, the wet FeS was placed in a HDPE tube and stored in a freezer. Once the wet FeS was frozen, it was put back in the cleaned reaction flask filled with 250 ml deionized water previously purged with N_2 and stirred for 10 minutes under N_2, followed by filtration. The filtration process of FeS slurry was much faster after frozen and usually done within a few minutes, which helped to minimize the oxidation of FeS. The procedure was repeated 3 times before FeS was dried under N_2 flow. The dried FeS was placed in 1.5 ml vials and preserved under N_2 flow in a 500 ml flask.

4.1.3 Experimental Design and Procedure

Sediment and surface water from the site was mixed to form a slurry with a dry solid to water ratio of 1:9 (weight) placed in a 250 ml glass flask. The sediment used for the incubation experiments was from the same 4 L glass jar. The water content was determined before the experiments and used to calculate the amount of surface water needed to make the slurry with a

dry solid to water ratio of 1:9. Before each incubation experiment, the sediment from the glass jar was mechanically homogenized on a roller for 8 hours. During the incubation, the flask was sealed with a rubber stopper that had inlet and outlet holes. Ultrahigh-purity N_2 was purged through the flask in order to maintain anaerobic conditions. The outlet gas was connected to a sulfide trap filled with the anti-oxidation reagent (AOR) (Brouwer and Murphy, 1994). The flow rate of N_2 was maintained 1-2 bubbles per second in the gas trap. The incubation flask was wrapped with aluminum film to prevent possible decomposition of MeHg which may be caused by exposure to light (Hammerschmidt and Fitzgerald, 2006). The experimental procedure and setup are shown in Fig. 4.1 and Fig. 4.2 respectively.

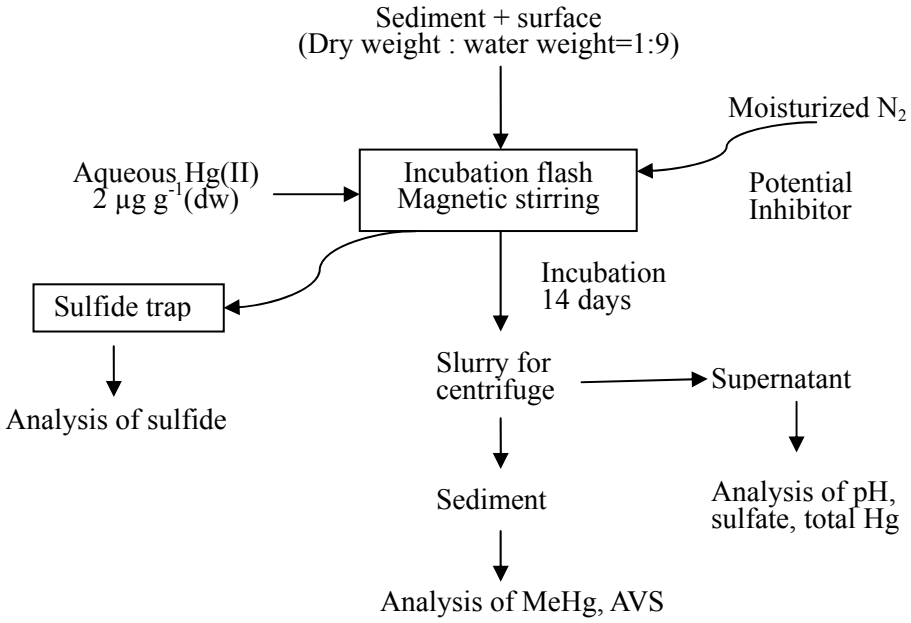

Figure 4.1 Experimental procedure for incubation experiments

After purging for half an hour to exclude oxygen from the system, the potential methylation-inhibitors were added into the slurry to a concentration of 0.25 mmol $(g\text{-}dw)^{-1}$ if soluble; otherwise the amended concentration was 0.5 mmol $(g\text{-}dw)^{-1}$. Subsequently, 1 mg mL^{-1} Hg(II) ($HgCl_2$ solution in 4.83% HNO_3) solution was spiked into the slurry for a final concentration of 2 μg (g-dw)-1. The Hg(II) solution was prepared by dissolving 0.1354 g $HgCl_2$ (99.9995%, Alfa Aesar) in DI water and 7 mL concentrated HNO_3 (trace metal grade) to a final volume of 100 mL in a volumetric flask. Experimental measurements showed that the pH of the sediment slurry decreased from 6.26 to 6.20 due to the addition of Hg(II) solution.

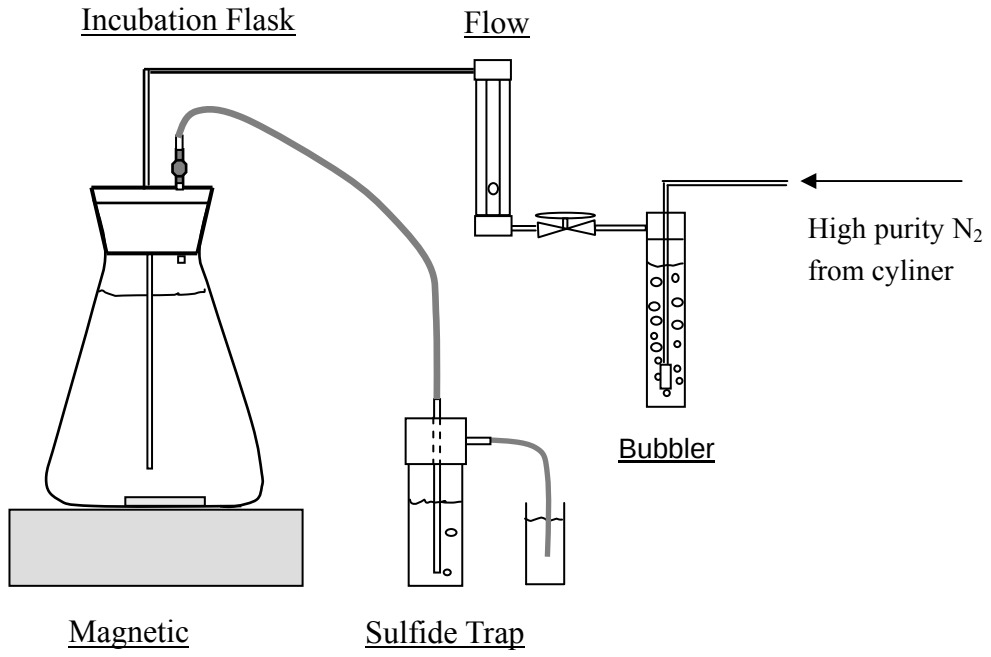

Figure 4.2 Experimental setup for incubation experiments

After incubation for 2 weeks, the slurry was removed and placed into 50 mL Teflon centrifuge tubes followed by coarse centrifugation. The supernatant was separated and filtered through 0.45 μm membrane filters (Whatman) prior to analysis for sulfate and THgD. The sediment obtained from coarse separation was frozen until analysis for MeHg. All processes involving sediment exposure were conducted using a glove box under N_2.

All the incubation experiments followed the same procedure except there was no potential inhibitor added to the slurry for the control experiments. The control was used to show how much MeHg was produced without addition of any potential inhibitors and thus show how effective the selected inhibitors inhibited Hg(II) methylation.

The experiments were conducted within 8 months after the collection of sediment and surface water. The inhibitor selection experiments were conducted in the first 3 months. Each batch of experiment took 14 days. The experiments were performed in the order shown in Fig. 4.6, control1, Fe^{2+}, MoO_4^{2-}, Fe_2O_3 and S^0. The experiments on effects of iron sulfides were conducted during the last 3 months. There were altogether 4 batches of experiments and included 3 different concentrations of CIS in the first two batches, and a control, 3 different concentrations of Syn-FeS in the last two batches. There was 2 months interval between experiments for inhibitor selection and the investigations focusing on iron sulfides. For all the incubation experiments, two replicates were run simultaneously.

4.1.4 Analytical Methods

The moisture content of the sediment was determined by overnight drying ~2.5 grams of sample at 105 ºC. Organic matter content was determined as weight loss on ignition (LOI) at 550

ºC for overnight of the 105 ºC dried sediment. The methods for analysis of MeHg and THg in sediments are shown in Section 3.1.3.

The moisture content of wet FeS was determined by weight change after drying under N_2 flow. The specific surface area of iron sulfides were measured following multipoint N_2-BET adsorption method (Autosorb-1, Quantachrome). Scanning electron microprobe (SEM) (Jeol 840A) was used to obtain SEM images of both CIS and Syn-FeS. In order to obtain a clear image, the sample was coated with pure gold dust for better conductivity. The major components of CIS and Syn-FeS were identified by XRPD spectra, obtained using a Bruker/Siemens D5000 automated powder X-ray diffractometer with CuKα radiation.

Acid volatile sulfide (AVS) in the sediment samples was converted to H_2S by adding 20 mL 6 M HCl to 15 mL suspension mixed with 85 mL deionized water to produce a final HCl concentration of 1 M. The evolved H_2S was purged from the sample and trapped in anti-oxidation reagent (AOR) followed by measurement using a sulfide ion selective electrode (ISE) (Oakton) coupled to a pH/mV meter (Brouwer and Murphy, 1994). Quantitative analysis was performed using a 4-point calibration curve with appreciate concentration span to cover the concentration of each collected sulfide sample ($R^2 \geq 0.999$ for the curve of potential~ natural logarithm of sulfide concentration). The recovery of a Na_2S standard following the same method as sediment samples for AVS measurement was 96.0%. Total free sulfide (mainly HS^- and H_2S) in supernatant and H_2S collected in the sulfide trap at the outlet of the incubation flask was also measured with ISE.

Sulfate in water and filtrates of the incubation slurry was determined by converting sulfate ions to a barium sulfate suspension and the resulting turbidity was measured using a HACH 2100AN turbidimeter following EPA method 9038. The quantitative analysis was performed using a 9-point calibration curve with 5 mg L^{-1} increments in the range of 0 to 40 mg L^{-1} ($R^2 \geq 0.9999$). The recovery of a prepared 14 mg L^{-1}standard was 101%.

Total dissolved mercury in the water portion from the slurry was measured based on EPA method 1631-Version E. The samples were preserved by adding pretested 0.5% (v:v) 12N HCl (Trace metal grade). Prior to analysis, all mercury in a sample aliquot was oxidized to Hg(II) with BrCl. After oxidation, the sample was sequentially reduced with $NH_2OH.HCl$ to destroy the free halogens, then reduced with $SnCl_2$ to convert Hg(II) to volatile Hg^0. Hg^0 was measured by using a duel gold trap-cold vapor atomic fluorescence spectrometry (CVAFS) analyzer (Tekran). The quantitative analysis was performed using a 5-point calibration curve ranging from 2 to 100 ng L^{-1}, a stable and accurate calibration was obtained (R^2 = 0.9999). The detection limit calculated as three times of the standard deviation of 15 reagent blanks was 0.82 ng L^{-1}.

4.2 Results and Discussion

4.2.1 Properties of Commercial Iron Sulfide and Synthetic Iron Sulfide

4.2.1.1 Commercial Iron Sulfide (CIS)

The original CIS obtained was composed of diverse sizes of particles (Fig. 4.3a). Before application, it was ground and sieved to less than 125 μm (mesh size). Its SEM image (Fig. 4.3b) was obtained at 250 times magnification using particles between 75-125 μm. The measured specific area of CIS was 1.7 $m^2 g^{-1}$.

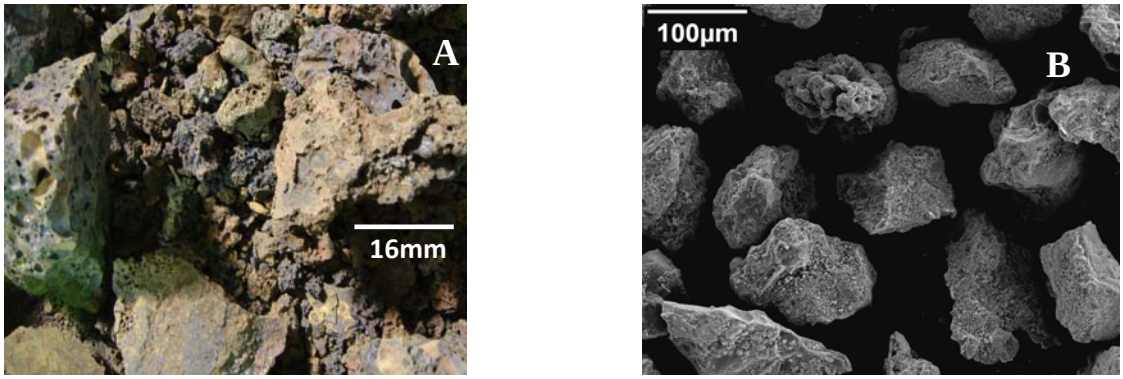

Figure 4.3 Images of (a) original commercial iron sulfide (CIS) obtained using a camera, (b) ground and screened (75-125 µm) CIS obtained by a JEOL 840A SEM at 250 × magnification.

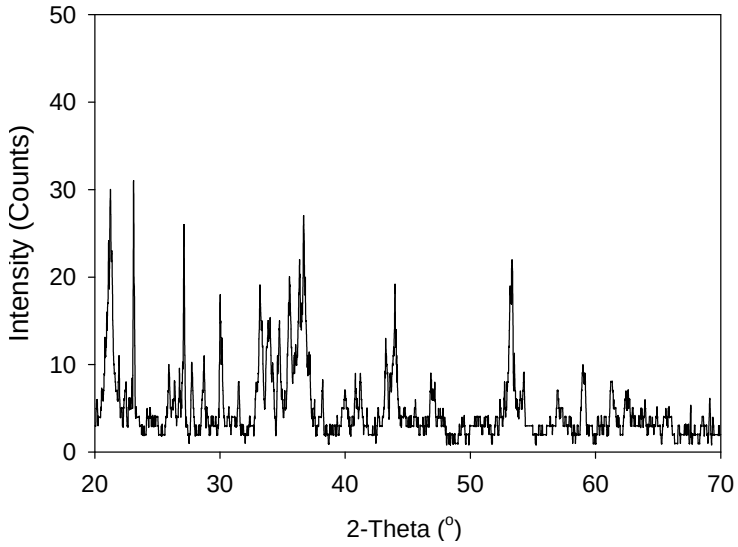

Figure 4.4 XRPD patter of commercial iron sulfide (CIS) obtained using a Bruker/Siemens D5000 automated powder X-ray diffractometer with Cu*K*a radiation.

Comparing the XRPD pattern (Fig. 4.4) of CIS to the standard patterns in the International Centre for Diffraction Data (ICDD) database, with the assistance of XRD pattern processing software (MDI Jade version 6.1), CIS was actually a complicated mixture of iron sulfides, hydrated iron oxide (FeOOH) , iron oxide (Fe_2O_3), elemental sulfur (S^0) and iron

sulfates (including hydrates). This mixture was the result of the oxidation of FeS. The oxidation occured mainly during its production and storage before arrival to the laboratory. In the presence of water, FeS was oxidized to FeOOH and S^0 (Eq. 4.1) and S^0 could be further oxidized to sulfate (Eq. 4.2). During the oxidation of FeS in the presence of water, H^+ ions were released (Burton et al., 2006).

$$FeS + 3/4H_2O + 1/2O_2 = FeOOH + S^0 \quad (4.1)$$

$$S^0 + H_2O + 3/2O_2 \rightarrow SO_4^{2-} + 2H^+ \quad (4.2)$$

The overall reaction

$$FeS + \frac{9}{4}O_2 + \frac{3}{2}H_2O \rightarrow FeOOH_{(s)} + 2H^+ + SO_4^{2-} \quad (4.3)$$

The iron sulfides in CIS included Mackinawite (FeS), Greigite (Fe_3S_4), Pyrrhotite ($_{Fe1-x}S$, mainly in form Fe_7S_8) and Pyrite (FeS_2). Greigite, pyrrhotite, and pyrite are products of FeS oxidation when water is not involved in the oxidation reactions (Berner, 1970; Rickard and Morse, 2005). Greigite and pyhhorite have been shown to contain mixed Fe(II) and Fe(III) valence states (Vaughan and Tossell, 1981; Pratt et al., 1994), formed from the oxidation of Mackinawite.

4.2.1.2 Synthetic Iron Sulfide (Syn-FeS)

The freshly prepared FeS was black in color. The specific surface area of the dried FeS measured by N_2-BET method was 7.8 $m^2\ g^{-1}$. The measured specific surface area of FeS (mackinawite) varies broadly (7 to 47 $m^2\ g^{-1}$) (Wolthers et al., 2003) as determined by the N_2-BET method. Fig. 4.5 shows the SEM image of the N_2-dried FeS particles. The image of FeS in

Fig. 5b fits the description as noted by others (Coles et al., 2000). Previous studies (Rickard et al., 2006) have demonstrated that the primary FeS precipitate formed from the reaction between Fe(II) and S(-II) in aqueous solutions at ambient temperatures and pressures is nanoparticulate stoichiometric mackinawite, $Fe_{1.00 \pm 0.01}S$, thus the prepared FeS should be mackinawite.

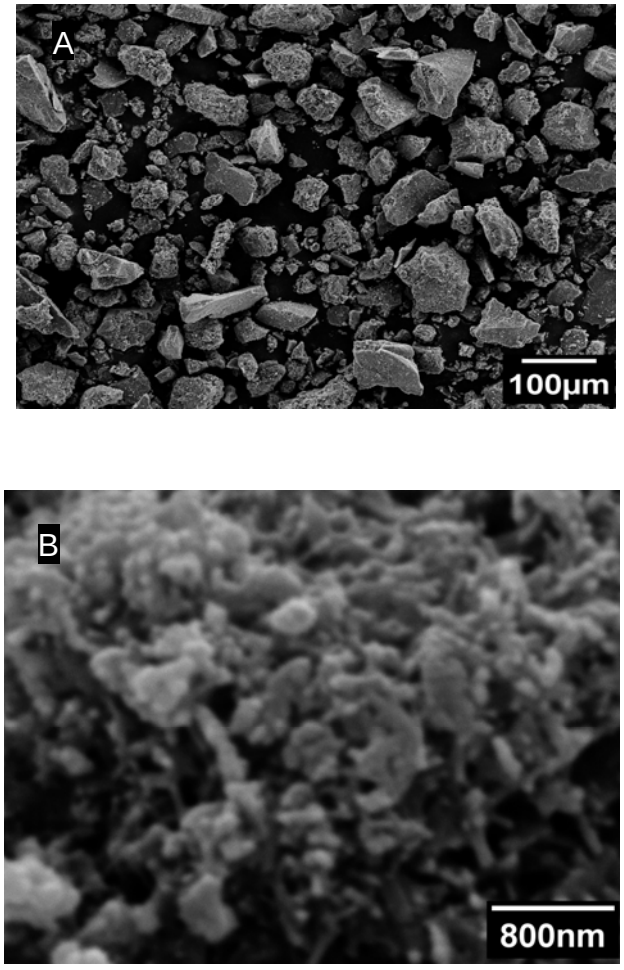

Figure 4.5 Images of laboratory prepared FeS by a JEOL 840A scanning electron microscope obtained at (a) 150 × magnification and (b) 30,000 × magnification.

The identity of the Syn-FeS was further confirmed by the XRPD pattern of the synthetic FeS shown in Fig. 5.7 of Chapter 5 for comparison with the pattern of the sample after sorption

of Hg(II). It was concluded that because of the nanoparticulate nature of FeS, XRPD methods routinely used to examine FeS give no pattern or show a broad peak at 5Å (17.6˚ 2θ) (Rickard and Morse, 2005). Consistent with this conclusion, the observed XRPD pattern of the Syn-FeS showed broad peaks with very low intensities. The broad peaks around 17.6˚ 2θ are indicative of FeS, with intensities and positions in reasonable agreement with peaks previously reported in the conventional XRPD pattern for FeS (Wolthers et al., 2003).

4.2.2 Sediment Properties

The collected sediment from Henderson Lake was neutral in pH (Table 4.1) and contained 26.3% solid and 2.88% organic matter (11.0% of the dry sediment). Sulfate was 175 μM in the collected surface water, which was in the low concentration range (10-300 μM) in the lake water (Suplee and Cotner, 2002). Total Hg was 84.4 μmol $(g\text{-}dw)^{-1}$ and the calculated MeHg/HgT ratio was 0.82%. The properties of the collected sediment are summarized in Table 4.1.

Table 4.1 Summary of sediment characterization

	pH of pore water	Solid %	Sulfate in sediment μmol $(g\text{-}dw)^{-1}$	THg ng $(g\text{-}dw)^{-1}$	AVS μmol $(g\text{-}dw)^{-1}$
Avg ± STD	6.84 ± 0.12	26.3 ± 0.08	8.10 ± 0.53	84.4 ± 4.9	30.4 ± 0.4
	pH of surface water	Organic Matter %	Sulfate in surface water, μM	MeHg ng $(g\text{-}dw)^{-1}$	
Avg ± STD	7.25 ± 0.02	2.88 ± 0.04	175 ± 0.0	0.69 ± 0.03	

dw: dry weight; STD: standard deviation from two replicates; AVS: acid volatile sulfide.

4.2.3 Effects of Selected Chemicals on Inhibition of Mercury Methylation

Based on the observations of the negative correlation between MeHg in sediment and sulfide in pore water (Benoit et al., 1999), the amendment of iron sulfide into the sediment slurry

should be able to inhibit the methylation of Hg(II) by creating a sulfidic condition. Studies have shown that the addition of Fe^{2+} into sediment slurry reduced the net rate of mercury methylation (Mehrotra and Sedlak, 2005). It is reported that the methylation of Hg(II) was suppressed under iron-reducing conditions (Warner et al., 2003). Based on these observations, we surmised that the amendment of either iron sulfides, Fe^{2+} or Fe_2O_3 into anoxic surface sediments should be able to inhibit the methylation of Hg(II).

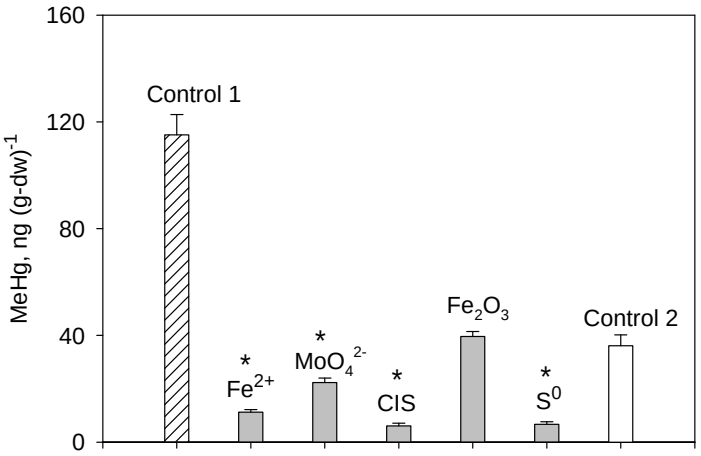

Figure 4.6 MeHg in slurry after amendment of selected inorganics.

For soluble Fe^{2+} and MoO_4^{2-}, the amended concentration was 0.25 mmol $(g\text{-}dw)^{-1}$. For CIS, Fe_2O_3 and S^0, which has very low solubility, amended concentration was 0.5 mmol $(g\text{-}dw)^{-1}$. For CIS, the concentration was nominal and calculated by assuming it had the same molecular weight as FeS. Control 1 was performed 1 week after sediment collection and control 2 was performed at about 7 months after sediment collection. Error bars represent the standard error from duplicate incubation. The asterisk (*) indicates a significant difference between the treatment and control 2 at $p < 0.05$

Elemental sulfur forms Hg(II)-polysulfides with Hg(II) and thus enhance the solubility of Hg(II) (Marvin-Dipasquale and Oremland, 1998), but to our knowledge, its effects on Hg(II) methylation has not been reported. If HgS0 is the dominant neutral mercury complex available

for methylation in sulfidic sediments (Benoit et al., 2001), the formation of charged Hg-disulfide complexes may inhibit the Hg(II) methylation. Thus, the amendment of S^0 should be able to reduce the net production of MeHg.

Therefore, Fe^{2+} (added as $FeCl_2.4H_2O$), molybdate (added as $Na_2MO_4.2H_2O$) (the well known methylation inhibitor of Hg(II)), iron sulfides, Fe_2O_3 and S^0 were selected as the potential methylation inhibitors and respectively amended into sediment slurry of incubation experiments. Considering availability, applicability and cost for possible capping application, an economical commercial iron sulfide (CIS) was selected as an amendment.

For soluble $FeCl_2.4H_2O$ or $Na_2MO_4.2H_2O$, an amendment concentration of 0.25 mmol $(g\text{-}dw)^{-1}$ was added to the sediment slurry; while for insoluble CIS, Fe_2O_3 or S^0, a concentration of 0.50 mmol (g-dw)-1 was applied. It should be noted that it was assumed CIS had the same molecular weight as FeS when weighing. Since MeHg produced in control 2 (performed 7 months after the collection of the sediment) was significantly lower than that in control 1 (performed 7 days after the collection of the sediment), time had a potential influence on net MeHg produced in the controls (Figure 4.6). If the decrease in MeHg production was significant compared to control 2, it was significant to control 1. Therefore, statistic comparison was made between the treatment and control 2. Compared to control 2, significant decrease of MeHg production occurred following treatment with either Fe^{2+}, MoO_4^{2-}, CIS or S^0 ($P < 0.05$). Commercial iron sulfide (CIS) and S^0 were the most effective in inhibition of methylation of the spiked Hg(II). MeHg produced in the presence of CIS was 6.1 ng $(g\text{-}dw)^{-1}$(performed 2 months after the collection of the sediment), which was only 5.3% of the 115.2 ng $(g\text{-}dw)^{-1}$ produced in

control 1 and 17% of the 36.1 ng (g-dw)$^{-1}$ produced in control 2. With S^0 amendment, MeHg production was 6.7 (g-dw)$^{-1}$. For reasons unclear, when S^0 was amended, H_2S produced (trapped in the outlet bottle) was 50 times greater than that produced when amended with CIS. Also because iron sulfides are good at binding mercury, organism, iron sulfide was selected for further investigation. Ferrous iron (Fe^{2+}) also effectively suppressed the net production of MeHg and Fe_2O_3 did not show significant inhibiting effects compared to control 2. In this study, either Fe^{2+}, CIS or S^0 appeared more effective on inhibition of Hg(II) methylation than molybdate, a widely accepted inhibitor for mercury methylation.

4.2.4 Inhibition of Mercury Methylation by CIS and Syn-FeS

CIS was first evaluated as a potential inhibitor for the incubation experiments. Since CIS is a mixture of FeS and its oxidation products, FeS (Mackniwite) was synthesized in the laboratory to investigate the effectiveness of FeS on the inhibition of Hg(II) methylation. The amendment concentration at 0.17, 0.50, and 1.5 mmol (g-dw)$^{-1}$ was respectively applied for either CIS or Syn-FeS. These concentrations were selected such that each higher concentration was three times of the lower concentration. In other words, 0.50 mmol (g-dw)$^{-1}$ is three times that of 0.17 mmol (g-dw)$^{-1}$ and 1.5 mmol (g-dw)$^{-1}$ is three times of 0.50 (g-dw)$^{-1}$. With amendment concentration 1.5 mmol (g-dw)$^{-1}$ for Syn-FeS, the incubation slurry could not be separated into the clear supernatant and sediment phases by centrifuge. As a result, at this concentration, data for Syn-FeS was not available in Fig. 4.7, 4.8, and 4.9.

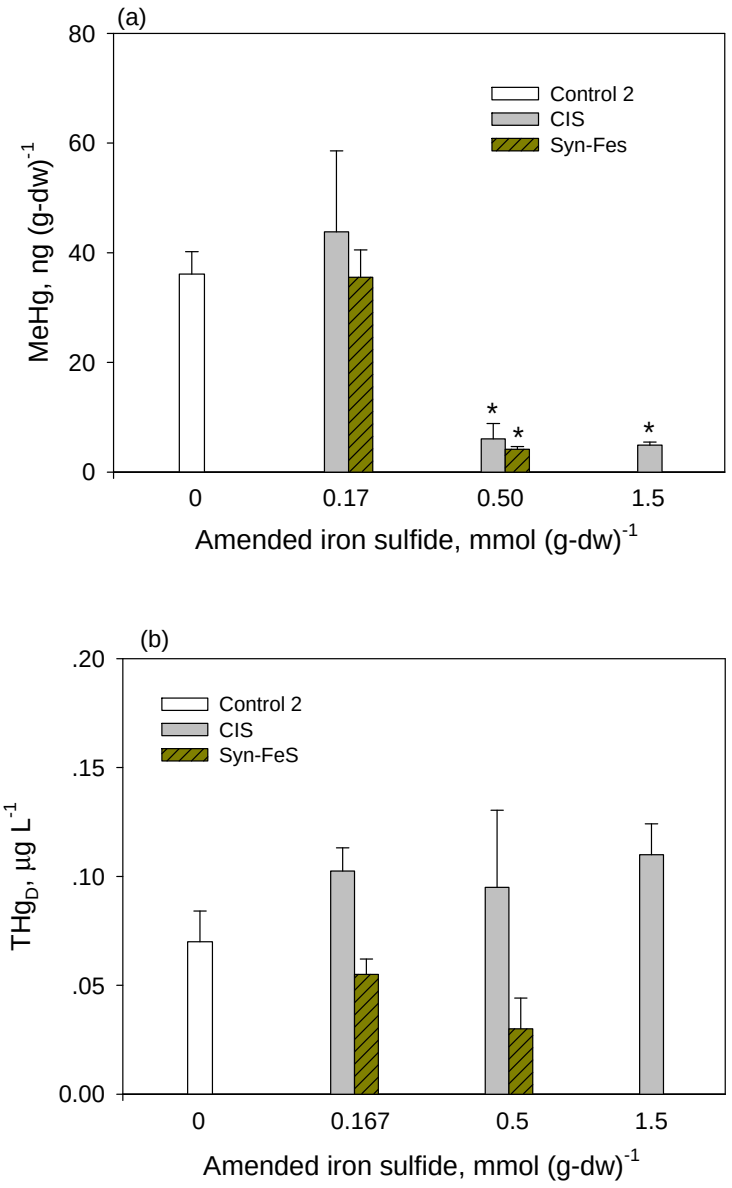

Figure 4.7 MeHg in sediment (a) and THg in supernatant (b) with amendment of iron sulfides. For CIS, the molecular concentrations were nominal and calculated by assuming it had the same molecular weight as FeS. Error bars represent the standard error from duplicate incubation. The asterisk (*) indicates a significant difference between the treatment and control 2 at $p < 0.05$.

When amendment concentration of either CIS or Syn-FeS was increased to 0.50 mmol $(g\text{-}dw)^{-1}$ (Figure 4.7a), MeHg produced significantly decreased compared to control 2 ($P < 0.05$). When the treatment concentration was 0.17 mmol $(g\text{-}dw)^{-1}$, there was no significant change of

MeHg production as compared to control 2. At equivalent amendment concentrations, Syn-FeS was as effective as the partially oxidized CIS as an inhibitor of Hg(II) methylation. With the increase in the amended concentrations, THgD in the slurry decreased for Syn-FeS and increased for CIS at $P < 0.1$, however there was no significant change at $P < 0.05$. The change of THgD in the water however was not as significant as the decrease of MeHg in the sediment slurries (Figure 4.7b).

With increase in concentrations of added CIS or Syn-FeS (Figure 4.8a), pH decreased ($P < 0.05$). For Syn-FeS, at treatment concentration of 0.50 mmol $(g\text{-}dw)^{-1}$, pH in the system was very close to the pH for treatment concentration at 0.17 mmol $(g\text{-}dw)^{-1}$. Both were slightly lower than the pH in the control 2. The pH decrease was possibly due to the release of H^+ in the sorption of Hg(II) by FeS, which was observed and explained in Section 5.2.3. For CIS, the pH decrease was greater than for Syn-FeS and was largely due to oxidation before the experiments began. In addition, small amount of H^+ was likely release from the sorption process. Sulfate in the supernatants increased with the increase in added concentrations of CIS and Syn-FeS. With an added concentration of 0.50 mmol $(g\text{-}dw)^{-1}$, sulfate was 4 times greater than control 2 for CIS and 2 times greater than control 2 for Syn-FeS. For CIS, increased sulfate concentration in the supernatant was most likely due to the production of sulfate as result of its oxidation before arrival to the laboratory. For Syn-FeS, increased sulfate could be a carry over from the reactant ($FeSO_4.(NH_4)_2(SO_4)_2\ .6H_2O$) during FeS preparation. A small portion would also be from FeS oxidation during handling and incubation experiments.

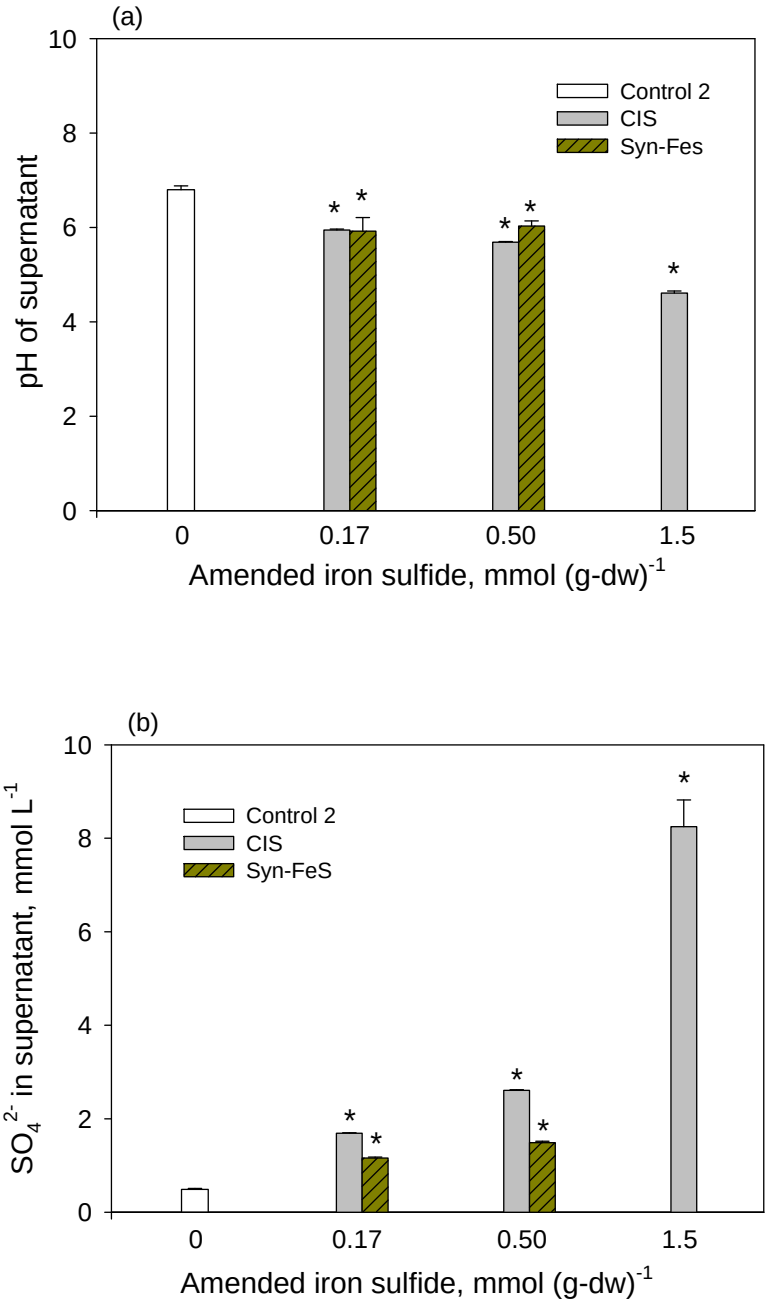

Figure 4.8 pH (a) and sulfate (b) in the supernatants with amendment of iron sulfides.

For CIS, the molecular concentrations were nominal and calculated by assuming it had the same molecular weight as FeS. Error bars represent the standard error from duplicate incubation. The asterisk (*) indicates a significant difference between the treatment and control 2 at $p < 0.05$

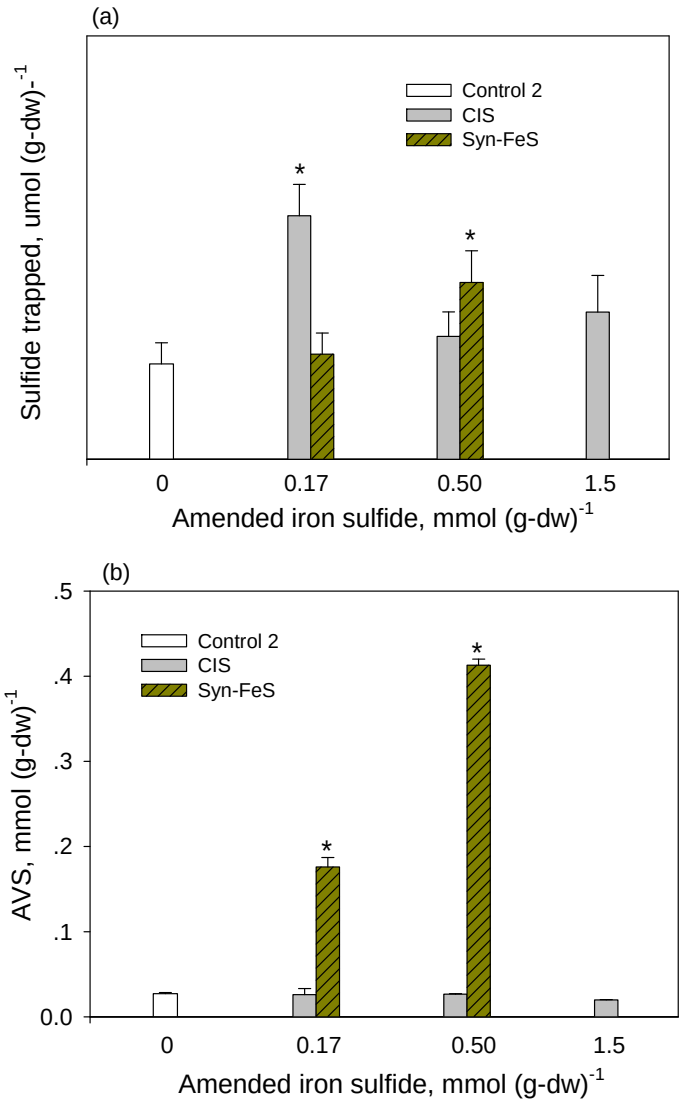

Figure 4.9 H_2S production (a) and acid volatile sulfide (AVS) in the slurry (b) with amendment of iron sulfides.

For CIS, the molecular concentrations were nominal and calculated by assuming it had the same molecular weight as FeS. Error bars represent the standard error from duplicate incubation. The asterisk (*) indicates a significant difference between the treatment and control 2 at $p < 0.05$

With iron sulfide addition, H_2S trapped in AOR increased during incubation (Fig. 4.9a). H_2S is toxic to aquatic organisms (Brouwer and Murphy, 1995). The increase in H_2S production

was likely a result of pH decrease in the slurries amended with iron sulfides. At lower pH, solubility of iron sulfide increases (Davison, 1991) and more dissolved sulfides are in the form of H_2S (Wang and Chapman, 1999). Log k_{a1} = -7.02 for $H_2S = H^+ + HS^-$ (Technology, 1997). The H_2S produced was less than 1 fold greater than control 2 for either CIS or Syn-FeS.

The amount of AVS in the sediment slurry after addition of 1M HCl is shown in Fig. 4.9b. With addition of Syn-FeS, the recovered AVS was proportional to the amended amounts and the recovery was about 80%. For CIS, there was no apparent change in recovered AVS as compared to the control.

To explain the difference between Syn-FeS and CIS in 1 hr AVS recovery from the amended sediments, AVS produced from Syn-FeS and CIS, was measured respectively using the test method for AVS. Wet Syn-FeS dissolved rapidly and the recovered H_2S was about 0.9 moles per mole Syn-FeS in 1 hr. Because Syn-FeS contained clusters of nanoparticles, it dispersed quickly under magnetic stirring and the reaction rate was very rapid. While for CIS, the recovered H_2S was 0.031 moles in 1 hr, 0.196 moles in 29 hrs and 0.247 moles in 70 hrs per mole CIS (nominal mole, assuming CIS in the form of FeS when weighing). Approaching 70 hours, recovered H_2S did not increase with time and the evolution reaction was close to completion. CIS particles (≤ 125 μm) were tightly packed and dispensed very slowly under magnetic stirring during incubation. Therefore, one reason for the low AVS recovery (Fig. 6b) is likely due to the low reaction rate between CIS and 1 M HCl controlled by the mass transfer rate in CIS particles. Another likely reason for the low recovery is that CIS is a mixture of many sulfur species, such as sulfates, elemental sulfur, goethite and iron sulfides. The iron sulfides in

CIS exist in many forms and some of them release less H_2S during acid evolution, such as pyrite which is conventionally not considered as the component of AVS in sediments (Rickard and Morse, 2005).

4.2.5 Discussion

Probably due to the decrease in activity of sulfate reducing bacteria, caused by the decomposition of organic matter during storage, MeHg produced in Control 2 (performed 7 months after sediment collection) was lower than that in Control 1 (performed 7 days after sediment collection). When compared to both Control 1 and Control 2, CIS or Syn-FeS amendment resulted in less MeHg production. Thus, both CIS and Syn-FeS was shown to effectively inhibit the transformation of Hg(II) to MeHg.

4.2.5.1 Total Dissolved Hg and Dissolution of Iron Sulfides in Syn-FeS and CIS

The solubility of FeS can be described by a pH-dependent reaction and a pH-independent reaction (Rickard, 2006). Since S^{2-} is found in no significant concentration in most aqueous solutions, the pH-dependent dissolution reaction of FeS can be conventionally represented by the bisulfide reaction, $FeS + H^+ = Fe^{2+} + HS^-$, with log Ksp = -3.00 ± 0.12 (Davison, 1991). Under acidic to neutral conditions, it is predominantly a pH-dependent reaction.

With increase in added concentrations of iron sulfides, the pH of the system decreased monotonically from neutral to slightly acidic (Fig. 4.8a). Under these conditions, bisulfide HS^- are produced by the dissolution of FeS. The dissolution of components in CIS such as Greigite (Fe_3S_4), Pyrrhotite ($Fe_{1-x}S$) and Pyrite (FeS_2) also produces bisulfide. The oxidation products of FeS, iron sulfides in CIS such as greigite and pyhhorite contain mixed Fe(II) and Fe(III)

(Vaughan and Tossell, 1981; Pratt et al., 1994) and pyrite contains S with oxidation state -1. Because of their special valence states, redox reactions are involved in the dissolution of the iron sulfides and HS^- and S^0 are produced. For example, the dissolution reaction of pyrite can be represented by $FeS_2 + H^+ = Fe^{2+} + HS^- + S^0$, with log Ksp = -16.4 (Rickard and Morse, 2005).

HS^- alone or together with S^0 can react with HgS^0 to form dissolved Hg-polysulfide complexes, which increases the solubility of HgS(s) (Paquette and Helz, 1997; Fabbri et al., 2001). Via precipitation reaction and adsorption to the added iron sulfides, concentration of dissolved Hg(II) in pore water is expected to be less than control. Due to increased dissolution of HgS(s) via the formation of Hg(II)-polysulfides, THgD concentrations in the slurries may not decrease correspondingly. This explains the non-significant change in THgD level for Syn-FeS or CIS addition, with increases in amended concentrations (Fig. 4.7b).

4.2.5.2 Inhibition of Hg(II) Methylation by Syn-FeS and CIS

It has also been proposed that the availability of Hg(II) for methylation is controlled by the concentration of neutral dissolved Hg complexes rather than Hg^{2+} or total dissolved Hg (THgD) (Benoit et al., 2001). This is consistent with the observation from this study that the amount of MeHg produced is not correlated to the THgD in the slurry water phase. Benoit et al. also proposed that HgS^0 is possibly the dominant neutral mercury complex available for methylation in sulfidic sediments, because HgS^0 is easily available for microbial methylation since it more readily diffuses across cell membranes compared to disulfide complexes (Benoit et al., 1999). Therefore, the inhibition effects following amendment with Syn-FeS is likely due to the lowered neutral mercury complexes (manily HgS^0) by formation of charged Hg-polysulfide

complexes in pore water between SH^- and HgS^0. This also explain why amended S^0 effectively inhibited Hg(II) methylation in the experiments of inhibitor selection (Fig. 4.6).

The commercial iron sulfide (CIS) used in this study was a mixture of the oxidation products of FeS, composed mainly of iron sulfide species, S^0, Fe_2O_3, FeOOH and some sulfates. Based on the experimental results and discussion in the last paragraphs, iron sulfide species and S^0 contribute to the inhibition of Hg(II) methyaltion probably by the reduction of bioavailable neutral mercury complexes, via formation of charged Hg-polysulfide complexes from HS^-, HgS^0 and S^0. With the CIS amendment, a iron-reducing condition was created by the introduction of Fe(III) in Fe_2O_3, FeOOH and some iron sulfide speices. From the inhibitor selection experiments, the iron-reducing conditions introduced by amendment of Fe_2O_3 did not significantly simulate or inhibit the Hg(II) methylation. Recent study has showed reduction of Fe(III) in FeOOH can oxidize S(-II) to form S^0 and then form Hg(II)-polysulfides that can subsequently facilitate the dissolution of HgS(s) (Slowey and Brown, 2007). If mainly HgS^0 is bioavailable for methylation, FeOOH found in CIS may also indirectly contribute to the inhibition of Hg(II) methylation by formation of charged Hg(II)-polysulfides.

4.2.5.3 Activity of Sulfate Reducing Bacteria And Amendment of Syn-FeS and CIS

The formation of MeHg is influenced by the supply of bioavailable Hg(II) and/or activity of methylating bacteria. Thus, the decrease in activity of the methylating bacteria might be another cause for the suppressed methylation of Hg(II) following CIS or Syn-FeS amendment. The toxicity of sulfides to the organism is generally related to H_2S instead of total sulfide (Brouwer and Murphy, 1995; Vismann, 1996). During the incubation experiments in this study,

H_2S was continuously removed from the incubation slurry by purging with N_2 and collected in the outlet bottle containing AOR. The total free sulfide measured in the supernatant was below the method detection limit using ISE (3 μM). The total free sulfide included HS^- and H_2S because S^{2-} exists only under basic conditions and is never a dominant species (Wang and Chapman, 1999). Also, with amendment of Syn-FeS at 0.50 mmol $(g\text{-}dw)^{-1}$, collected H_2S in the outlet bottle was less than 2 times in control 2. At this amendment concentration, the amount of collected H_2S was not significantly different between the CIS treatment and control 2 ($P < 0.05$) (Fig. 4.9a). Based on these observations, there was no evidence shown that the CIS or Syn-FeS amendment lowered the activity of the mathylating bacteria. However, to determine if the inhibition of Hg(II) methylation was related to the decrease in activity of sulfate reducing bacteria, it would be necessary to monitor the activity of these bacteria in slurry amended with iron sulfides, which was outsides the scope of this study.

4.3 Summary

The amendment of iron sulfides into sediment slurries can greatly inhibit the formation of MeHg. The effectiveness of the CIS indicates that other species of iron sulfides also worked effectively in the inhibition of Hg(II) methylation. The oxidation of FeS does not significantly reduce its effectiveness regarding the inhibition of Hg(II) methylation. Thus, it should be possible to reduce the MeHg concentration in the surface sediments by placing a layer of iron sulfides between the mercury contaminated sediments and a layer of conventional sand cap, even if the oxidation of FeS occurs.

Chapter 5 Immobilization of Aqueous Hg(II) by Iron Sulfides

5.1 Material and Methods

Chemicals used in this work were analytical grade or plus. Deionized water was produced from a Corning Mega Purification System (15.0 MΩ). Glassware and Teflon tubes were soaked in 4 M HCl for at least 24 hours before rinsing with DI water and drying for use.

5.1.1 Preparation and Characterization of FeS

Wet FeS was prepared from $FeSO_4.(NH_4)_2(SO_4)_2.6H_2O$ (Mohr's salt) and $Na_2S.9H_2O$ at room temperature (24˚C) using the method described in Chapter 4. After rinsed with DI water for 3 times, FeS was dried under N_2 flow. The dried FeS was placed in 1.5 ml vials and preserved under N_2 flow in a 500 ml flask.

As stated in Chapter 4, the specific surface area of N_2-dried FeS was measured following the multipoint N_2-BET adsorption method and SEM images were obtained using Scanning Electron Microprobe (SEM). The major components of the synthetic material before and after sorption were identified by XRPD spectra, obtained using a Bruker/Siemens D5000 automated powder X-ray diffractometer with Cu$K\alpha$ radiation.

5.1.2 Experimental Design and Procedure

A 5 mM Hg(II) stock solution was prepared by dissolving $HgCl_2$ (99.9995%, Alfa Aesar) in 32 mM HNO_3 solution (trace metal grade concentrated HNO_3 dissolved in deionized water). This stock solution was stored in a PTFE bottle for later experiments. Except for the experiments to test the capacity of FeS to retain mercury, a final concentration of 0.4 g L^{-1} of FeS was applied.

The pH of the initial mercury solutions before FeS addition was adjusted to 5.6 with the exception of experiments determing pH effects on mercury retention. The sorption vessels were sealed with a rubber stopper containing inlet and outlet holes. N_2 was maintained in the head space of the vessels during the experiments in order to maintain anaerobic conditions.

For the dynamic experiments used to determine retention rates, samples were retrieved in specific time intervals. Samples were filtered through 0.45 μm PTFE syringe filters (Whatman) in order to minimize the delay between sampling and separation. Filtration was completed within 30 seconds after sampling.

The equilibrium experiments were conducted using either 50 ml glass centrifuge tubes or 500 ml glass flasks depending on the required volumes of relative experiments. Hg(II) solutions of designated concentrations were prepared by diluting the 5 mM stock solution with deionized water, and pH of the solutions was adjusted using 0.2 M NaOH. After purging for half an hour to exclude oxygen from the system, FeS was added into the solution. Magnetic stirring by a PTFE stirrer bar was used to maintain the homogeneity of the suspension. After 24 hours, the suspension was filtered using a glass vacuum filtration unit using 0.45 μm nitrocellulose membrane (Fisher Science). No significant adsorption of mercury to the membrane was detected.

The aeration experiments were conducted following a procedure similar to that of the equilibrium experiments during the first 24 hours. After purging for 24 hours with N_2, the purge gas was switched to compressed air with an approximate flow rate of 50 ml min^{-1}.

5.1.3 Analytical Methods

All filtrates were preserved with concentrated HNO_3 to pH less than 2 before analyzing for mercury. Because HgS is completely soluble in aqua regia (Mikac et al., 2002), the retained solid samples from the filtration were digested together with the filter membrane in 10 ml aqua regia (2.5 ml concentrated HCl mixed with 7.5 ml HNO_3). No mercury was detected from the digested blank filter membrane. The recovery of mercury by this method was 98 ± 2.6% (n = 14). After settling within 48 hours, both the retained solid and the membrane itself were dissolved completely without any visible suspension. The oxidized mercury was reduced to volatile elemental form by addition of stannous chloride and quantitatively measured by CVAAS (Mercury Instruments, LabAnalyzer 254). The qualitative analysis was performed using a 7-point calibration curve ranging from 0 to 1.2 μg L^{-1}, a stable and accurate calibration was obtained (R^2 ≥ 0.999).

pH was measured using a combination electrode (Sensorex) coupled to a pH meter (Jenco Model 60). Analysis of total iron in filtrates was performed using ICP-MS (Perkin Elmer Sciex, Elan 9000).

FeS was estimated using the method for AVS measurement. FeS was converted to H_2S by adding 20 ml 6 M HCl to 15 ml suspension mixed with 85 ml deionized water to produce a final HCl concentration of 1 M (Allen et al., 1993). The evolved H_2S was purged from the sample and trapped in an anti-oxidation buffer followed by measurement using a sulfide ion selective electrode (Oakton) (Brouwer and Murphy, 1994).

5.2 Results and Discussion

5.2.1 Dynamic Sorption

These experiments were designed to investigate the sorption rate of Hg(II) onto the synthetic FeS and help determine the time for the sorption process to reach an approximate equilibrium. For these experiments, 0.4 g L^{-1} FeS and Hg(II) solution with an initial pH 5.6 was applied. From Fig. 5.1, within 3 minutes after FeS addition, more than a half of the initial Hg(II) is removed from the aqueous phase, with 99.99% Hg(II) removed within 20 minutes. This confirmed that a period of 24 hours should be sufficient for the suspension to reach equilibrium. Base on this observation, a period of 24 hours was chosen for the following equilibrium experiments.

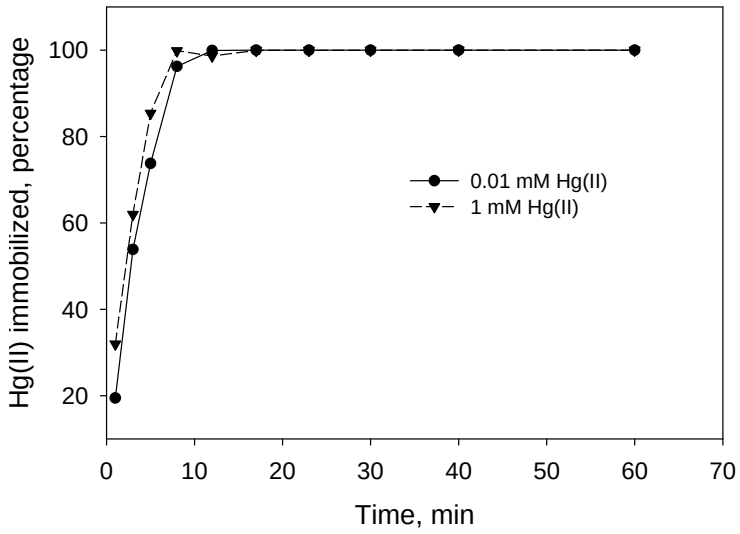

Figure 5.1 Dynamic Hg(II) sorption by FeS
Added FeS 0.4 g L^{-1}; Initial pH of Hg(II) solutions 5.6. The legends in the figure represent the initial Hg(II) concentrations before FeS addition.

5.2.2 Initial, Equilibrium pH and Hg(II) Immobilization

When 0.4 g L^{-1} (4.55 mM L^{-1}) FeS is added to a 1 mM Hg(II) solution, the Hg(II) loaded to FeS is 0.22 mol (mol FeS) $^{-1}$. Fig. 5.2a shows the relation between the initial pH of solutions before FeS addition and the equilibrium pH of the suspensions 24 hours after FeS addition, for 0.01, 0.1 and 1 mM initial Hg(II) concentrations respectively. Although the equilibrium pH increased with increase in initial pH of the Hg(II) solutions, the relationship was not proportional. When the initial pH increased from 3 to 8, the equilibrium pH increases approximately from 6 to 7. When the equilibrium pH exceeded 7, the data tended to be linear. This phenomenon can be explained by the dissolution of FeS. The solubility of FeS is described by a pH-dependent reaction and a pH-independent reaction. The pH-dependent dissolution reaction can be represented by $FeS + 2H^+ = Fe^{2+} + H_2S$, with $\log Ksp^* = -3.6$ (Davison, 1991). The pH-independent dissolution reaction involves the formation of the aqueous FeS cluster complex and can be represented by $FeS = FeS^0$, with $\log K_0(FeS) = -5.7$ (Rickard, 2006).

Under acidic conditions, it is predominantly a pH-dependent reaction. The dissolution of FeS consumes hydrogen ions thus increases the pH of the suspension, which explains the "pH buffering effect" of FeS at lower initial pH shown in Fig. 5.2a. Under alkaline conditions, it becomes a pH-independent dissolution and the solubility of FeS is much lower than its solubility under acidic conditions. Thus the equilibrium pH tends to be proportional to the initial pH. The overall tendency is that FeS solubility decreases with increasing pH. Fig. 5.2c shows the relation between unreacted FeS and suspension pH, which was obtained by modeling using MINTEQA2. The equilibrium constant used for mackniwite was 3.6 and the reaction between

FeS and Hg(II) was assumed via precipitation for cases when Hg(II) is present. When Hg(II)/Fe ≤ 0.22, no significant loss of FeS from dissolution would occur if the initial pH of Hg(II) solutions is close to neutral.

Under acidic conditions, solubility of FeS increases rapidly with decrease in pH of the suspension When the initial pH was around 2.5 (equilibrium pH < 5), apparent loss of FeS was observed in the suspensions. This is consistent with the modeling results shown in Fig. 5.2c. Because of the loss of FeS from dissolution under low pH as expected, the sorption of Hg(II) decreases (Fig. 5.2b, two data points shown at lower pH were due to this reason). Further experiments with lower initial pH were not performed due to significant loss of FeS particles. When equilibrium pH > 5.5, mercury in the aqueous phase increased with equilibrium pH. The same relatioship was observed for experiments with initial mercury concentrations of 0.01, 0.1 and 1 mM. It appeared that, at the same equilibrium pH, the mercury concentration in the aqueous phase was not apparently related to the initial concentration in the solution and the amount of mercury removed in the concentration range investigated. This was likely due to the increased dissolution of FeS nanoparticles at higher pH. It was observed that FeS was better dispersed and the suspension became darker with increase in pH. When the equilibrium pH was greater than 7.2, colorless filtrates was not obtained when filtered through a 0.45 μm membrane filter. The filtrates became darker with increase in pH, suggesting that more FeS passed through the membrane.

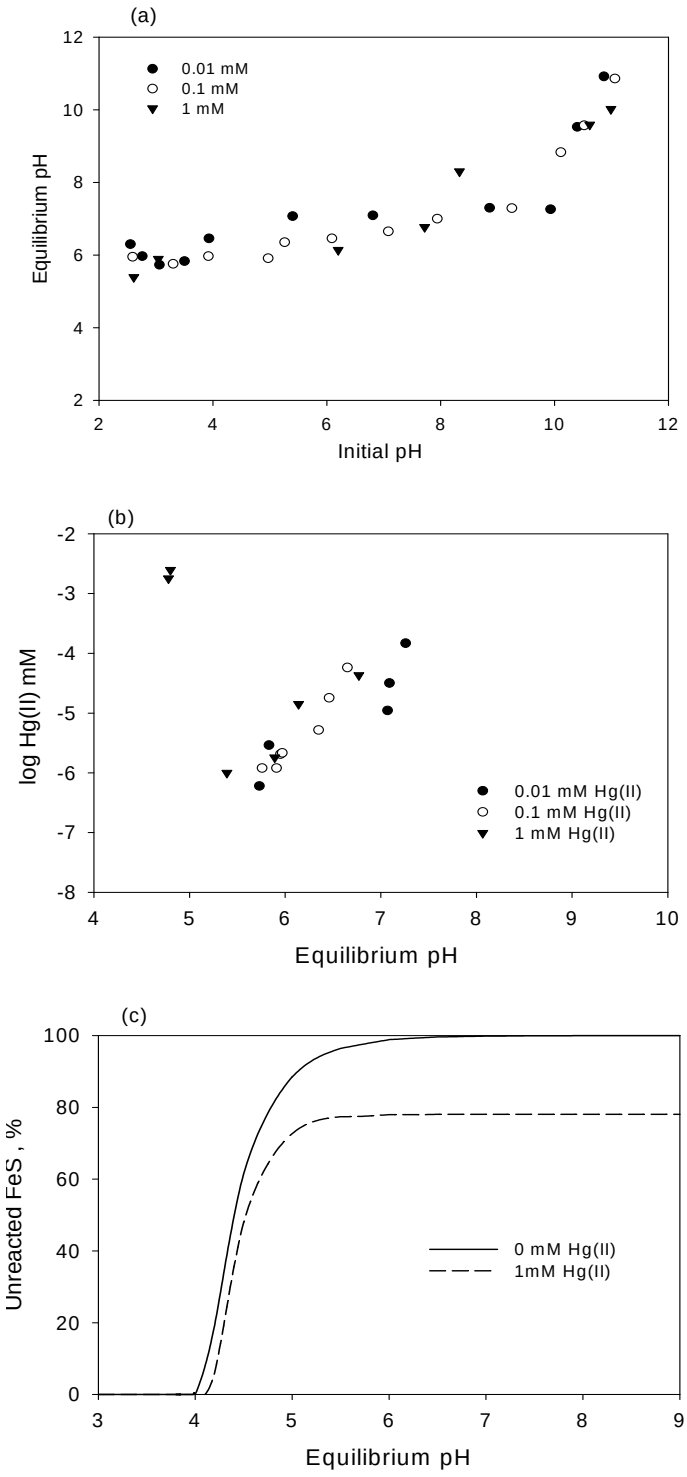

Figure 5.2 pH and the immobilization of Hg(II). FeS added 0.4 g L^{-1}
(a) Relation between equilibrium pH, 24 hours after FeS addition, and initial pH of Hg(II) solution before FeS addition; (b) effects of equilibrium pH on dissolved Hg(II) concentrations; (c) modeling results of unreacted FeS solids in the suspension vs. equilibrium pH.

The slight increase of dissolved Hg(II) may also be explained by surface adsorption. It is generally assumed that the $HgOH^+$ ions are much more reactive than Hg^{2+} (Macnaugh.Mg and James, 1974; Jean and Bancroft, 1986). With increasing pH, the surface potential of FeS decreases, becoming less positive or more negative. The point of zero surface charge for FeS lies at pH ~7.5 (Wolthers et al., 2005). It is easier for positively charged $HgOH^+$ to react with negative surfaces. However, the concentration of $HgOH^+$ decreases with increasing pH due to the formation of $Hg(OH)_2$ (Schuster, 1991). The effects of the decreasing surface potential and of decreasing concentration of $HgOH^+$ ions oppose each other, so that only small effects of pH on adsorption would be expected (Barrow and Cox, 1992). This is consistent with our experimental results.

5.2.3 Maximum Capacity of FeS for Immobilization of Hg(II)

Capacity of FeS for immobilizing Hg(II) was tested by changing added FeS concentrations with fixed initial Hg(II) concentration (1 mM) and also by changing Hg(II) concentrations with fixed initial FeS concentration (0.4 g L^{-1}). For both cases, initial pH of Hg(II) solutions was adjusted to 5.6 before FeS addition. For the case with initial Hg(II) concentration fixed at 1 mM (Fig. 5.3a), when the added FeS was in the range of 0.4 to 0.28 g L^{-1}, close to 100% of Hg(II) was removed from solution, with Hg(II) concentrations in filtrates less than 0.37 μg L^{-1}. When added FeS decreased from 0.24 to 0.16 g L^{-1}, Hg(II) removal decreased only marginally. Further decrease of added FeS in the suspension resulted in significant decrease in the percent removal of Hg(II). Although the maximum immobilization capacity reached 0.72 mol Hg(II) (mol FeS) $^{-1}$ when added FeS was as low as 0.08 g L^{-1} (loaded Hg(II)/FeS = 1.1), only 66% of

initial Hg(II) was removed. For the case with initial FeS fixed at 0.4 g L^{-1} (Fig. 5.4a), Hg(II) removed was proportional to the initial Hg(II) concentrations until a maximum capacity 0.75 mol Hg(II) (mol FeS) $^{-1}$ was reached at initial Hg(II) concentration 3.5 mM. At this maximum value, the mole ratio of loaded Hg(II)/FeS was 0.77 and the Hg(II) removed was 98.3%.

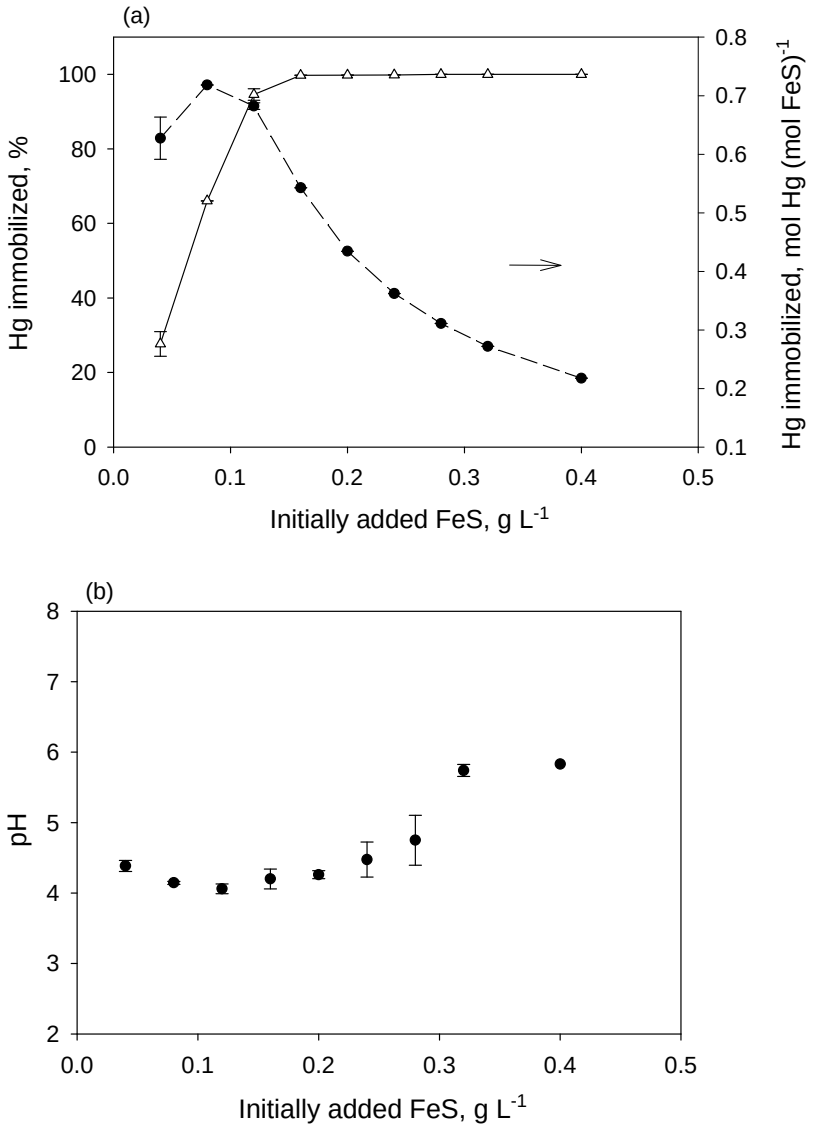

Figure 5.3 Sorption of Hg(II) in suspensions with different FeS concentrations Initial Hg(II) 1 mM at pH 5.6. (a) Removed Hg (II) vs. initial FeS concentrations; (b) equilibrium pH vs. initial FeS concentrations.

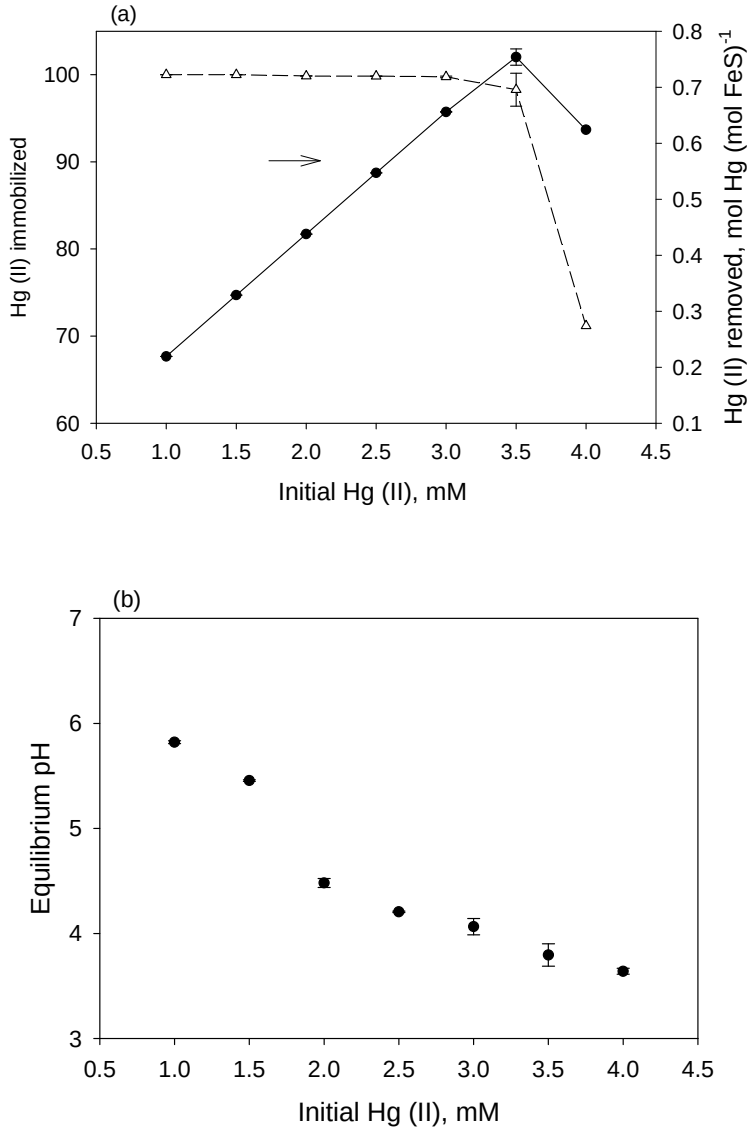

Figure 5.4 Sorption of Hg(II) in suspensions with different initial Hg(II) concentrations Added FeS 0.4 g L^{-1} and initial pH 5.6. (a) Removed Hg (II) vs. initial Hg(II) concentrations; (b) equilibrium pH vs. initial Hg(II) concentrations.

From Fig. 5.3 and Fig. 5.4, the overall tendency observed was that pH decreased with the increased Hg(II)/FeS mole ratio. When Hg(II)/FeS ~ 2.2, the equilibrium pH was near the initial pH 5.6. Decrease in pH has also been observed for sorption of Pb^{2+} and Cd^{2+} onto FeS (Coles et al., 2000). It is hard to explain the pH decrease by simple precipitation reaction alone, because neither OH^- nor H^+ is involved in this reaction. The pH decrease should be largely caused by

the surface adsorption. As stated earlier, it is usually assumed that the charged and hydrolyzed Hg(II) species are much more reactive than Hg^{2+} (Macnaugh.Mg and James, 1974; Jean and Bancroft, 1986). A surface adsorption model (Eq. 5.1) (James and Healy, 1972; Macnaugh.Mg and James, 1974) explains the pH decrease prompted by the interaction between hydrolyzed Hg(II) species and mineral surface.

$$M_{aq}^{n+} + mH_2O = M(OH)_m^{(n-m)+} + mH^+ \qquad (5.1)$$
$$\overline{S} + M(OH)_m^{(n-m)+} = \cdot M(OH)_m^{(n-m)+}$$

Below pH ~7.5 (Wolthers et al., 2005) the positively charged FeS surface attracts OH^- ions and could be an explanation for the decrease of suspension pH.

5.2.4 Hg(II) Immobilization and Fe^{2+} Release

The precipitation reaction can be expressed as $FeS + xHg^{2+} = xFe^{2+} + (Hg_xFe_{1-x})S$ ($0 < x \leq 1$). When x = 1, the ion replacement by Hg^{2+} from FeS solids is complete and HgS is formed; when x < 1, Fe(II) in FeS solids is partially replaced by Hg^{2+} and (Hg,Fe)S is formed. For the ion exchange reaction, equal moles of Fe^{2+} ions are released with the removal of Hg^{2+} ions. Based on this, by measuring the released Fe^{2+} in the solution, the portion of Hg(II) immobilized via ion exchange can be determined if no significant Fe^{2+} is released by dissolution. For these experiments, with loaded Hg(II)/FeS ≤ 0.22 at initial pH 5.6, it has been shown that the final pH was close to neutral (Fig. 5.2). This was confirmed by the measured pH of the suspension (Fig. 5.5). The pH varied from 6.9 to 5.8 when the initial Hg(II) increased from 0.01 to 1 mM. Under these conditions, no significant dissolution of FeS occurs, which is especially true when initial Hg(II) is near 1 mM (Fig. 5.2c). The curves for 0.01 mM and 0.1 mM initial Hg(II) (which are

not shown) should lie between the two curves shown on Fig. 5.2c and very close to the curve without the presence of Hg(II). Iron speciation shows that Fe^{2+} accounts for more than 95% of total dissolved iron (Table 1) for pH from 5.8-6.9. The measured total dissolved S(II) concentration was around 30 μM under the experimental conditions and was used to obtain the speciation data (Table 5.1) using MINTEQA2. Based on the modeling results for dissolution of FeS (Fig. 5.2c) and speciation of iron, total iron concentrations in the filtrates represent the approximate Fe^{2+} concentrations released by the ion exchange reaction between Hg(II) and FeS.

Table 5.1 Percentage of major dissolved iron species

pH	Fe^{2+} %	$Fe(HS)_2aq$ %	$Fe(OH)^+$%
4	98.48	1.51	
4.5	97.31	2.43	
5	97.52	2.45	
5.5	97.59	2.50	0.01
6	97.40	2.66	0.04
6.5	96.96	3.12	0.12
7	95.43	4.28	0.38
7.5	92.54	5.91	1.16
8	89.40	6.98	3.55

A linear relation was observed (Fig. 5.5) between equilibrium molar Fe^{2+} concentrations in the filtrate and molar Hg(II) concentrations removed. It should be noted that with loaded Hg(II)/FeS ≤ 0.22 at initial pH 5.6, approximately 100% Hg(II) was removed from the aqueous phase (Fig. 5.1). The slope of the linear regression was 0.773 with an intercept of -0.0223, which meant that under the experimental conditions, approximately 77% of the Hg(II) was immobilized via ion exchange and 23% of the Hg(II) was immobilized by adsorption. Fig. 5.5 also showed that the pH decreased with increasing initial Hg(II) concentrations, which is consistent with the observation shown on Fig. 5.4 but with smaller Hg(II)/FeS loadings.

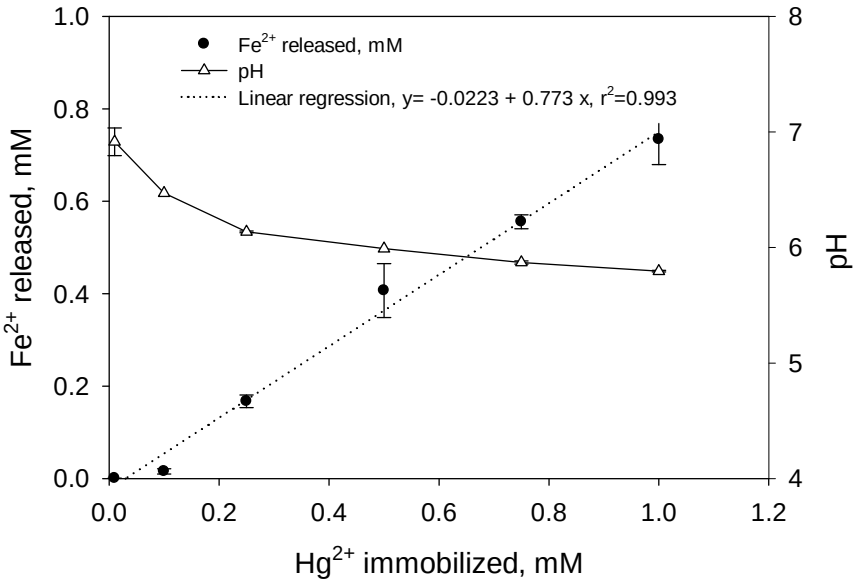

Figure 5.5 Iron releases with different initial concentrations of Hg(II)

Added FeS 0.4 g L^{-1} and initial pH 5.6. Under these experimental conditions, close to 100% of added Hg(II) is removed from the aqueous phase.

5.2.5 XRPD Analysis

The XRPD patterns A and B shown in Fig. 5.6 are for the N_2-dried FeS and 'FeS' from the sorption experiments respectively. The major components in the samples were identified with the assistance of the XRD pattern processing software (MDI Jade version 6.1) loaded with ICDD database. The positions of the peaks for pattern A associated with FeS (ICDD 15-0037) are marked with the number 0. It was concluded that because of the nanoparticulate nature of FeS, XRPD methods routinely used to examine FeS give no pattern or show a broad peak at 5Å (17.6˚ 2θ) (Rickard and Morse, 2005). Consistent with this conclusion, the observed XRPD pattern (Fig. 5.6A) of the synthetic FeS showed broad peaks with very low intensities. The broad peaks around 17.6˚ 2θ are indicative of FeS, with intensities and positions in reasonable agreement with peaks previously reported in the conventional XRPD pattern for FeS (Wolthers et al., 2003).

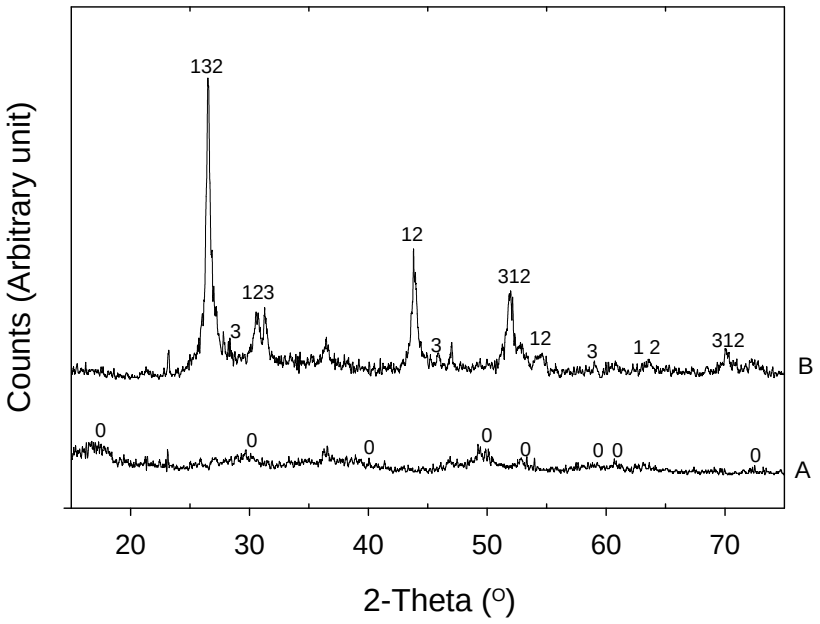

Figure 5.6 XRPD patters for N_2-dried (a) Fresh FeS and (b) 'FeS' after sorption
Added FeS 0.4 g L^{-1} and initial pH 5.6. Numbers on the graph are used to mark the approximate peak positions of major components of the samples. 0–Mackinawite (FeS), 1–Metacinnabar (HgS), 2–Mercury iron sulfide, 3–Cinnabar (HgS)

In contrast to pattern A in Fig. 5.6, peaks appear in pattern B which indicates the formation of mercury sulfides, including mercury-iron sulfide. The positions of major peaks of mercury sulfide complexes in pattern B are marked with 1 for metacinnabar (HgS, ICDD 06-0261), 2 for mercury-iron sulfide and 3 for cinnabar (HgS, ICDD 06-0256). The highest intensity peak of cinnabar occurs at around 31.2˚ 2θ. The formula for mercury-iron sulfide is given as $(Hg_{0.89}Fe_{0.11})S$ (ICDD 50-1151) in the ICDD database and is referred to as (Hg,Fe)S in this paper, because it may not be the only form of mercury-iron sulfide existing in the sample. The patter for (Hg,Fe)S is very similar to that for metacinnabar. For the major peaks with high intensities, peaks of (Hg,Fe)S overlap those of HgS and are separated slightly at the top with those for (Hg,Fe)S on the right side.

Besides those marked, there are 4 peaks shown both on pattern A and pattern B. These peaks were caused by compounds not containing mercury. Checking the standard patterns, the peak at 21.2˚ 2θ could be from a hydrated iron oxide goethite (α-FeOOH, ICDD 29-0713) and the peak at 23.2˚ 2θ could be from elemental sulfur possibly in two forms (ICDD 42-1278 and 08-0247), where the peak intensities are highest. It is very likely that the other two peaks at around 36.3 and 46.9˚ 2θ are in part from another hydrated iron oxide lepidocrocite (γ-FeOOH, ICDD 08-0098), which has major peaks at these two positions. These two peaks are also present in the XRPD pattern of synthetic FeS reported by other researchers though no explanation was provided (Coles et al., 2000). The presence of elemental sulfur and hydrated iron(III) oxides indicates minor oxidation of FeS has occurred possibly during its preparation, sorption experiments and XRPD analysis via the reaction $FeS + H_2O + O_2 = FeOOH + S^0$.

Practical experience has shown that, even after taking elaborate precautions such as conducting all work under an Ar atmosphere, it is not possible to keep freshly synthesized machinawite for more than a few days in solution without some oxidation occurring (Morse and Arakaki, 1993).

5.2.6 Oxidation and Hg(II) Retention

In the presence of water, FeS is oxidized to FeOOH and S^0 can be further oxidized to sulfate (Eq. 4.1 to 4.3). After 24 hours of aeration, no FeS was detected by the measurement method for AVS, which means FeS has been completely oxidized.

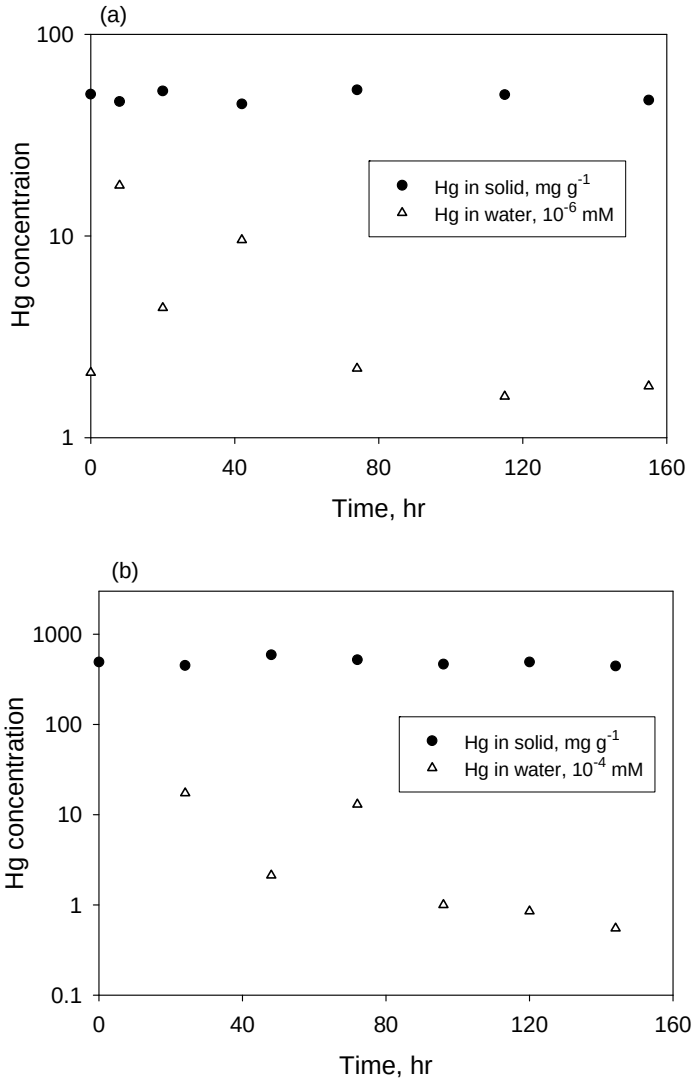

Figure 5.7 Hg concentrations in suspended solid and water during aeration
Added FeS 0.4 g L^{-1} and initial pH of solutions 5.6. At time '0', the purge gas was switched to air from N_2. (a) Initial Hg(II) 0.1 mM, (b) Initial Hg(II) 1 mM

From Fig. 5.7, we concluded that only a small amount of mercury was released into the water phase after switching the purge gas from N_2 to air, but compared to the amount retained on the solid phase it was negligible. There was no significant loss of mercury from the solid phase during 160 hours of aeration. For metacinnabar and cinnabar, aeration of the suspension does not cause mercury releases from the two compounds. For Hg(II) adsorbed on FeS solid, if FeS is

oxidized according to the reaction above, it should be released from FeS which would result in a significant increase in mercury concentration in the water phase. Such an increase of mercury in the water phase was not observed. This was probably due to the formation of FeOOH during oxidation and released Hg(II) was adsorbed onto FeOOH after its release from FeS. Studies (Barrow and Cox, 1992, 1992; Gunneriusson and Sjoberg, 1993; Bonnissel-Gissinger et al., 1999; Brown and Parks, 2001; Kim et al., 2004; Slowey and Brown, 2007) have shown that FeOOH itself is a good adsorbent for Hg(II).

After complete oxidation of synthetic FeS, FeOOH was separated by filtration and dried at 65˚C. The measured specific area of FeOOH (N_2-BET) was 44.7 m^2 g^{-1}, which was greater than the measured specific area of FeS (7.8 m^2 g^{-1}). However, its ability to immobilize Hg(II) was smaller than FeS which was not surprising because Hg(II) was removed by adsorption onto FeOOH. With the addition of 0.4 g L^{-1} FeOOH into 0.1 mM Hg(II) solution at pH 5.6, the capacity for FeOOH was 0.0044 Hg(II)/FeOOH (mole ratio). The loaded mole ratio was 0.022 and 0.22 Hg(II)/FeS for 0.1 mM and 1 mM Hg(II) solutions for the two cases in Fig. 8. Considering close to 100% of Hg(II) is immobilized and only 23% by adsorption, the portion retained by adsorption is about 0.0051 and 0.051 mol Hg(II) (mol loaded FeS)$^{-1}$ for 0.1 mM and 1 mM Hg(II) solutions respectively. Thus we can conclude that it is possible for FeOOH to adsorb the Hg(II) released from FeS in 0.1 mM case, but it only accounts for about 10% of total Hg(II) retained by adsorption in the 1 mM case. In this case, it is impossible for FeOOH to adsorb all of the Hg(II) released from FeS after its oxidation.

HgS can adsorb Hg(II) in acidic solutions. An capacity of 1.84 mmol Hg(II) (mol HgS)$^{-1}$ has been detected in 1 mM HCl solution (Hasany et al., 1999). In less acidic solution, more Hg(II) could be adsorbed per mole of HgS. Under such condition, HgS can be another source for adsorption of released Hg(II). Another possibility is the adsorption of Hg(II) onto (Hg,Fe)S. (Hg,Fe)S should be more resistant to oxidation than FeS especially after some of its active sites on the surface are covered by adsorbed Hg(II) complexes.

5.2.7 Sorption of Hg(II) onto Commercial Iron Sulfide

While the sorption study was mainly focused on Syn-FeS , the sorption ability of CIS was investigated by adding 0.4 g L^{-1} into Hg(II) solution at different initial concentrations. The initial pH of the solution was about 5.6.

Table 5.2 Hg(II) removed and equilibrium pH by commercial iron sulfide

Initial Hg(II), mM	0.01	0.1	0.5	1
Equilibrium pH	6.64	5.94	3.71	3.61
Hg(II) removed, %	100	100	92.1	69.0
Hg(II) removed, g Hg (gCIS)$^{-1}$	0.005	0.05	0.230	0.345

CIS: commercial iron sulfide

With initial CIS fixed at 0.4 g L^{-1}, the amount of Hg(II) removed increased with the increase of the initial Hg(II) concentration, while the percentage of Hg(II) removed decreased. In the investigated range of Hg(II) concentration, the maximum capacity 0.345 g Hg(II) (g CIS)$^{-1}$ was reached, with 69% Hg(II) was removed (Table 5.2). When added Syn-FeS was 0.4 g L^{-1} with a initial pH of 5.6, 100% Hg(II) was removed from the 1mM solution and the equilibrium pH was 5.82. For Syn-FeS, the maximum capacity of 0.75 mol Hg(II) (mol FeS) $^{-1}$ was reached at initial Hg(II) concentration 3.5 mM (Fig. 5.4). At this maximum value, the mole ratio of

loaded Hg(II)/FeS was 0.77 and the Hg(II) removed was 98.3%. From the comparison above, CIS is a good sorbent for Hg(II), but it is not as good as Syn-FeS. The reasons for the lower sorption ability were the low content of iron sulfides in CIS and extremely low equilibrium pH, which were both mainly caused by the oxidation of original FeS in CIS.

5.3 Summary

FeS has a great capacity to remove Hg(II) from solution. Although sorption process of Hg(II) to FeS includes both precipitation and adsorption, the primary mechanism for FeS to immobilize Hg(II) is via precipitation, which accounts about 77% of total Hg(II) immobilized.

Because FeS is very reactive to oxygen, steps should be taken to stabilize FeS before it can be applied as a component of an active capping material. Once Hg(II) is removed, no significant mercury will be released into the water when the system is expose to oxidizing conditions. Oxidation product FeOOH, precipitation products HgS and (Hg,Fe)S of FeS might be the most important mechanism for the retention of released Hg(II) after the oxidation of FeS.

Chapter 6 Remediation of Mercury-Contaminated Sediment with Iron Sulfides

6.1 Experimental Methods

6.1.1 Sediment

Sediment used in the capping experiments was collected from the Henderson Lake as described in chapter 4. Hg(II) stock solution with a concentration of 1 mg mL^{-1} (in the form of $HgCl_2$ dissolved in 4.7% HNO_3) was spiked into the sediment to reach a final concentration of 40 μg-Hg (g-dry sediment)$^{-1}$, which was analogous to the THg concentrations in the sediments from Pompton Lake used in the conventional capping experiments described in Chapter 3. After enrichments, the sediment was mechanically rotated for 24 hours to make it uniform. The pH of pore water was 6.84 for the original sediment and 6.60 for the Hg(II) enriched sediments.

6.1.2 Experimental Setup

Using Hg(II) enriched sediment, three cases were investigated in the capping experiments as shown in Fig. 6.1. Case (1) and case (2) were both uncapped. For case (1), there was only one sub-case (A) and no any chemical was amended into the Hg(II) enriched sediment. For case (2), either 0.5 mmol (4.4% wt) CIS (commercial iron sulfide) (B) or 0.5 mmol (4.4% wt) Syn-FeS (C) was amended into Hg(II) enriched sediment. For case (3), a layer of 8 mm cap was placed over the sediment and 4 sub-cases (D, E, F and G) were set up using different capping materials. For D, clean sand was used as the cap. For E, 8 mm CIS was used. For case F, the lower 5 mm cap was a mixture of 25% (wt) AquaBlok capping material and 75% sand, and the upper 3 mm was

sand. For Case G, the lower 5 mm cap was a mixture of 25% (wt) dry Syn-FeS and 75% sand, and the upper 3 mm was sand. The capping materials used are shown in Fig. 6.3. Altogether for both capped and uncapped cases, seven sub-cases were investigated and details are summarized in Table 6.1. For each case, two duplicates were applied.

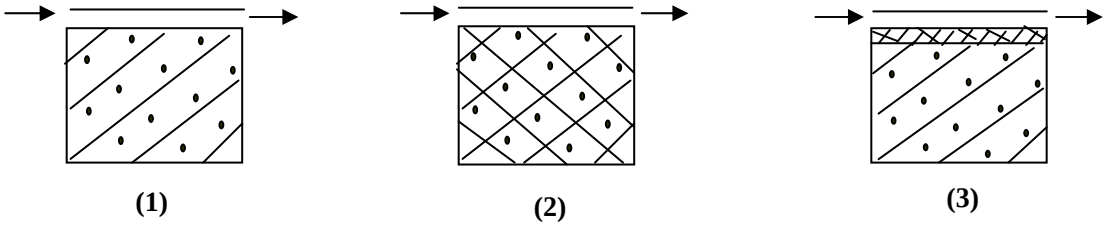

Figure 6.1 Schematic of experimental design.
(1) Aqueous Hg(II) enriched sediment below overlying water; (2) Aqueous Hg(II) enriched sediment amended with selected potential inhibitor (3) 8 mm cap layer below overlying water, sediment spiked with aqueous Hg(II) below the cap.

Table 6.1 Summary of the experimental design for active capping experiments

Experiments	(1)	(2)		(3)			
	A	B	C	D	E	F	G
Cap layer	No	No	No	8 mm Clean sand	8 mm CIS	3 mm sand + 5 mm AquaBlok Mix	3 mm sand + 5 mm Syn-FeS Mix
Chemicals amended in Sediment layer	Hg(II)	Hg(II), CIS	Hg(II), Syn-FeS	Hg(II)	Hg(II)	Hg(II)	Hg(II)

The experimental setup was analogous to those used for the conventional capping experiments described in Chapter 3. During experiments, water was pumped into the chambers at a flow rate of 2 L m^{-2} hr^{-1}. The height of the overlying water was maintained at 10 mm by setting the inlet of the outlet tube 10 mm higher than the sediment or cap surface. The effluent water was collected for THg, sulfate, and pH analysis. The top of each cell was covered with a glass plate to

minimize vaporization of water and prevent the dust. Redox conditions at varied depths were monitored in one duplicate for each case using Pt electrodes.

After 9 months of operations, the sediment and cap to a depth of 18 mm in each chamber was sectioned with 2 mm vertical resolution for analysis of THg and MeHg. The details of the method used were described in Chapter 3. The analytical methods for THg, MeHg, sulfate and pH were the same as described in the previous chapters.

6.1.3 Capping Material

Sand used in the experiments was play sand from a hardware store. It was cleaned with laboratory detergent and then dried in an oven at 105˚C. It was sieved to less than 500 μm before usage (Fig. 6.3D). Commercial iron sulfide (CIS) used in cell E was ground and sieved to less than 500 μm and greater than 50 μm (Fig. 6.3E).

Figure 6. 2 Original AquaBlok capping material

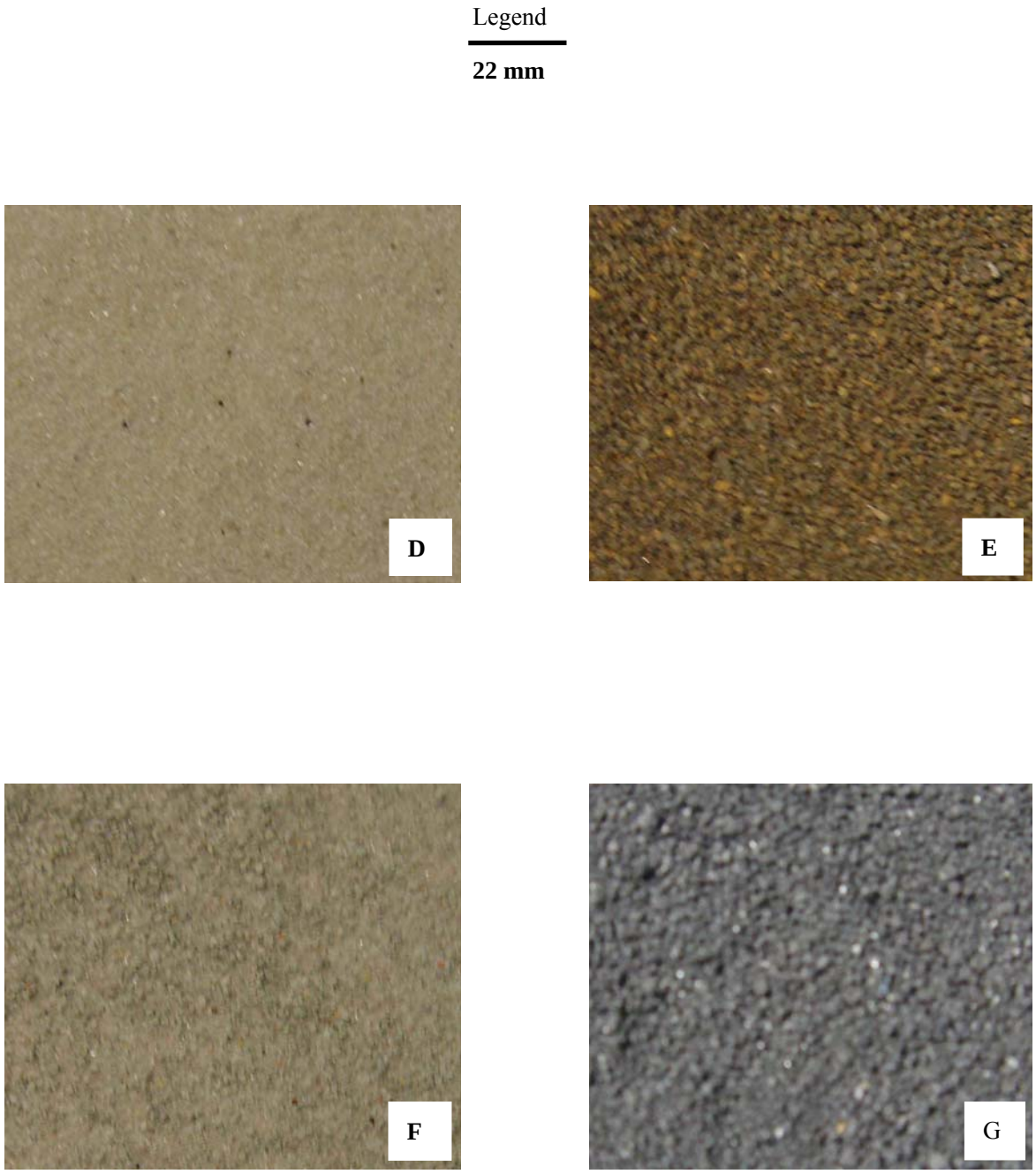

Figure 6.3 Capping materials used in the experiments.
D, sand used for chamber D. **E**, CIS used for chamber E. **F**, a mixture of 25% (wt) ground AquaBlok capping material and 75% sand. **G**, a mixture of 25% (wt) Syn-FeS and 75% sand.

The original AquaBlok capping material sent to the laboratory was composed of particles with diverse sizes ranging from ~5 mm to ~20 mm (Fig. 2). These particles were actually small rocks coated with clay amended with 4% elemental sulfur. Because the sizes of the particles were too big for the small-scale simulation cells, the coat which was the active part of the particles was broken off the inner rocks, ground and sieved to less than 500 μm as the capping material for the experiments. Then, it was mixed with sand prepared according to a ratio of 1:3 (weight) (Fig. 3F).

Laboratory synthesized wet FeS (Syn-FeS) was purged with high purity N_2 in a flask sealed with a rubber stopper having inlet and outlet holes. During the purge process, the Syn-FeS clumps were broken into smaller particles by shaking. When it was half dry, sand was added into the flask and mixed with Syn-FeS according to a sand/Syn-FeS ratio of 1:3 (dry weight). Large particles were further broken into smaller ones using a spatula. N_2 was kept purged into the mixture until it was dry. Most sand particles were coated with Syn-FeS at the end of this process. It was sieved to less than 1 mm before application (Fig. 3G)

6.2 Results and Discussion

6.2.1 Redox Conditions in Caps and Sediments

Because the cells were loosely covered with glass plates, they were not airtight. The dissolved oxygen in the feed water and the diffusion of air into the cells kept aerobic conditions in the overlying water and the surface sediment or cap right below the water-sediment/cap interface.

Table 6.2 Moisture of sediment/cap with depths in cells

Depth* mm	1	3	5	7	9	11	13	15	17
A	81.9	81.1	79.7	79.3	78.5	76.1	74.4	73.9	73.1
B	74.4	80.8	79.6	78.9	77.2	75.5	74.4	73.3	72.4
C	75.3	82.7	78.4	75	73.7	73.2	72.3	71.1	71.1
D	22.9	22.0	21.7	25.1	58.1	65.2	66.0	66.5	67.1
E	44.4	34.1	33.0	32.2	65.3	66.5	67.1	67.3	67.6
F	26.0	28.6	30.3	34.2	52.8	61.2	65.5	68.3	68.1
G	22.1	25.7	29.2	33.5	62.3	63.1	66.1	66.8	67.3

Note: (1) Each depth represents the depth at the middle of each slicing section.
(2) The data shown are the average of samples from two duplicate cells.

For uncapped cells, the consolidation of the sediments should have occurred via gravity. The surface sediments absorbed extra moisture from the overlying water which led to a higher porosity (Table 6.2) and no apparent consolidation occurred. Therefore, there was no significant motion of the Pt electrodes (fixed at certain depths of the cells) relative to the sediments. At the end of the experiment, the depths of the Pt electrodes shown in Fig. 6.4 were approximately at the depths when the experiment started. For capped cells D, F and G, with sand as the major composition of the caps, the bulk density of caps were greater, which led to the consolidation of sediments beneath the caps. This was shown by the lower moisture contents compared to that of the original sediment, which was 73.7%. This was also true for capped cell E, using CIS as the cap.

In capped cells, the caps had higher bulk density and lower porosity, therefore, at the end of the capping experiments, the top of the caps dropped around 2-4 mm due to the consolidation of sediments beneath the caps. This resulted in the relative motion between sediment/cap and Pt

electrodes. The depths of the Pt electrodes shown were the actual positions of the electrodes (Fig. 6.5) in sediment/cap at the end of the experiment.

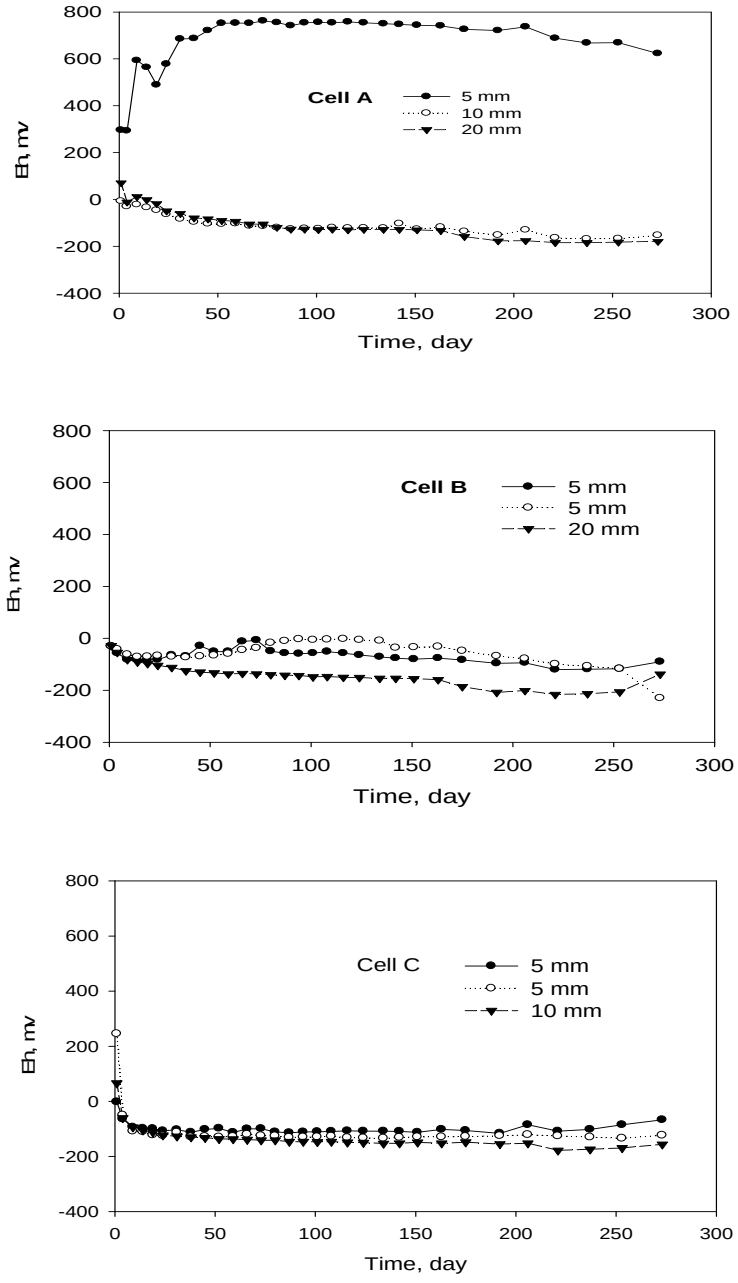

Figure 6.4 Redox in uncapped cells

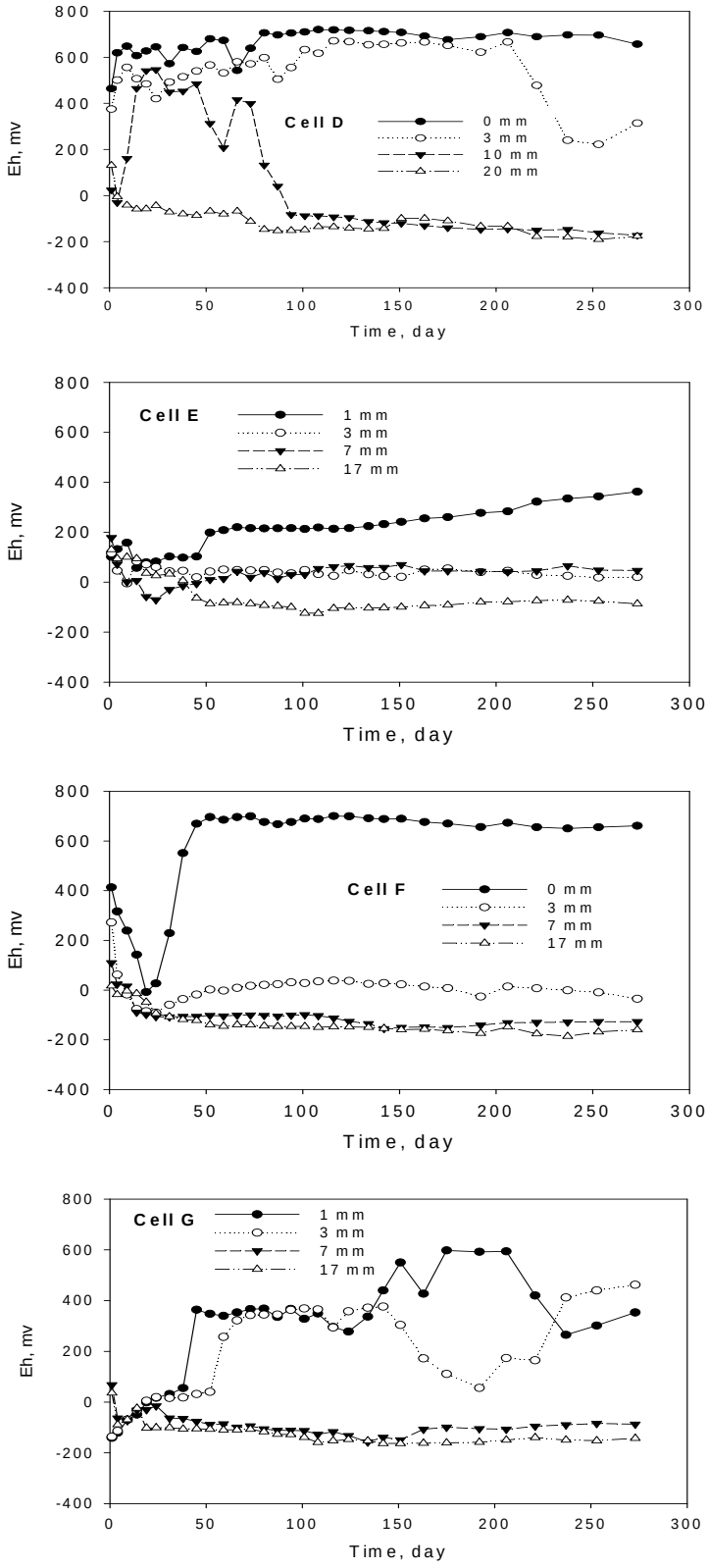

Figure 6.5 Redox in capped cells

For uncapped cell A, it was aerobic at a depth of 5 mm and anaerobic below a depth of 10 mm. Therefore, the transition from aerobic to anaerobic occurred between 5 mm and 10 mm. For uncapped cell C, which was amended with Syn-FeS, it was anaerobic below 5 mm during the experiment. Syn-FeS is a strong reductant and was well distributed in the sediment as nano-sized particles, little oxygen would diffuse through before it is oxidized. This explains the difference of redox conditions in sediment of cell A and C. The redox potential at depth of 5 mm of cell C increased gradually during the experiment, which indicated the oxidation of Syn-FeS in the surface sediment. CIS contains different species of iron sulfides and it is not as strong a reductant as FeS. This is the reason why the redox potential at 5 mm of cell B which was amended with CIS was not as low as that of cell C at the same depth. Overall, for cells B and C, it was anaerobic at the depth of 5 mm at the end of the experiment and the transition from aerobic to anaerobic occurred between 0 to 5 mm. The addition of iron sulfide creates a more reducing condition in the top sediment in uncapped cells.

For capped cells, it was anaerobic at the bottom of the cap (at depth 7 mm in Fig. 6.5) after trapped oxygen was released or consumed. This process took about 3 months for cell D with sand cap, which was longer compared to other capped cells. This is because unlike other cells, there was no components in the sand cap which could consume oxygen. It was anaerobic in the sediments beneath the caps with a thickness of 8 mm.

6.2.2 pH in Effluent Water

For uncapped cells, the overall tendency of pH of the effluent water increased with time during the experimental time span except a small decrease shortly after the initiation of the

experiment (Fig. 6.6). At this time, the releases of H^+ ions from sediments into the overlying water led to the decrease of the pH in the effluent water, which was mainly caused by the oxidation of iron sulfides in the surface sediment below water-sediment interface, for example, the oxidation of FeS in the presence of water.

$$FeS + 3/4H_2O + 1/2O_2 = FeOOH + S^0 \quad (4.1)$$

$$S^0 + H_2O + 3/2O_2 \rightarrow SO_4^{2-} + 2H^+ \quad (4.2)$$

The overall reaction

$$FeS + \frac{9}{4}O_2 + \frac{3}{2}H_2O \rightarrow FeOOH_{(s)} + 2H^+ + SO_4^{2-} \quad (4.3)$$

The pH in the effluent water of 3 uncapped cells were lower compared to the pH in the pore water of Hg(II) amended sediments, which was 6.6. The pH of cell A varied from ~4.6 to ~6.5 during the experiments, and the pH of cell B and cell C varied from ~3.8 to ~5.7. With the consumption of iron sulfides in the surface sediments, the rate of the oxidation reaction decreases and less H^+ ions were released, pH in the effluent water increased for each cell with time. Because additional iron sulfides were amended into sediments in cell B and cell C before initiation of water flow, more H^+ ions were released in the effluent water and pH in the effluent water from these two cells were lower than that from cell A.

For cell D which had a 8 mm layer of sand cap over the sediment, the trend of pH change in effluent water was very similar to that of the uncapped cells, which increased with time except a sharper decrease shortly after the initiation of the experiment. The release rate of H^+ ions was balanced among the mass transfer rate of O_2 from water to sediment, the oxidation reaction rate

and the mass transfer rate of H^+ from sediment to the effluent water through the sand cap. Because of the layer of sand cap, it took a longer time for H^+ ions produced in the sediments to enter the overlying water. Also, because of the sand cap, O_2 could not penetrate in the sediment as deep as in cell A (Fig. 6.4 and Fig. 6.5). After about 3 months, it was anaerobic in the sediment under the sand cap. The overall release rate of H^+ ions in cell D was lower compared to that in cell A.

Because iron sulfides were exposed to the dissolved oxygen in the overlying water directly, pH in the effluent of cell E was the lowest among all capped and uncapped cells. pH in the effluent of cell E varied from ~3.4 to ~5.2 and kept decreasing until around 6 months.

pH profiles in effluents of cells F and G had similar trend. Since the initiation of the experiment, pH decreased monotonically until it reached the lowest value in each cell in approximately one month. Then, pH started to increase until the end of the experiments. The existence of the sharp decrease was related to the layer of 3 mm sand cap and was a result of the combination of mass transfer and reaction. For cell F and G, it appeared that pH was more sensitive to the redox conditions because pH values diverged in the two duplicate for both cells F and G. For cell G, the decrease of pH was mainly caused by the oxidation of S0 (Eq. 4.1) produced in the oxidation reaction of Syn-FeS with presence of water in the cap beneath the sand cap (Eq. 4.2). For cell F, the decrease of pH was caused by the oxidation of S0 amended in the AquaBlok capping material.

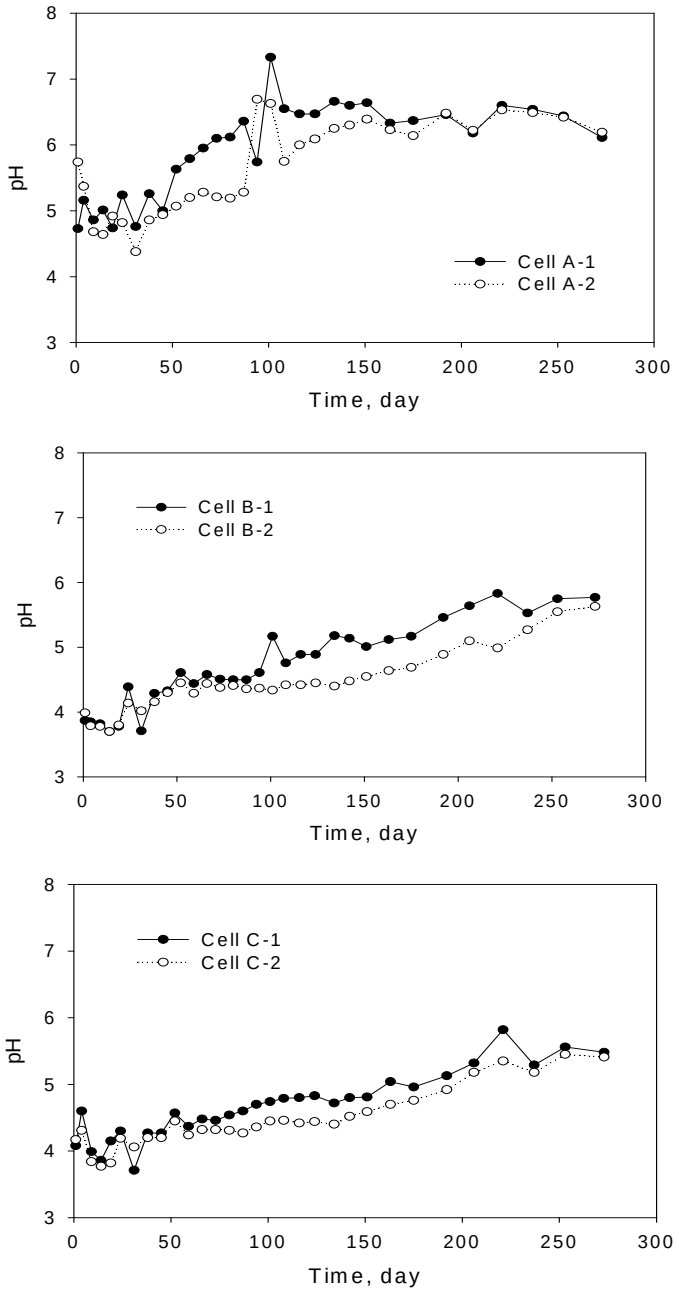

Figure 6.6 pH in effluent water of uncapped cells
For each cell, the results from two replicate cells are shown in the figures

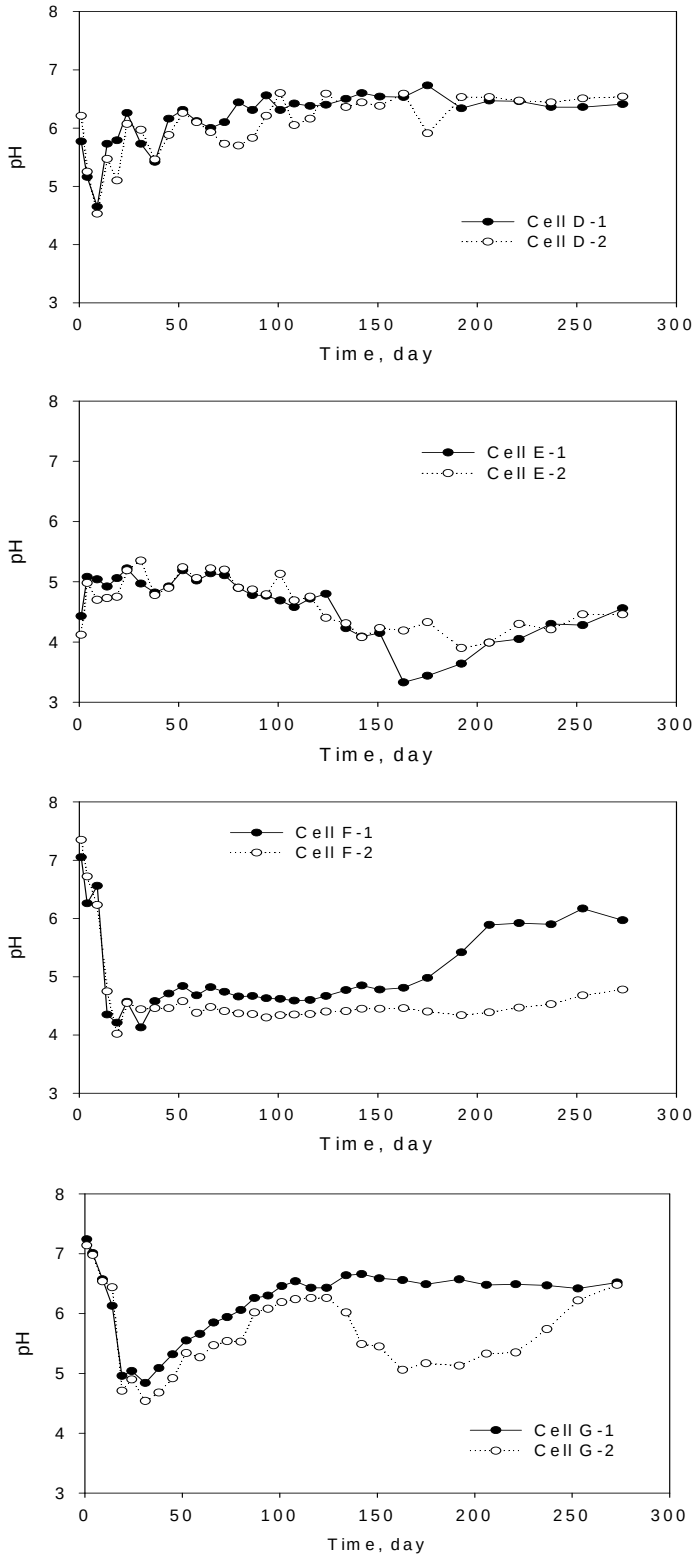

Figure 6.7 pH in effluent water of capped cells

6.2.3 Sulfate Releases to the Effluent Water

With presence of water, SO_4^{2-} ions were released into the water during the oxidation of S^0, which is the intermediate product of oxidation reaction of FeS. From the stoichiometry (Eq. 4.2), the amount of sulfate produced was one half of that of H^+ produced during the oxidation process (in mole), therefore, sulfate concentration was high when pH was low in the effluent water. For this reason, the sulfate profile (Fig. 6.8) and the pH profile (Fig. 6.6 and Fig. 6.7) oppose each other in all the cells. As it approached 9 months (the end of the experiment), sulfate concentration was close to zero for all other cells except cell E, in which CIS was the cap. At this time, the oxidation of sulfides was almost complete in the aerobic zone of either sediments or caps.

The total sulfate released into water was calculated by integrating the curves in Fig. 6.8 using the equation,

$$n = \sum_i Q \cdot C_i \cdot \Delta t_i \qquad (6.1)$$

Where,

n: Total sulfate released to the overlying water.

Q: The flow rate of overlying water, 10 ml/hr.

i: ith sample collected.

C_i: Sulfate concentration in effluent water of sample i.

Δt_i: Time interval between sample i and sample (i-1) were collected.

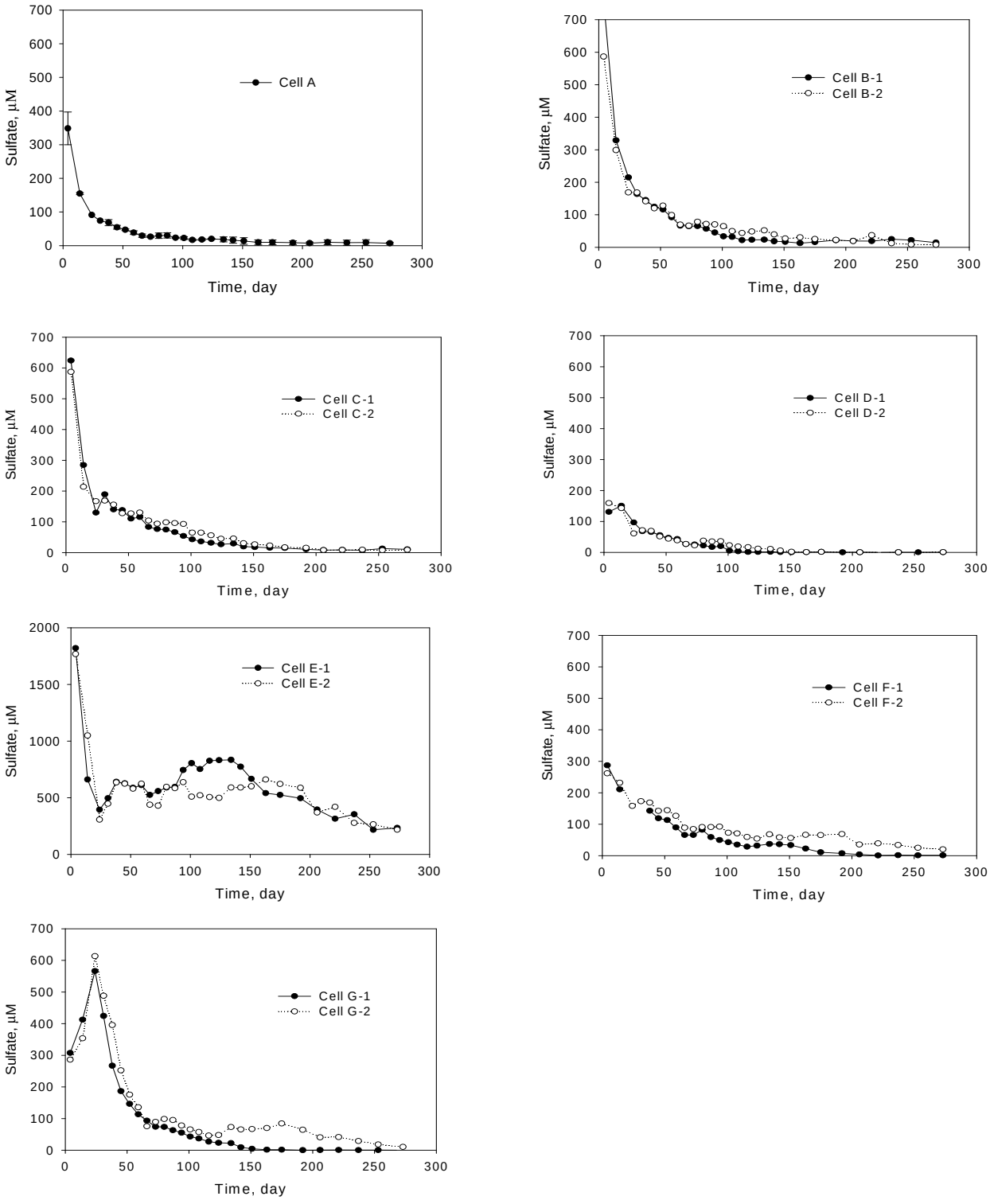

Figure 6.8 Sulfate in the effluent water
For each cell, the results from two replicate cells are shown in the figures

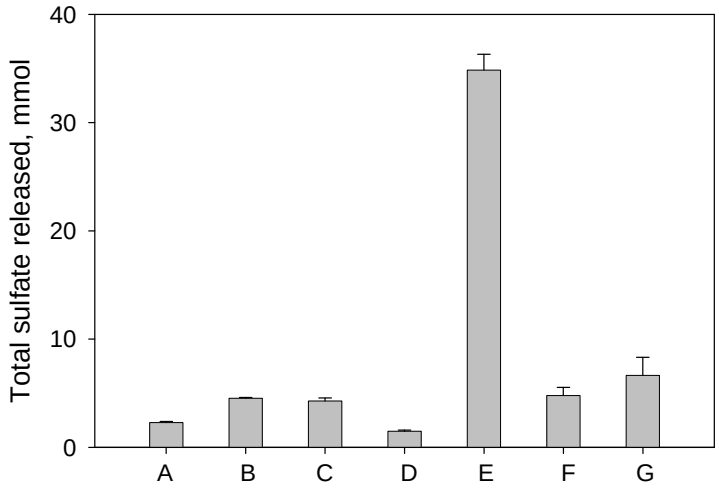

Figure 6.9 Total sulfate released into overlying water

Among all either capped or uncapped cells, total sulfate released in cell D was the least during the experimental period, with a value of 1.5 mmol (Fig. 6.9). Total sulfate released in cell A was 2.3 mmol. The less release of sulfate with sand cap was mainly due to the more anaerobic conditions in the sediment under the cap. Because of the higher concentration of iron sulfides amended in the sediments of uncapped cells B and C, more sulfate ions were released into the effluent water in uncapped cells B and C compared to cell A as expected. Total sulfate released in cells B and C had very close values, with 4.5 mmol for cell B and 4.3 mmol for cell C. For capped cells F and G, the value was 4.7 mmol and 6.7 mmol respectively. For cell F, in the second layer of the cap, S^0 was 4% of the AquaBlok capping material, which means that it was 1% of the mixed cap with 75% being sand. While for cell G, Syn-FeS was 25% of the mixed cap with sand. This explains why less sulfate was released in cell F compared to cell G. Sulfate released from cell E was the highest, which was 34.8 mmol and approximately 5 times of that from cell G, with 3 mm sand cap over Syn-FeS. There were two reasons for this large amount release of sulfate. One was that some sulfate was in CIS before application because CIS was a

mixture of oxidation products of FeS and sulfate was produced during the oxidation (Eq. 4.3). The other reason was due to release of sulfate via the oxidation of iron sulfides after application. CIS was exposed to dissolved oxygen in overlying water because there was not a layer of sand above it as cell G.

Assuming in the aerobic zone of the mixed cap in cell G, Syn-FeS had been completely converted to sulfate by the end of the experiment. This was true because Syn-FeS was nanosized and sulfate release rate was close to zero at this time. With this assumption, the depths of aerobic zone can be estimated from the total released sulfate. From Eq. 4.3, equal mole of sulfate is released when Syn-FeS is completely oxidized to sulfate. Thus, thickness of the aerobic zone can be estimated from

$$n = \frac{f_{FeS} \cdot \rho_{Mix} \cdot A \cdot h}{M_{FeS}} \tag{6.2}$$

Where,

n: Total sulfate released to the overlying water, 6.7×10^{-3} mol in cell G.

f_{FeS}: mass fraction of Syn-FeS in the mixed cap layer, which was 25%.

M_{FeS}: molecular weight of FeS, 87.9 g mol^{-1}.

ρ_{mix}: Density of mixed cap of Syn-FeS and sand, 1.4 g mL^{-1}.

A: Cross section area of cap in cells, 50cm^2.

h: The thickness of the aerobic zone, cm.

Solving Eq. 6.2 for h, h equals 0.34 mm, which is consistent with the observed redox distribution in cell G. With a layer of 3 mm sand cap over Syn-FeS amended cap, only 0.34 mm layer of Syn-FeS was oxidized in the 5 mm mixed cap. This is consistent with the observation

that color change from black to orange (the color of FeOOH) occurred only at the interface between sand layer and the mixed layer, and the major part of the mixed layer remained black during the experiment.

6.2.4 Releases of Total Mercury into Overlying Water

Effluent water samples were collected with an interval of 2 months since the initiation of the capping simulation experiments. Altogether 4 samples were collected and analyzed for each cell. THg concentration showed little variation among the 4 samples for each cell and they were averaged (Fig. 6.10).

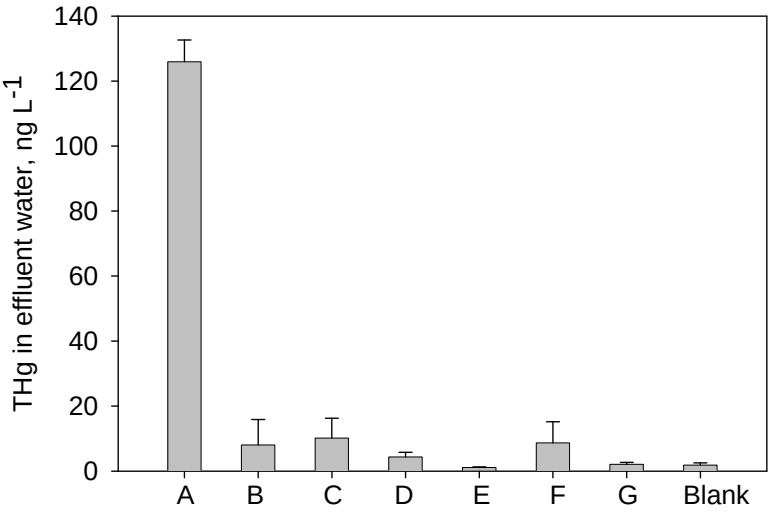

Figure 6.10 Total Hg concentrations in effluent water

Among all the cells, cell A had the highest concentration in effluent water, which was 130 ng L^{-1}. With amendment of CIS and Syn-FeS in cells F and G, THg in effluent water was 8 ng $L^{-1}$and 10 ng L^{-1} respectively. The THg concentration in pore water of the sediment obtained after centrifugation was 110 ng L^{-1} for cell A, 100 ng L^{-1} for cell B and 60 ng L^{-1} for cell C. Obviously,

such significant decrease of THg in effluent water of cells F and G was not solely caused by the lowered THg in pore water of the sediments. The first 2 mm layer of sediment in cells B and C had lower moisture, 74.4% and 75.3% respectively, compared to 81.9% in cell A (Table 6.2). It was actually observed that there was sediment particles floating at the water-sediment interface in cell A. While in cells B and C, a hard and brown crust was formed at the sediment surface. The major components of the crust might be sediment mixed with the oxidation products of iron sulfides. It is very possible that the high THg concentration in effluent water of cell A was largely due to the escape of tiny sediment particles. These samples for THg were unfiltered before extraction. In cells B and C, the sediment surface was fixed by the formation of a layer of crust and no floating particles were observed at the surface.

Total Hg released from uncapped cells was greatly reduced for all capped cells compared to cell A. The major reason was that with a layer of cap, little sediment particle could diffuse into the water phase and THg in effluent water rather than that in feed water mainly came from pore water by diffusion through the cap.

With Syn-FeS amended into sand cap, there was no apparent mercury released into the overlying water because THg concentration in the effluent water of cell G was at the same level with that in the blank cell, which had only DI water in it. It is interesting to note that THg in the effluent water of cell E was lower than that of the blank cell. This is because iron sulfides are good sorbent for mercury and extracted mercury from feed water. Sand cap alone (cell D) reduced the release of THg, but it appeared not as effective as iron sulfides. Compared to other caps, AquaBlok capping material was not as effective in blocking mercury, which was possibly

due to the increased solubility of HgS (cinnabar) with the presence of dissolved S^0 (Paquette and Helz, 1997; Fabbri et al., 2001) by formation of Hg-polysulfides (Appendix A).

6.2.5 Mercury Migration in Sediment and Cap

After 9 months of operation, the top sediment and cap was sectioned with 2 mm vertical resolution. Total Hg distribution in sediment/cap is shown in Fig. 6.11 for the two replicates of each cell. Each depth shown in the figure represents the average depth of each section. For example, the first section was from "0" to "2 mm" and is represented as "1 mm" in depth.

No evidence shows that significant amount of mercury had been released into the overlying water for capped cells during the experimental period. The increase of THg concentration in the last section of cap and the decrease of THg concentration in the first section of sediment in each capped cell were caused by the intermixing between cap and sediment at the cap-sediment interface. Mixing between cap and sediment particles at the interface was practically impossible to avoid in the simulation cells. Even for uncapped cell, mercury migration was not significant. It appeared that a small decrease of THg concentration occurred in the first 2 mm sediment of cell A. This was not surprising considering the strong partitioning of mercury to the solid phase. Total Hg spiked into the sediment was around 40 μg $(g\text{-}dw)^{-1}$, while THg in pore water was only 110 ng L^{-1} for this enriched sediment, 100 ng L^{-1} when it was amended with CIS and 60 ng L^{-1} when it was amended with Syn-FeS. The calculated partition coefficients would be 364 L g^{-1}, 400 L g^{-1} and 667 L g^{-1}, comparable to those for sediments collected from Pompton Lake, which varied from 79 (for sandy sediment from area 2) to 573 L g^{-1} (Table 3.1).

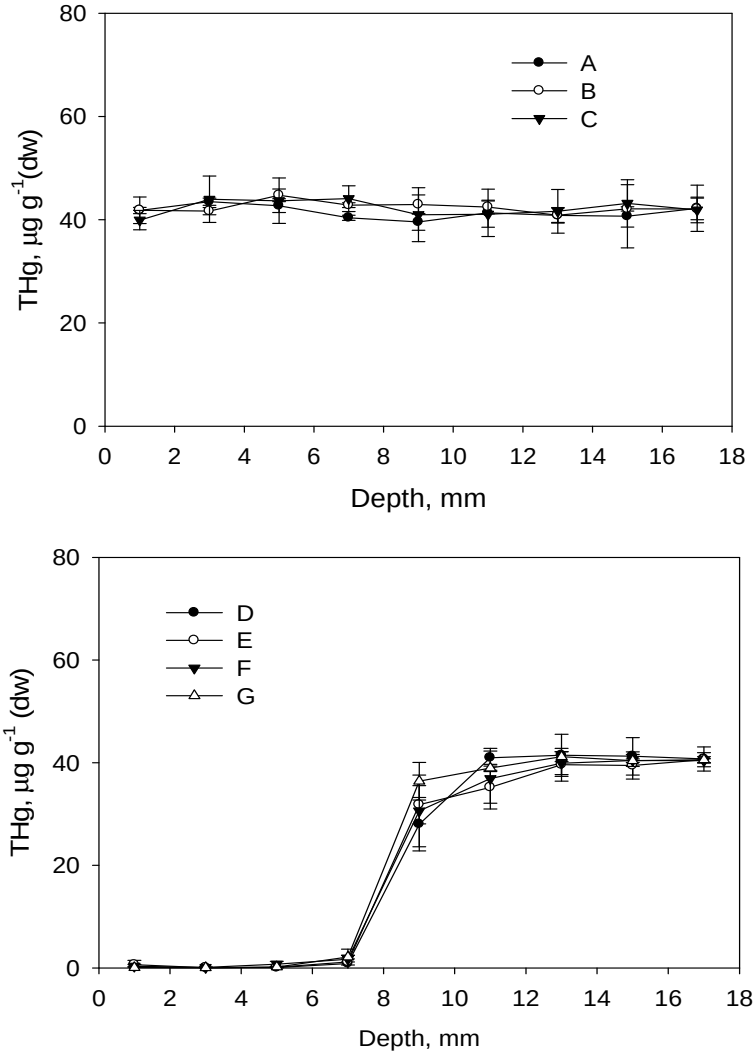

Figure 6.11 Total Hg profiles in sediment/caps

Each depth shown in the figure represents the average depth of each section. For example, the first section was from "0" to "2 mm" and is represented as "1 mm" in depth.

Modeling was performed for uncapped cell A and capped cell D, using Eq. 3.4 and Eq. 3.5. The value of ka is 5.5×10^{-8} m s^{-1}. The estimated bulk density ρ_b and ε_w for sediment in cell A are 267 g L^{-1} and 0.89 respectively. The estimated bulk density ρ_b and ε_w for sediment under the cap in cell D are 420 g L^{-1} and 0.79 respectively. The sand properties are the same as those shown in Section 3.3. Because there were always some sediment particles in sand caused by intermixing, a value of 2.2 L g^{-1} was selected as the partition coefficient between sand and pore

water instead of the measure value 0.038 L g^{-1} for clean sand. The parameters used for modeling are shown in Table 6.3.

Table **6.3** Parameters for modeling simulation

	Cap/ Uncapped situation	Layer	t day	$D_{THg(eff)}$ m^2 s^{-1}	R_f	C_{THg0} ng L^{-1}	Solid-water Kd L g^{-1}
Cell A	Uncapped	Sediment	273	5.4×10^{-10}	97200	110	364
Cell D	Capped	Cap	273	1.5×10^{-10}	3420	0	2.2
		Sediment		5.5×10^{-10}	153000	110	364

For uncapped cell A, THg concentration decrease in the sediment is observed only in the surface sediment with depth less than 2 mm (Fig. 6.12). Mercury from the sediment is released to the overlying water directly. This is consistent with the experimental observations shown in Fig. 6.11.

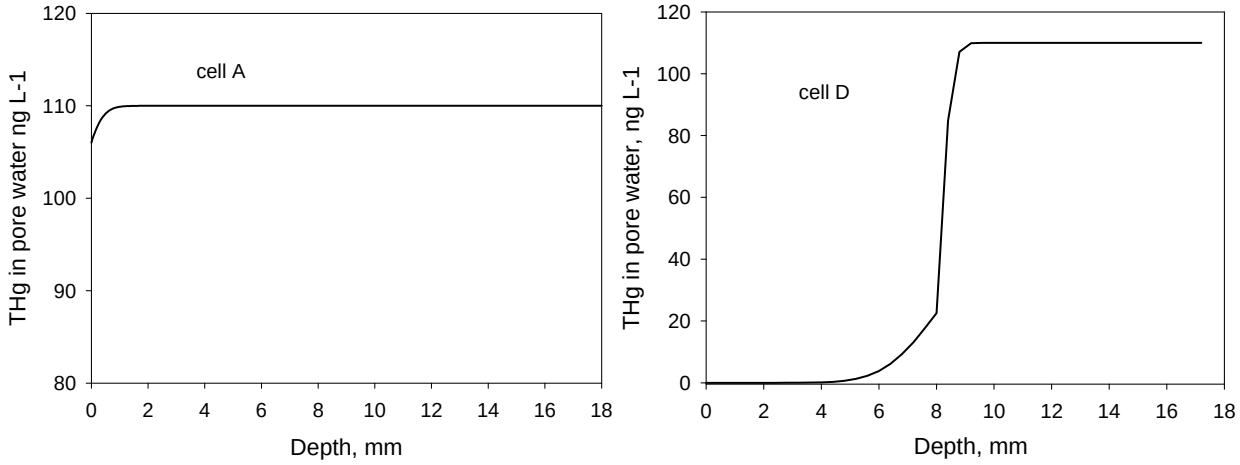

Figure 6.12 Modeling total Hg profiles in sediment/caps

For capped cell D, THg concentration decrease in the sediment is observed in the sediment with depth also less than 2 mm (Fig. 6.12). Significant increase of THg with a 2 mm thickness is shown in the cap above the sediment layer. Therefore, decrease in THg observed in

the first section of sediment and increase in THg observed in the last section of the cap (Fig.11) were also caused by mass transfer besides the intermixing. The released mercury from sediment was contained in the sand cap and no significant release of mercury into the overlying water occurs.

6.2.6 Inhibition of Mercury Methylation

Section samples from duplicate 1 of cells A, C, D and G were analyzed for MeHg. Total Hg concentration had little variation in sediments of these 4 cells except the first section in capped cells caused by intermixing between cap and sediment (Fig. 6.13b). Contrary to the uniformity of THg in sediment, variations in the distribution of MeHg in sediment were observed (6.13a).

For uncapped cells A and C, MeHg concentration first increased and then decreased quickly and maintained approximately uniform at this low concentration. It should be noted that the depth of each data point shown on Fig. 6.13 represents the average of the starting depth and ending depth for each section. MeHg in sediment for cells A and C exhibited similar variation. For each of these two uncapped cells, in the top 12 mm sediment, MeHg concentration first increased to reach a maximum and then decreased. In the sediment below 12 mm, MeHg was maintained approximately uniform at this value. This is consistent with the observations that MeHg production occurs most actively in the surface layer of sediments and the thickness of the active layer varies, such as 0-2.5 cm (Han et al., 2007), 0-3 cm (Bloom et al., 1999), 0-15cm (Sunderland et al., 2004). In this study, it was 0-1.2 cm in the sediment of the simulation cells, which is smaller than those observed under field conditions.

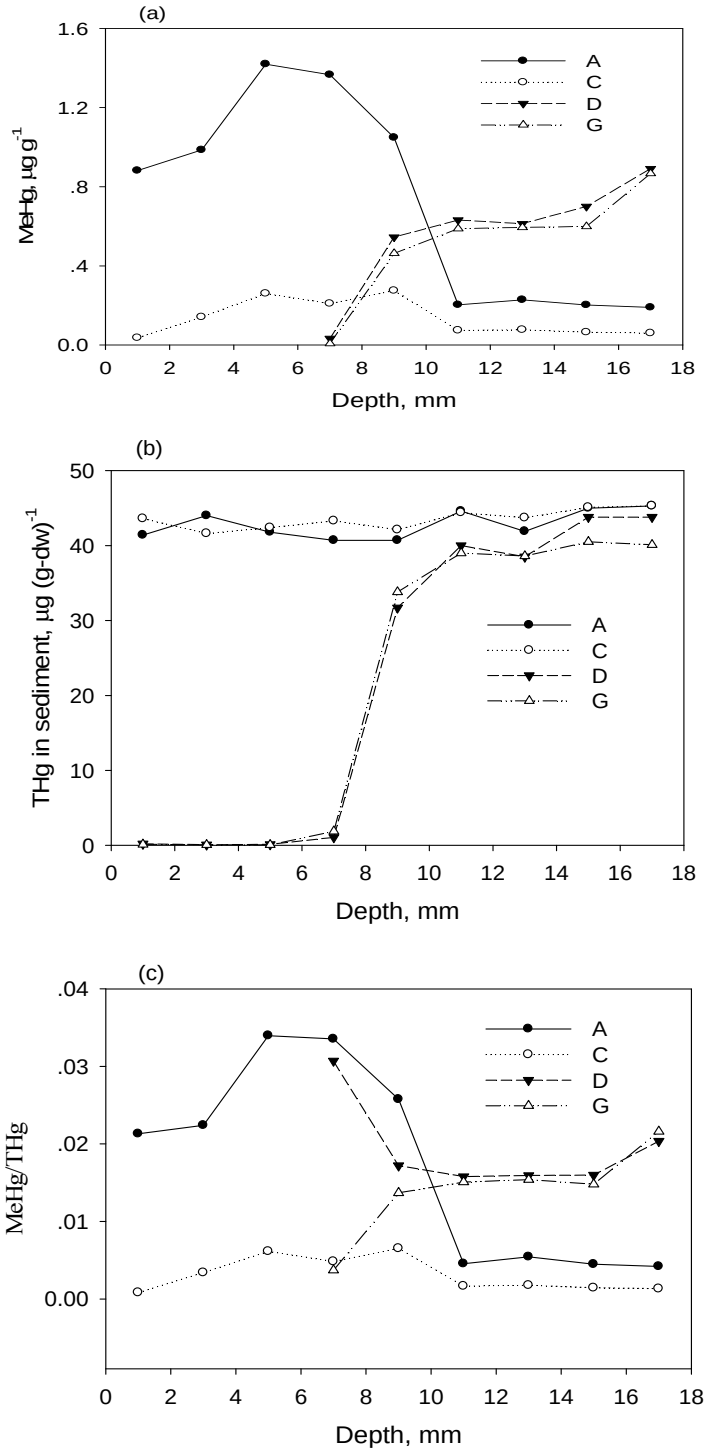

Figure 6.13 MeHg in cells A, C, D and G
MeHg profiles in sediment/cap of duplicate 1 (b) total Hg profiles in sediment/cap of duplicate 1 (c) MeHg/THg ratio in sediment/cap of duplicate 1

In capped cells, because THg concentration for the first 3 samples of the cap lay was close to zero, MeHg analysis was not conducted. Overall, MeHg concentration decreased because of the placement of cap. The profile of MeHg concentration in cell D is very close to that in cell G and it is difficult to see apparent inhibition effect of the amended Syn-FeS (Fig. 6.13a). However, for the first two points shown in Fig. 6.13c, MeHg/THg ratios in cell G are smaller than those in cell D. For cell D, the MeHg/THg ratios for the first two points were very close to those of uncapped cell A, which did not have amendment of Syn-FeS. For cell G, MeHg/THg ratio for the first point was very close to that of uncapped cell C at the same depth, which had amendment of 4.4% (wt) of Syn-FeS, and this ratio for the second point was higher compared to that of cell C. For cell G, the first point at depth 7 mm stands for section 6-8 mm, the last sample of cap layer. Appropriate THg concentration for this section was 1.86 μg $(g\text{-}dw)^{-1}$, which means that the cap in this section was mixed with approximately 4.7% (wt) sediment and Syn-FeS counted about 24% (wt) of the sample. The second point at depth 9 mm stands for section 8-10 mm, the first layer of the sediment beneath cap. Appropriate THg concentration for this section was 33.8 μg $(g\text{-}dw)^{-1}$, which means that sediment in this section was mixed with approximately 15.5% (wt) cap material and Syn-FeS was estimated to be 3.9% (wt) in the sample.

MeHg/THg ratio varied from 0.42% to 3.4% in sediment of cell A, 0.08% to 0.65% in sediment of cell C, 1.6% to 3.1% and 0.37% to 2% in cap and sediment of cell D and cell G respectively. With amendment of FeS, MeHg production was inhibited in sediment.

6.3 Summary

The introduction of FeS creates a more reducing condition in the surface sediment of the uncapped cell and in the sediment beneath the cap of the capped cell. The oxidation of FeS amended into sand cap led to the release of additional H^+ and sulfate ions into overlying water, thus the pH of the effluent water decreased. If the sand cap over the layer amended with FeS is thick enough to produce a reducing condition, the oxidation of FeS would not occur.

Amended FeS either in sediment or cap blocked mercury from being released into overlying water. Contrary to the uniformity of THg in sediment of uncapped cells, variations in the distribution of MeHg in sediment existed. Methylation was most active in the surface sediment and the maximum concentration of MeHg occured a few millimeters below the sediment surface. With amendment of FeS, the distribution of MeHg followed the same trend as that without addition of FeS, but MeHg/THg ratio was much lower. When FeS was amended into the cap, MeHg/THg ratio was decreased in the intermixing zone between the cap and sediment. Overall, the amendment of FeS inhibited the transformation of mercury to MeHg.

Chapter 7 Conclusions and Recommendations

7.1 Conclusions

7.1.1 Conventional Capping with Sand

Laboratory simulation cells were employed to evaluate the effectiveness of a sand cap for containing mercury-contaminated sediments and the resultant impacts on the mercury fate beneath the cap. Experimental observations in simulations cells with a 10 mm sand cap showed no significant mercury migration into a cap layer over a period of approximately 8 months. The total mercury flux in the overlying water was undetectable for the capped case, compared to that from uncapped sediment. This indicates that the sand cap can delay and reduce the migration of mercury into the overlying water. Experimental observations also showed that the presence of a cap decreased the proportion of MeHg. Redox potential and oxygen concentration measurements showed aerobic conditions extended only a few millimeters into the sand cap, causing reducing conditions throughout the underlying contaminated sediment. It is postulated that the sediment beneath the cap was less conducive to mercury methylation which tends to occur at the sediment surface where microbial activity is high and newly sedimented highly degradable organic carbon is concentrated.

Modeling results show that capping material with higher partitioning coefficient of mercury between the solid and pore water has a high capacity to delay mercury release and contain mercury released from sediment. With a 300 mm cap which has a partitioning coefficient similar to clean sediment for mercury, the released mercury from sediment beneath the cap only

penetrates about 1 quarter of the cap and no significant mercury has been released into the water in 2000 years. Under field conditions, the mass transfer coefficient ka might be larger due to the larger energy of flowing water. Also, mercury release rate may be significantly increased by the destruction of the cap layer from the disturbance caused by human activities, ground water flow and burrowing organism, etc. Thus, the modeling results represent the case under ideal conditions.

7.1.2 Iron sulfides and Inhibition of Mercury Methylation

By amending either Syn-FeS or a commercial iron sulfide (CIS) into sediment slurries spiked with Hg(II) (from $HgCl_2$ solution) under anoxic conditions, the inhibition effects of iron sulfides on the methylation of mercury were investigated. Analysis of XRPD spectra of CIS indicated that CIS was a mixture of the oxidation products of FeS, which included but were not limited to Mackinawite (FeS), Greigite (Fe_3S_4), Pyrrhotite ($Fe_{1-x}S$), Pyrite (FeS_2) and elemental sulfur (S^0). Experimental results showed that both Syn-FeS and CIS were good inhibitors of Hg(II) methylation. With an amended concentration of 0.5 mmol (g-dry weight)$^{-1}$, MeHg produced was 3.6% for Syn-FeS and 5.3% for CIS of that produced in the control experiments. Larger surface area and higher content of iron sulfide possibly helped explain why Syn-FeS was more effective as compared to CIS. Total dissolved mercury (THg_D) in sediment slurry decreased with the increase of amended Syn-FeS concentration and increased with the increase of amended CIS concentration, but the change was not as significant as the decrease of MeHg in the sediment slurries. The results indicated that MeHg production was not correlated to THg_D in these experiments.

The amendment of sulfides into sediment slurries can greatly inhibit the formation of MeHg. The effectiveness of the CIS indicates that other species of iron sulfides also worked effectively in the inhibition of Hg(II) methylation. The oxidation of FeS does not significantly reduce its effectiveness regarding the inhibition of Hg(II) methylation. Thus, it should be possible to reduce the MeHg concentration in the surface sediments by placing a layer of solid FeS between the mercury contaminated sediments and a layer of conventional sand cap, even if the oxidation of FeS occurs.

7.1.3 Iron Sulfides and Mobility of Mercury

As one of the major constituents of AVS in anoxic sediments, mackinawite (FeS) is known for its ability to scavenge trace metals. The interaction between aqueous Hg(II) (added as $HgCl_2$) and Syn-FeS (which was proved to be mackinawite) was studied via batch sorption experiments conducted under anaerobic conditions. Due to the release of H^+ ions during formation of hydrolyzed Hg(II) species which is more reactive than Hg^{2+} in surface adsorption, the equilibrium pH decreased with the increase in Hg(II)/FeS molar ratio. Counteracting the loss of FeS solids at lower pH, the maximum capacity for FeS to remove aqueous Hg(II) was approximately 0.75 mol Hg(II) (mol FeS)$^{-1}$. The comparison of XRPD patterns of Syn-FeS sorbent before and after sorption showed that the major products formed from the interaction between Syn-FeS and the aqueous Hg(II) were metacinnabar, cinnabar, and mercury iron sulfides.

At low initial pH of Hg(II) solutions under low to moderate Hg(II) loadings, equilibrium pH increases by consuming H^+ via dissolution of FeS. As long as there is no significant loss of FeS by dissolution, the effects of pH on immobilization of Hg(II) are very small. With higher

Hg(II)/FeS loadings, even at a neutral initial pH, the equilibrium pH decreases because less unreacted FeS is present to neutralize H^+ released by hydrolysis of Hg(II) which is promoted by adsorption.

Because of the low solubility of mercury sulfides compared to FeS, FeS has a great capacity to remove Hg(II) from solution. Although sorption process of Hg(II) to FeS includes both precipitation and adsorption, the primary mechanism for FeS to immobilize Hg(II) is via precipitation, which accounts about 77% of total Hg(II) immobilized.

CIS is also good at immobilizing Hg(II) but not as good as pure FeS. Therefore, the oxidation of iron sulfide mineral decreases its ability to immobilize Hg(II). Because FeS is very reactive to oxygen, steps should be taken to stabilize FeS before it can be applied as a component of an active capping material. Once Hg(II) is removed, no significant mercury will be released into water when the system is expose to oxidizing conditions. Oxidation product FeOOH, precipitation products HgS and (Hg,Fe)S of FeS might be the most important mechanism for the retention of released Hg(II) after the oxidation of FeS.

7.1.4 Remediation of Mercury-Contaminated Sediment with Iron Sulfides

The introduction of iron sulfides creates a more reducing condition in the surface sediment of the uncapped cell and in the sediment beneath the cap of the capped cell. The oxidation of FeS amended into sand cap leads to the releases of additional H^+ and sulfate ions into overlying water, thus the pH of the effluent water decreases. With 3 mm sand cap over the layer amended with FeS, the oxidation occurred only at the interface between sand layer and the mixed layer during 9 months. Approaching the end of the experiment, the system approximately

reached an equilibrium state and the release rate of both ions was close to zero. If the sand cap over the layer amended FeS is thick enough to produce a reducing condition, the oxidation of FeS would not occur.

Amendment of FeS in uncapped sediment can reduce the release of mercury by two means. First, a layer of brown crust formed from the oxidation products of iron sulfides fixes fine sediment particles at the sediment surface. Second, it is by its reaction with Hg(II) and binding of mercury to its surface, and thus reduce THg concentration in pore water. With FeS amended into sand as cap, from the analysis of effluent water, there was no apparent mercury released into the overlying water compared to the blank experiment, which had only DI water in the cell. This is also confirmed by the THg profile in the cap and sediment. The increase of THg concentration in the last section of cap and the decrease of THg concentration in the first section of sediment in each capped cell were caused by the intermixing between cap and sediment at the cap-sediment interface. Mixing between cap and sediment particles at the interface was practically impossible to avoid in the simulation cells. Even for uncapped cell, mercury migration was not significant during 9 months because of the strong binding of mercury to solid phase.

Contrary to the uniformity of THg in sediment of uncapped cells, variations in the distribution of MeHg in sediment existed. Methylation was most active in the surface sediment and the maximum concentration of MeHg occured a few millimeters below the sediment surface. With amendment of FeS, the distribution of MeHg followed the same trend as that without addition of FeS, but MeHg/THg ratio was much lower. When FeS was amended into the cap, MeHg/THg ratio was decreased in the intermixing zone between the cap and sediment. Overall, the amendment of FeS inhibits the transformation of mercury to MeHg.

7.2 Recommendations

7.2.1 Mechanism of Inhibition of Iron Sulfides on Mercury Methylation

The mechanism of the methylation processes in sediment itself is still a question. It has been suggested that lipid soluble species such as $HgCl_2$ or HgS_0 (aq) may diffuse passively through biological membranes and thus be available for methylation (Jay et al., 2000). Studies with certain bacteria suggest that uptake of Hg(II) very likely occurs by a facilitated mechanism rather than by passive diffusion of neutrally charged Hg(II) species across the cell membrane, and the uptake of Hg(II) under anaerobic conditions was not proportional to the abundance of neutrally charged mercury species but was dependent on the total concentration of mercury in the samples (Golding et al., 2002; Kelly et al., 2003).

Correspondingly, there are two different mechanisms that have been suggested for the inhibition of mercury methylation by sulfides in sediment pore water. One is that the reduced MeHg production is caused by the reduction in the solubility of Hg(II) ions via precipitation of HgS(s) (Compeau and Bartha, 1983; Winfrey and Rudd, 1990). The other suggests that it could be due to the lower neutral mercury complexes concentration associated with the formation of charged Hg-polysulfide complexes in pore water (Benoit et al., 2001).

To understand the actual mechanism of sulfide inhibition effects on mercury methylation, it is necessary to understand what species of mercury in the sediments are bioavailable for the sulfate reducing bacteria and what happens to the bacteria after addition of FeS. In this work, no attention was paid on the behavior of bacteria. Further study with focus on the behavior of bacteria during the process might help reveal the mystery.

7.2.2 Effective Methods to Make FeS Applicable Under In-Situ Conditions

The oxidation of FeS with the presence of water eventually leads to the formation of FeOOH, H^+ and sulfate. Therefore, the oxidation of FeS decreases its effectiveness in containing mercury and may also decrease its effectiveness in inhibiting the methylation of mercury. From the simulation experiment, the oxidation was caused mainly by oxygen dissolved in water. Two methods may be effective to prevent the oxidation of FeS in cap: one is to place a layer of a layer of stable material over FeS layer to generate an anaerobic condition and the other is to stabilize FeS to prevent its oxidation.

Syn-FeS is composed of nanosized particles. For laboratory investigation purpose only, it was mixed with sand and placed over the sediment before the initiation of water. Under field conditions, the capping material has to be spread over the sediment, passing through the water column. Because of the nanosized property of Syn-FeS, mechanical methods relying on gravitational settling of cap materials in the water column may not be appropriate. The settling process would be very slow and FeS would be partially oxidized in anoxic water during settling. Therefore, it is important to make FeS in a form easy for application. This may be combined with the stabilization of FeS.

7.2.3 Natural Iron Sulfide Ore

Though Syn-FeS is very effective at containing and inhibiting the methylation of mercury, it might not be economical to use it in the cap. The natural iron sulfide minerals might be a good choice for field application.

Pyrrhotite (FeS) and pyrite (FeS_2) ores seem good candidates for field application. Iron sulfides have great affinity for mercuric ions, evidenced by the solubility product for HgS, the sorption study of Hg(II) on iron sulfide minerals (Brown et al., 1979), and our study using CIS as sorbent. Major sulfide components in CIS are Mackinawite (FeS), Greigite (Fe_3S_4), Pyrrhotite ($Fe_{1-x}S$, mainly in form Fe_7S_8) and Pyrite (FeS_2). Also, the slurry experiments in Chapter 5 demonstrates that CIS is a good inhibitor of mercury methylation.

Iron sulfides are common minerals to mined throughout the world and usually may be quite accessible in localities where mercury contamination is dominant. For example, most massive sulfide mining operations (Pb, Zn, Cu) separate and discard huge amounts (thousands of tons) of iron sulfides annually (Brown et al., 1979).

The major problem with the application of iron sulfide minerals is possibly the acidification of the water system caused by the oxidation of the minerals. The oxidation of the iron sulfide minerals can be minimized by placing a layer of sand over the mineral layer.

Bibliography

Allen, H. E., Fu, G. M., and Deng, B. L. (1993). Analysis of Acid-Volatile Sulfide (AVS) and Simultaneously Extracted Metals (SEM) for the Estimation of Potential Toxicity in Aquatic Sediments. *Environmental Toxicology and Chemistry,* 12(8), 1441-1453.

Alli, A., Jaffe, R., and Jones, R. (1994). Analysis of Organomercury Compounds in Sediments by Capillary GC with Atomic Fluorescence Detection. *Hrc-Journal of High Resolution Chromatography,* 17(11), 745-748.

Aminzaki, L., Elhassani, S., Majeed, M. A., Clarkson, T. W., Doherty, R. A., et al. (1976). Perinatal Methylmercury Poisoning in Iraq. *American Journal of Diseases of Children,* 130(10), 1070-1076.

Andersson, P., Borg, H., and Karrhage, P. (1995). Mercury in Fish Muscle in Acidified and Limed Lakes. *Water Air and Soil Pollution,* 80(1-4), 889-892.

Arakaki, T. and Morse, J. W. (1993). Coprecipitation and Adsorption of Mn(II) with Mackinawite (FeS) under Conditions Similar to Those Found in Anoxic Sediments. *Geochimica Et Cosmochimica Acta,* 57(1), 9-14.

Azcue, J. M., Zeman, A. J., Mudroch, A., Rosa, F., and Patterson, T. (1998). Assessment of Sediment and Porewater after One Year of Subaqueous Capping of Contaminated Sediments in Hamilton Harbour, Canada. *Water Science and Technology,* 37(6-7), 323-329.

Babiarz, C. L., Hurley, J. P., Hoffmann, S. R., Andren, A. W., Shafer, M. M., et al. (2001). Partitioning of Total Mercury and Methylmercury to the Colloidal Phase in Freshwaters. *Environmental Science & Technology,* 35(24), 4773-4782.

Bakir, F., Damluji, S. F., Aminzaki, L., Murtadha, M., Khalidi, A., et al. (1973). Methylmercury Poisoning in Iraq - Interuniversity Report. *Science,* 181(4096), 230-241.

Barkay, T., Gillman, M., and Turner, R. R. (1997). Effects of Dissolved Organic Carbon and Salinity on Bioavailability of Mercury. *Applied and Environmental Microbiology,* 63(11), 4267-4271.

Barrow, N. J. and Cox, V. C. (1992). The Effects of pH and Chloride Concentration on Mercury Sorption .1. By Goethite. *Journal of Soil Science,* 43(2), 295-304.

Barrow, N. J. and Cox, V. C. (1992). The Effects of pH and Chloride Concentration on Mercury Sorption .2. By a Soil. *Journal of Soil Science,* 43(2), 305-312.

Behra, P., Bonnissel-Gissinger, P., Alnot, M., Revel, R., and Ehrhardt, J. J. (2001). XPS and XAS Study of the Sorption of Hg(II) onto Pyrite. *Langmuir,* 17(13), 3970-3979.

Benning, L. G., Wilkin, R. T., and Barnes, H. L. (2000). Reaction Pathways in the Fe-S System below 100 Degrees C. *Chemical Geology,* 167(1-2), 25-51.

Benoit, J. M., Gilmour, C. C., and Mason, R. P. (2001). Aspects of Bioavailability of Mercury for Methylation in Pure Cultures of Desulfobulbus Propionicus (1pr3). *Applied and Environmental Microbiology,* 67(1), 51-58.

Benoit, J. M., Gilmour, C. C., Mason, R. P., and Heyes, A. (1999). Sulfide Controls on Mercury Speciation and Bioavailability to Methylating Bacteria in Sediment Pore Waters. *Environmental Science & Technology,* 33(6), 951-957.

Benoit, J. M., Gilmour, C. C., Mason, R. P., Riedel, G. S., and Riedel, G. F. (1998). Behavior of Mercury in the Patuxent River Estuary. *Biogeochemistry,* 40(2-3), 249-265.

Benoit, J. M., Mason, R. P., and Gilmour, C. C. (1999). Estimation of Mercury-Sulfide Speciation in Sediment Pore Waters Using Octanol-Water Partitioning and Implications for Availability to Methylating Bacteria. *Environmental Toxicology and Chemistry,* 18(10), 2138-2141.

Berman, M. and Bartha, R. (1986). Levels of Chemical Versus Biological Methylation of Mercury in Sediments. *Bulletin of Environmental Contamination and Toxicology,* 36(3), 401-404.

Berner, R. A. (1962). Tetragonal Iron Sulfide. *Science,* 137(3531), 669-&.

Berner, R. A. (1964). Iron Sulfides Formed from Aqueous Solution at Low Temperatures and Atmospheric Pressure. *Journal of Geology,* 72(3), 293-306.

Berner, R. A. (1970). Sedimentary Pyrite Formation. *American Journal of Science,* 268(1), 1-23.

Bloom, N. (1989). Determination of Picogram Levels of Methylmercury by Aqueous Phase Ethylation, Followed by Cryogenic Gas-Chromatography with Cold Vapor Atomic Fluorescence Detection. *Canadian Journal of Fisheries and Aquatic Sciences,* 46(7), 1131-1140.

Bloom, N. S. (1992). On the Chemical Form of Mercury in Edible Fish and Marine Invertebrate Tissue. *Canadian Journal of Fisheries and Aquatic Sciences,* 49(5), 1010-1017.

Bloom, N. S., Gill, G. A., Cappellino, S., Dobbs, C., McShea, L., et al. (1999). Speciation and cycling of mercury in Lavaca Bay, Texas, sediments. *Environmental Science & Technology,* 33(1), 7-13.

Bloom, N. S. and Preus, E. *Anoxic Sediment Incubation to Assess the Methylation Potential of Mercury Contaminated Solids.* Paper presented at the 2nd International symposium Contaminated Sediment, Ectoxicology, Quebec, Canada (2003, May 26-28).

Bloom, N. S., Watras, C. J., and Hurley, J. P. (1991). Impact of Acidification on the Methylmercury Cycle of Remote Seepage Lakes. *Water Air and Soil Pollution,* 56, 477-491.

Bodaly, R. A., Hecky, R. E., and Fudge, R. J. P. (1984). Increases in Fish Mercury Levels in Lakes Flooded by the Churchill River Diversion, Northern Manitoba. *Canadian Journal of Fisheries and Aquatic Sciences,* 41(4), 682-691.

Bonnissel-Gissinger, P., Alnot, M., Lickes, J. P., Ehrhardt, J. J., and Behra, P. (1999). Modeling the Adsorption of Mercury(II) on (hydr)oxides II: Alpha-FeOOH (Goethite) and Amorphous Silica. *Journal of Colloid and Interface Science,* 215(2), 313-322.

Boszke, L., Kowalski, A., Glosinska, G., Szarek, R., and Siepak, J. (2003). Environmental Factors Affecting Speciation of Mercury in the Bottom Sediments; An Overview. *Polish Journal of Environmental Studies,* 12(1), 5-13.

Brouwer, H. and Murphy, T. (1995). Volatile Sulfides and Their Toxicity in Fresh-Water Sediments. *Environmental Toxicology and Chemistry,* 14(2), 203-208.

Brouwer, H. and Murphy, T. P. (1994). Diffusion Method for the Determination of Acid-Volatile Sulfides (AVS) in Sediment. *Environmental Toxicology and Chemistry,* 13(8), 1273-1275.

Brown, G. E. and Parks, G. A. (2001). Sorption of Trace Elements on Mineral Surfaces: Modern Perspectives from Spectroscopic Studies, and Comments on Sorption in the Marine Environment. *International Geology Review,* 43(11), 963-1073.

Brown, J. R., Bancroft, G. M., Fyfe, W. S., and Mclean, R. A. N. (1979). Mercury Removal from Water by Iron Sulfide Minerals - Electron-Spectroscopy for Chemical-Analysis (ESCA) Study. *Environmental Science & Technology,* 13(9), 1142-1144.

Burton, E. D., Bush, R. T., and Sullivan, L. A. (2006). Acid-Volatile Sulfide Oxidation in Coastal Flood Plain Drains: Iron-Sulfur Cycling and Effects on Water Quality. *Environmental Science & Technology,* 40(4), 1217-1222.

Cai, Y., Jaffe, R., Alli, A., and Jones, R. D. (1996). Determination of Organomercury Compounds in Aqueous Samples by Capillary Gas Chromatography Atomic Fluorescence Spectrometry Following Solid-Phase Extraction. *Analytica Chimica Acta,* 334(3), 251-259.

Callister, S. M. and Winfrey, M. R. (1986). Microbial Methylation of Mercury in Upper Wisconsin River Sediments. *Water Air and Soil Pollution,* 29(4), 453-465.

Canfield, D. E., Raiswell, R., and Bottrell, S. (1992). The Reactivity of Sedimentary Iron Minerals toward Sulfide. *American Journal of Science,* 292(9), 659-683.

Carpi, A., and Lindberg S.E. (1997). Sunlight-Mediated Emission of Elemental Mercury from Soil Amended with Municipal Sewage Sludge. *Environmental Science and Technology*, 31(7), 2085-2091.

Celo, V., Lean, D. R. S., and Scott, S. L. (2006). Abiotic Methylation of Mercury in the Aquatic Environment. *Science of the Total Environment,* 368(1), 126-137.

Chen, Y., Bonzongo, J. C., and Miller, G. C. (1996). Levels of Methylmercury and Controlling Factors in Surface Sediments of The Carson River System, Nevada. *Environmental Pollution,* 92(3), 281-287.

Chen, Y., Bonzongo, J. C. J., Lyons, W. B., and Miller, G. C. (1997). Inhibition of Mercury Methylation in Anoxic Freshwater Sediment by Group VI Anions. *Environmental Toxicology and Chemistry,* 16(8), 1568-1574.

Choy, B. and Reible, D. D. (2001). *Diffusion Model of Environmental Transport*. Lewis Publishers, New York.

Coles, C. A., Rao, S. R., and Yong, R. N. (2000). Lead and Cadmium Interactions with Mackinawite: Retention Mechanisms and the Role of pH. *Environmental Science & Technology,* 34(6), 996-1000.

Compeau, G. and Bartha, R. (1983). Effects of Sea Salt Anions on the Formation and Stability of Methylmercury. *Bulletin of Environmental Contamination and Toxicology,* 31(4), 486-493.

Compeau, G. and Bartha, R. (1984). Methylation and Demethylation of Mercury under Controlled Redox, pH, and Salinity Conditions. *Applied and Environmental Microbiology,* 48(6), 1203-1207.

Compeau, G. C. and Bartha, R. (1985). Sulfate-Reducing Bacteria - Principal Methylators of Mercury in Anoxic Estuarine Sediment. *Applied and Environmental Microbiology,* 50(2), 498-502.

Davison, W. (1991). The Solubility of Iron Sulfides in Synthetic and Natural-Waters at Ambient-Temperature. *Aquatic Sciences,* 53(4), 309-329.

Davison, W., Phillips, N., and Tabner, B. J. (1999). Soluble Iron Sulfide Species in Natural Waters: Reappraisal of Their Stoichiometry and Stability Constants. *Aquatic Sciences,* 61(1), 23-43.

DeLaune, R. D., Jugsujinda, A., Devai, I., and Patrick, W. H. (2004). Relationship of Sediment Redox Conditions to Methyl Mercury in Surface Sediment of Louisiana Lakes. *Journal of*

Environmental Science and Health Part a-Toxic/Hazardous Substances & Environmental Engineering, 39(8), 1925-1933.

Drever, J. I. (1997). *The Geochemistry of Natural Waters: Surface and Groundwater Environments.* (3rd ed.). Prentice Hall, Upper Saddle River, N.J.

Dyrssen, D. and Kremling, K. (1990). Increasing Hydrogen-Sulfide Concentration and Trace-Metal Behavior in the Anoxic Baltic Waters. *Marine Chemistry,* 30(1-3), 193-204.

Ehrhardt, J. J., Behra, P., Bonnissel-Gissinger, P., and Alnot, M. (2000). XPS Study of the Sorption of Hg(II) onto Pyrite FeS_2. *Surface and Interface Analysis,* 30(1), 269-272.

Ekstrom, E. B., Morel, F. M. M., and Benoit, J. M. (2003). Mercury Methylation Independent of the Acetyl-Coenzyme a Pathway in Sulfate-Reducing Bacteria. *Applied and Environmental Microbiology,* 69(9), 5414-5422.

Fabbri, D., Locatelli, C., Snape, C. E., and Tarabusi, S. (2001). Sulfur Speciation in Mercury-Contaminated Sediments of a Coastal Lagoon: the Role of Elemental Sulfur. *Journal of Environmental Monitoring,* 3(5), 483-486.

Fleming, E. J., Mack, E. E., Green, P. G., and Nelson, D. C. (2006). Mercury Methylation from Unexpected Sources: Molybdate-Inhibited Freshwater Sediments and an Iron-Reducing Bacterium. *Applied and Environmental Microbiology,* 72(1), 457-464.

Fujiki, M. and Tajima, S. (1992). The Pollution of Minamata Bay by Mercury. *Water Science and Technology,* 25(11), 133-140.

Furutani, A. and Rudd, J. W. M. (1980). Measurement of Mercury Methylation in Lake Water and Sediment Samples. *Applied and Environmental Microbiology,* 40(4), 770-776.

Gambrell, R. P., DeLaune, R. D., Patrick, W. H., and Jugsujinda, A. (2001). Mercury Distribution in Sediment Profiles of Six Louisiana Lakes. *Journal of Environmental Science and Health Part a-Toxic/Hazardous Substances & Environmental Engineering,* 36(5), 661-676.

Ganguli, P. M., Mason, R. P., Abu-Saba, K. E., Anderson, R. S., and Flegal, A. R. (2000). Mercury Speciation in Drainage from the New Idria Mercury Mine, California. *Environmental Science & Technology,* 34(22), 4773-4779.

Garbaciak, S., Spadaro, P., Thornburg, T., and Fox, R. (1998). Sequential Risk Mitigation and the Role of Natural Recovery in Contaminated Sediment Projects. *Water Science and Technology,* 37(6-7), 331-336.

Gilmour, C. C. and Henry, E. A. (1991). Mercury Methylation in Aquatic Systems Affected by Acid Deposition. *Environmental Pollution,* 71(2-4), 131-169.

Gilmour, C. C. and Henry, E. A. (1992). Mercury Methylation by Sulfate-Reducing Bacteria - Biogeochemical and Pure Culture Studies. *Abstracts of Papers of the American Chemical Society,* 203, 140-GEOC.

Gilmour, C. C., Henry, E. A., and Mitchell, R. (1992). Sulfate Stimulation of Mercury Methylation in Fresh-Water Sediments. *Environmental Science & Technology,* 26(11), 2281-2287.

Gilmour, C. C., Riedel, G. S., Ederington, M. C., Bell, J. T., Benoit, J. M., et al. (1998). Methylmercury concentrations and Production Rates across a Trophic Gradient in the Northern Everglades. *Biogeochemistry,* 40(2-3), 327-345.

Golding, G. R., Kelly, C. A., Sparling, R., Loewen, P. C., Rudd, J. W. M., et al. (2002). Evidence for Facilitated Uptake of Hg(II) by Vibrio Anguillarum And Escherichia Coli under Anaerobic and Aerobic Conditions. *Limnology and Oceanography,* 47(4), 967-975.

Grieb, T. M., Driscoll, C. T., Gloss, S. P., Schofield, C. L., Bowie, G. L., et al. (1990). Factors Affecting Mercury Accumulation in Fish in the Upper Michigan Peninsula. *Environmental Toxicology and Chemistry,* 9(7), 919-930.

Guimaraes, J. R. D., Ikingura, J., and Akagi, H. (2000). Methyl Mercury Production and Distribution in River Water-Sediment Systems Investigated through Radiochemical Techniques. *Water Air and Soil Pollution,* 124(1-2), 113-124.

Guimaraes, J. R. D., Meili, M., Malm, O., and Brito, E. M. D. (1998). Hg Methylation in Sediments and Floating Meadows of a Tropical Lake in the Pantanal Floodplain, Brazil. *Science of the Total Environment,* 213(1-3), 165-175.

Gunneriusson, L. and Sjoberg, S. (1993). Surface Complexation in the H^+-Goethite (Alpha-FeOOH)-Hg(II)-Chloride System. *Journal of Colloid and Interface Science,* 156(1), 121-128.

Hall, B. D., St Louis, V. L., Rolfhus, K. R., Bodaly, R. A., Beaty, K. G., et al. (2005). Impacts of Reservoir Creation on the Biogeochemical Cycling of Methyl Mercury and Total Mercury in Boreal Upland Forests. *Ecosystems,* 8(3), 248-266.

Hamasaki, T., Nagase, H., Sato, T., Kito, H., and Ose, Y. (1991). Production of Methyltin Compounds Related to Possible Conditions in the Environment. *Applied Organometallic Chemistry,* 5(2), 83-90.

Hamblin, P. F., Zhu, D. Z., Chiocchio, F., He, C., and Charlton, M. N. (2000). Monitoring Suspended Sediment Plumes by Optical and Acoustical Methods with Application to Sand Capping. *Canadian Journal of Civil Engineering,* 27(1), 125-137.

Hammerschmidt, C. R. and Fitzgerald, W. F. (2004). Geochemical Controls on the Production and Distribution of Methylmercury in Near-Shore Marine Sediments. *Environmental Science & Technology,* 38(5), 1487-1495.

Hammerschmidt, C. R. and Fitzgerald, W. F. (2006). Photodecomposition of Methylmercury in an Arctic Alaskan Lake. *Environmental Science & Technology,* 40(4), 1212-1216.

Han, S., Obraztsova, A., Pretto, P., Choe, K. Y., Gieskes, J., et al. (2007). Biogeochemical Factors Affecting Mercury Methylation in Sediments of the Venice Lagoon, Italy. *Environmental Toxicology and Chemistry,* 26(4), 655-663.

Harada, M. (1995). Minamata Disease - Methylmercury Poisoning in Japan Caused by Environmental-Pollution. *Critical Reviews in Toxicology,* 25(1), 1-24.

Harmon, S. M., King, J. K., Gladden, J. B., and Newman, L. A. (2007). Using Sulfate-Amended Sediment Slurry Batch Reactors to Evaluate Mercury Methylation. *Archives of Environmental Contamination and Toxicology,* 52(3), 326-331.

Hasany, S. M., Saeed, M. M., and Ahmed, M. (1999). Retention of Hg(II) by Solid Mercury Sulfide from Acidic Solution. *Separation Science and Technology,* 34(3), 487-499.

Hintelmann, H., Keppel-Jones, K., and Evans, R. D. (2000). Constants of Mercury Methylation and Demethylation Rates in Sediments and Comparison of Tracer and Ambient Mercury Availability. *Environmental Toxicology and Chemistry,* 19(9), 2204-2211.

Horvat, M., Liang, L., and Bloom, N. S. (1993). Comparison of Distillation with Other Current Isolation Methods for the Determination of Methyl Mercury-Compounds in Low-Level Environmental-Samples .2. Water. *Analytica Chimica Acta,* 282(1), 153-168.

Hosokawa, Y. (1993). Remediation Work for Mercury Contaminated Bay - Experiences of Minamata Bay Project, Japan. *Water Science and Technology,* 28(8-9), 339-348.

James, R. O. and Healy, T. W. (1972). Adsorption of Hydrolyzable Metal-Ions at Oxide-Water Interface .1. Co(II) Adsorption on SiO_2 and TiO_2 as Model Systems. *Journal of Colloid and Interface Science,* 40(1), 42-&.

Jay, J. A., Morel, F. M. M., and Hemond, H. F. (2000). Mercury Speciation in the Presence of Polysulfides. *Environmental Science & Technology,* 34(11), 2196-2200.

Jean, G. E. and Bancroft, G. M. (1986). Heavy-Metal Adsorption by Sulfide Mineral Surfaces. *Geochimica Et Cosmochimica Acta,* 50(7), 1455-1463.

Jernelov, A. (1970). Release of Methyl Mercury from Sediments with Layers Containing Inorganic Mercury at Different Depths. *Limnology and Oceanography,* 15(6), 958-&.

Kaplan, D. I., Knox, A. S., and Myers, J. (2002). Mercury Geochemistry in Wetland and Its Implications for In-Situ Remediation. *Journal of Environmental Engineering-Asce,* 128(8), 723-732.

Kelly, C. A., Rudd, J. W. M., and Holoka, M. H. (2003). Effect of pH on Mercury Uptake by an Aquatic Bacterium: Implications for Hg Cycling. *Environmental Science & Technology,* 37(13), 2941-2946.

Kerin, E. J., Gilmour, C. C., Roden, E., Suzuki, M. T., Coates, J. D., et al. (2006). Mercury Methylation by Dissimilatory Iron-Reducing Bacteria. *Applied and Environmental Microbiology,* 72(12), 7919-7921.

Kerry, A., Welbourn, P. M., Prucha, B., and Mierle, G. (1991). Mercury Methylation by Sulfate-Reducing Bacteria from Sediments of an Acid Stressed Lake. *Water Air and Soil Pollution,* 56, 565-575.

Kim, C. S., Rytuba, J. J., and Brown, G. E. (2004). EXAFS study of Mercury(II) Sorption to Fe- and Al-(hydr)oxides I. Effects of pH. *Journal of Colloid and Interface Science,* 271(1), 1-15.

King, J. K., Kostka, J. E., Frischer, M. E., and Saunders, F. M. (2000). Sulfate-Reducing Bacteria Methylate Mercury at Variable Rates in Pure Culture and in Marine Sediments. *Applied and Environmental Microbiology,* 66(6), 2430-2437.

King, J. K., Kostka, J. E., Frischer, M. E., Saunders, F. M., and Jahnke, R. A. (2001). A Quantitative Relationship That Remonstrates Mercury Methylation Rates in Marine Sediments Are Based on the Community Composition and Activity of Sulfate-Reducing Bacteria. *Environmental Science & Technology,* 35(12), 2491-2496.

Korthals, E. T. and Winfrey, M. R. (1987). Seasonal and Spatial Variations in Mercury Methylation and Demethylation in an Oligotrophic Lake. *Applied and Environmental Microbiology,* 53(10), 2397-2404.

LA-DEQ. (2004). *Surveillance-Fish Consumption and Swimming Advisories*. http://www.deq.louisiana.gov/portal/tabid/80/Default.aspx

Larsson, P., Collvin, L., Okla, L., and Meyer, G. (1992). Lake Productivity and Water Chemistry as Governors of the Uptake of Persistent Pollutants in Fish. *Environmental Science & Technology,* 26(2), 346-352.

Le Roux, S. M., Turner, A., Millward, G. E., Ebdon, L., and Appriou, P. (2001). Partitioning of Mercury onto Suspended Sediments in Estuaries. *Journal of Environmental Monitoring,* 3(1), 37-42.

Lee, Y. H., Hultberg, H., and Andersson, I. (1985). Catalytic Effect of Various Metal-Ions on the Methylation of Mercury in the Presence of Humic Substances. *Water Air and Soil Pollution,* 25(4), 391-400.

Liu, J., Reible, D. D., Valsaraj, K., Devai, I., and Delaune, R. D. (2007). Observations of Mercury Fate and Transport Beneath a Sediment Cap. *Land Contamination & Reclamation,* 15(4), 401-411.

Liu, J., Valsaraj, K. T., Devai, I., and DeLaune, R. D. (2008). Immobilization of Aqueous Hg(II) by Mackinawite (FeS) , *Journal of Hazardous Materials* , In press, doi:10.1016/j.jhazmat.2008.1001.1006

Macalady, J. L., Mack, E. E., Nelson, D. C., and Scow, K. M. (2000). Sediment Microbial Community Structure and Mercury Methylation in Mercury-Polluted Clear Lake, California. *Applied and Environmental Microbiology,* 66(4), 1479-1488.

Macnaugh.Mg and James, R. O. (1974). Adsorption of Aqueous Mercury (II) Complexes at Oxide-Water Interface. *Journal of Colloid and Interface Science,* 47(2), 431-440.

Mailman, M., Stepnuk, L., Cicek, N., and Bodaly, R. A. (2006). Strategies to Lower Methyl Mercury Concentrations in Hydroelectric Reservoirs and Lakes: A review. *Science of the Total Environment,* 368(1), 224-235.

Martian-Doimeadios, R. C. R., Wasserman, J. C., Bermejo, L. F. G., Amouroux, D., Nevado, J. J. B., et al. (2000). Chemical Availability of Mercury in Stream Sediments from the Almaden area, Spain. *Journal of Environmental Monitoring,* 2(4), 360-366.

Marvin-DiPasquale, M. and Agee, J. L. (2003). Microbial Mercury Cycling in Sediments of the San Francisco Bay-Delta. *Estuaries,* 26(6), 1517-1528.

Marvin-Dipasquale, M. C. and Oremland, R. S. (1998). Bacterial Methylmercury Degradation in Florida Everglades Peat Sediment. *Environmental Science & Technology,* 32(17), 2556-2563.

Mason, R. P., Fitzgerald, W. F., and Morel, F. M. M. (1994). The Biogeochemical Cycling of Elemental Mercury - Anthropogenic Influences. *Geochimica Et Cosmochimica Acta,* 58(15), 3191-3198.

Mason, R. P., Kim, E. H., Cornwell, J., and Heyes, D. (2006). An Examination of the Factors Influencing the Flux of Mercury, Methylmercury and Other Constituents from Estuarine Sediment. *Marine Chemistry,* 102(1-2), 96-110.

Mason, R. P. and Lawrence, A. L. (1999). Concentration, Distribution, and Bioavailability of Mercury and Methylmercury in Sediments of Baltimore Harbor and Chesapeake Bay, Maryland, USA. *Environmental Toxicology and Chemistry,* 18(11), 2438-2447.

Masscheleyn, P. H. and Patrick, W. H. (1993). Biogeochemical Processes Affecting Selenium Cycling in Wetlands. *Environmental Toxicology and Chemistry,* 12(12), 2235-2243.

Matilainen, T. (1995). Involvement of Bacteria in Methylmercury Formation in Anaerobic Lake Waters. *Water Air and Soil Pollution,* 80(1-4), 757-764.

Matilainen, T. and Verta, M. (1995). Mercury Methylation and Demethylation in Aerobic Surface Waters. *Canadian Journal of Fisheries and Aquatic Sciences,* 52(8), 1597-1608.

Matilainen, T., Verta, M., Niemi, M., and Uusirauva, A. (1991). Specific Rates of Net Methylmercury Production in Lake-Sediments. *Water Air and Soil Pollution,* 56, 595-605.

Mauro, J. B. N., Guimaraes, J. R. D., and Melamed, R. (1999). Mercury Methylation in a Tropical Macrophyte: Influence of Abiotic Parameters. *Applied Organometallic Chemistry,* 13(9), 631-636.

Mehrotra, A. S., Horne, A. J., and Sedlak, D. L. (2003). Reduction of Net Mercury Methylation by Iron in Desulfobulbus Propionicus (1pr3) Cultures: Implications for Engineered Wetlands. *Environmental Science & Technology,* 37(13), 3018-3023.

Mehrotra, A. S. and Sedlak, D. L. (2005). Decrease in Net Mercury Methylation Rates Following Iron Amendment to Anoxic Wetland Sediment Slurries. *Environmental Science & Technology,* 39(8), 2564-2570.

Mikac, N., Foucher, D., Niessen, S., and Fischer, J. C. (2002). Extractability of HgS (Cinnabar and Metacinnabar) by Hydrochloric Acid. *Analytical and Bioanalytical Chemistry,* 374(6), 1028-1033.

Miskimmin, B. M., Rudd, J. W. M., and Kelly, C. A. (1992). Influence of Dissolved Organic-Carbon, Ph, and Microbial Respiration Rates on Mercury Methylation and Demethylation in Lake Water. *Canadian Journal of Fisheries and Aquatic Sciences,* 49(1), 17-22.

Morrison, K. A. and Therien, N. (1991). Experimental Evaluation of Mercury Release from Flooded Vegetation and Soils. *Water Air and Soil Pollution,* 56, 607-619.

Morse, J. W. and Arakaki, T. (1993). Adsorption and Coprecipitation of Divalent Metals with Mackinawite (Fes). *Geochimica Et Cosmochimica Acta,* 57(15), 3635-3640.

Morse, J. W. and Luther, G. W. (1999). Chemical Influences on Trace Metal-Sulfide Interactions in Anoxic Sediments. *Geochimica Et Cosmochimica Acta,* 63(19-20), 3373-3378.

Nriagu, J. O. (1979). *The Biogeochemistry of Mercury in the Environment.* Elsevier/North Holland, Biomedical Press, New York.

Pak, K. R. and Bartha, R. (1998). Mercury Methylation and Demethylation in Anoxic Lake Sediments and by Strictly Anaerobic Bacteria. *Applied and Environmental Microbiology,* 64(3), 1013-1017.

Pak, K. R. and Bartha, R. (1998). Mercury Methylation by Interspecies Hydrogen and Acetate Transfer between Sulfidogens and Methanogens. *Applied and Environmental Microbiology,* 64(6), 1987-1990.

Palermo, M., Maynord, S., Miller, J., and Reible, D. (1998). *Guidance for In-Situ Subaqueous Capping of Contaminated Sediments* (EPA 905-B96-004). Chicago, IL. http://www.epa.gov/glnpo/sediment/iscmain/about.html.

Palermo, M. R. (1998). Design Considerations for In-Situ Capping of Contaminated Sediments. *Water Science and Technology,* 37(6-7), 315-321.

Paquette, K. E. and Helz, G. R. (1997). Inorganic Speciation of Mercury in Sulfidic Waters: the Importance of Zero-Valent Sulfur. *Environmental Science & Technology,* 31(7), 2148-2153.

Parkman, H. and Meili, M. (1993). Mercury in Macroinvertebrates from Swedish Forest Lakes - Influence of Lake Type, Habitat, Life-Cycle, and Food Quality. *Canadian Journal of Fisheries and Aquatic Sciences,* 50(3), 521-534.

Patric, W. H., Gambrell, R. P., and Faulkner, S. P. (1996). *Redox Measurement of Soils, Method of Soil Analysis, Part 3. Chemical Methods.*, 1255-1273. Soil Science Society of America, Madison.

Pratt, A. R., Muir, I. J., and Nesbitt, H. W. (1994). X-Ray Photoelectron and Auger-Electron Spectroscopic Studies of Pyrrhotite and Mechanism of Air Oxidation. *Geochimica Et Cosmochimica Acta,* 58(2), 827-841.

Rajendran, A., Kumar, M. D., and Bakker, J. F. (1992). Control of Manganese and Iron in Skagerrak Sediments (Northeastern North-Sea). *Chemical Geology,* 98(1-2), 111-129.

Ramlal, P. S., Rudd, J. W. M., Furutani, A., and Xun, L. Y. (1985). The Effect of pH on Methyl Mercury Production and Decomposition in Lake-Sediments. *Canadian Journal of Fisheries and Aquatic Sciences,* 42(4), 685-692.

Rask, M. and Verta, M. (1995). Concentrations and Amounts of Methylmercury in Water and Fish in the Limed and Acid Basins of a Small Lake. *Water Air and Soil Pollution,* 80(1-4), 577-580.

Ravichandran, M., Aiken, G. R., Reddy, M. M., and Ryan, J. N. (1998). Enhanced Dissolution of Cinnabar (Mercuric Sulfide) by Dissolved Organic Matter Isolated from the Florida Everglades. *Environmental Science & Technology,* 32(21), 3305-3311.

Regnell, O., Hammar, T., Helgee, A., and Troedsson, B. (2001). Effects of Anoxia And Sulfide on Concentrations of Total and Methyl Mercury in Sediment and Water in Two Hg-Polluted Lakes. *Canadian Journal of Fisheries and Aquatic Sciences,* 58(3), 506-517.

Reible, D. D., Thibodeaux, L. J., Valsaraj, K. T., Lin, F., Dikshit, M., et al. *Pollutant Fluxes to Aqueous Systems Via Coupled Biological and Physico-chemical Bed Sediment Processes.* Paper presented at the Conference on Aquatic Sediments, Milwaukee, WI (1993, June 14-16).

Richman, L. A., Wren, C. D., and Stokes, P. M. (1988). Facts and Fallacies Concerning Mercury Uptake by Fish in Acid Stressed Lakes. *Water Air and Soil Pollution,* 37(3-4), 465-473.

Rickard, D. (1995). Kinetics of FeS Precipitation .1. Competing Reaction-Mechanisms. *Geochimica Et Cosmochimica Acta,* 59(21), 4367-4379.

Rickard, D. (2006). The Solubility of FeS. *Geochimica Et Cosmochimica Acta,* 70(23), 5779-5789.

Rickard, D., Griffith, A., Oldroyd, A., Butler, I. B., Lopez-Capel, E., et al. (2006). The Composition of Nanoparticulate Mackinawite, Tetragonal Iron(II) Monosulfide. *Chemical Geology,* 235(3-4), 286-298.

Rickard, D. and Morse, J. W. (2005). Acid Volatile Sulfide (AVS). *Marine Chemistry,* 97(3-4), 141-197.

Rodgers, D. W. and Beamish, F. W. H. (1983). Water-Quality Modifies Uptake of Waterborne Methylmercury by Rainbow-Trout, Salmo-Gairdneri. *Canadian Journal of Fisheries and Aquatic Sciences,* 40(6), 824-828.

Rothermich, M. M., Hayes, L. A., and Lovley, D. R. (2002). Anaerobic, Sulfate-Dependent Degradation of Polycyclic Aromatic Hydrocarbons in Petroleum-Contaminated Harbor Sediment. *Environmental Science & Technology,* 36(22), 4811-4817.

Schuster, E. (1991). The Behavior of Mercury in the Soil with Special Emphasis on Complexation and Adsorption Processes - a Review of the Literature. *Water Air and Soil Pollution,* 56, 667-680.

Sellers, P., Kelly, C. A., Rudd, J. W. M., and MacHutchon, A. R. (1996). Photodegradation of Methylmercury in Lakes. *Nature,* 380(6576), 694-697.

Shin, E. B. and Krenkel, P. A. (1976). Mercury Uptake by Fish and Biomethylation Mechanisms. *Journal Water Pollution Control Federation,* 48(3), 473-501.

Slemr, F., Schuster, G., and Seiler, W. (1985). Distribution, Speciation, and Budget of Atmospheric Mercury. *Journal of Atmospheric Chemistry,* 3(4), 407-434.

Slowey, A. J. and Brown, G. E. (2007). Transformations of Mercury, Iron, and Sulfur during the Reductive Dissolution of Iron Oxyhydroxide by Sulfide. *Geochimica Et Cosmochimica Acta,* 71(4), 877-894.

Steffan, R. J., Korthals, E. T., and Winfrey, M. R. (1988). Effects of Acidification on Mercury Methylation, Demethylation, and Volatilization in Sediments from an Acid-Susceptible Lake. *Applied and Environmental Microbiology,* 54(8), 2003-2009.

Sunderland, E. M., Gobas, F. A. P. C., Heyes, A., Branfireun, B. A., Bayer, A. K., et al. (2004). Speciation and Bioavailability of Mercury in Well-Mixed Estuarine Sediments. *Marine Chemistry,* 90(1-4), 91-105.

Suplee, M. W. and Cotner, J. B. (2002). An Evaluation of the Importance of Sulfate Reduction and Temperature to P Fluxes from Aerobic-Surfaced, Lacustrine Sediments. *Biogeochemistry,* 61(2), 199-228.

National Institute of Standards and Technology. 1997. Critical Stability Constants of Metal Complexes Database. NIST Standard Reference Database 46, Gaitherburg, MD.

Thibodeaux, L. J. (1999). *Environmental Chemodynamics: Movement of Chemicals in Air, Water, and Soil* (2nd ed.). John Wiley & Sons, New York.

Thoma, G. J., Reible, D. D., Valsaraj, K. T., and Thibodeaux, L. J. (1993). Efficiency of Capping Contaminated Sediments in-Situ .2. Mathematics of Diffusion Adsorption in the Capping Layer. *Environmental Science & Technology,* 27(12), 2412-2419.

Turner, A., Millward, G. E., and Le Roux, S. M. (2001). Sediment-water Partitioning of Inorganic Mercury in Estuaries. *Environmental Science & Technology,* 35(23), 4648-4654.

U.S.EPA. (1997). *Mercury Study Report to Congress Volume III: Fate and Transport of Mercury in the Environment* (EPA-452/R-97-005). Washington, D.C. www.epa.gov/mercury/report.htm

U.S.EPA. (2005). *Contaminated Sediment Remediation Guidance for Hazardous Waste Sites* (EPA-540-R-05-012). Office of Solid Waste and Emergency Response, Washington, D.C. http://www.epa.gov/superfund/health/conmedia/sediment/pdfs/guidance.pdf

U.S.EPA and U.S.DOE. (1999). *Understanding Variation in Partition Coefficient, Kd values. Volume I - Kd model, measurement methods, and application of chemical reaction codes.* (EPA-402-R-99-004). Office of Radiation and Indoor Air, Office of Solid Waste and Emergency Response, and Office of Environmental Restoration, Washington, D. C.

Ullrich, S. M., Tanton, T. W., and Abdrashitova, S. A. (2001). Mercury in the Aquatic Environment: a Review of Factors Affecting Methylation. *Critical Reviews in Environmental Science and Technology,* 31(3), 241-293.

Van Der Zee, C., Slomp, C. P., Rancourt, D. G., De Lange, G. J., and Van Raaphorst, W. (2005). A Mossbauer Spectroscopic Study of the Iron Redox Transition in Eastern Mediterranean Sediments. *Geochimica Et Cosmochimica Acta,* 69(2), 441-453.

Vaughan, D. J. and Tossell, J. A. (1981). Electronic-Structure of Thiospinel Minerals - Results from Mo Calculations. *American Mineralogist,* 66(11-1), 1250-1253.

Vismann, B. (1996). Sulfide Species and Total Sulfide Toxicity in the Shrimp Crangon. *Journal of Experimental Marine Biology and Ecology,* 204(1-2), 141-154.

Wang, F. Y. and Chapman, P. M. (1999). Biological Implications of Sulfide in Sediment - a Review Focusing on Sediment Toxicity. *Environmental Toxicology and Chemistry,* 18(11), 2526-2532.

Wang, Q. R., Kim, D., Dionysiou, D. D., Sorial, G. A., and Timberlake, D. (2004). Sources and Remediation for Mercury Contamination in Aquatic Systems - a Literature Review. *Environmental Pollution,* 131(2), 323-336.

Warner, K. A., Roden, E. E., and Bonzongo, J. C. (2003). Microbial Mercury Transformation in Anoxic Freshwater Sediments under Iron-Reducing and Other Electron-Accepting Conditions. *Environmental Science & Technology,* 37(10), 2159-2165.

Watras, C. J. and Huckabee, J. W. (Eds.). (1994). *Mercury Pollution: Integration And Synthesis*. P473. Lewis publishers.

Watson, J. H. P., Cressey, B. A., Roberts, A. P., Ellwood, D. C., Charnock, J. M., et al. (2000). Structural and Magnetic Studies on Heavy-Metal-Adsorbing Iron Sulphide Nanoparticles Produced by Sulphate-Reducing Bacteria. *Journal of Magnetism and Magnetic Materials,* 214(1-2), 13-30.

Wharton, M. J., Atkins, B., Charnock, J. M., Livens, F. R., Pattrick, R. A. D., et al. (2000). An X-ray Absorption Spectroscopy Study of the Coprecipitation of Tc and Re with Mackinawite (FeS). *Applied Geochemistry,* 15(3), 347-354.

Wheatley, B. and Paradis, S. (1995). Exposure of Canadian Aboriginal Peoples to Methylmercury. *Water Air and Soil Pollution,* 80(1-4), 3-11.

Wiener, J. G. and Stokes, P. M. (1990). Enhanced Bioaccumulation of Mercury, Cadmium and Lead in Low-Alkalinity Waters - an Emerging Regional Environmental Problem. *Environmental Toxicology and Chemistry,* 9(7), 821-823.

Winfrey, M. R. and Rudd, J. W. M. (1990). Environmental-Factors Affecting the Formation of Methylmercury in Low pH Lakes. *Environmental Toxicology and Chemistry,* 9(7), 853-869.

Wolfenden, S., Charnock, J. M., Hilton, J., Livens, F. R., and Vaughan, D. J. (2005). Sulfide Species as A Sink for Mercury in Lake Sediments. *Environmental Science & Technology,* 39(17), 6644-6648.

Wolthers, M., Charlet, L., Van der Linde, P. R., Rickard, D., and Van der Weijden, C. H. (2005). Surface Chemistry of Disordered Mackinawite (FeS). *Geochimica Et Cosmochimica Acta,* 69(14), 3469-3481.

Wolthers, M., Van der Gaast, S. J., and Rickard, D. (2003). The Structure of Disordered Mackinawite. *American Mineralogist,* 88(11-12), 2007-2015.

Wren, C. D. and Maccrimmon, H. R. (1983). Mercury Levels in the Sunfish, Lepomis-Gibbosus, Relative to pH and Other Environmental Variables of Precambrian Shield Lakes. *Canadian Journal of Fisheries and Aquatic Sciences,* 40(10), 1737-1744.

Wright, D. R. and Hamilton, R. D. (1982). Release of Methyl Mercury from Sediments - Effects of Mercury Concentration, Low-Temperature, and Nutrient Addition. *Canadian Journal of Fisheries and Aquatic Sciences,* 39(11), 1459-1466.

Appendix A Reactions of Hg(II), Sulfide and S^0

Reactions	log K (298 K)
$FeS(s, amorphous) + H^+ = Fe^{2+} + HS^-$	-2.95
$FeS(s, macknawite) + H^+ = Fe^{2+} + HS^-$	-3.6
$FeS(s, greigite) + H^+ = Fe^{2+} + HS^-$	-4.4
$FeS(s, pyrrohotite) + H^+ = Fe^{2+} + HS^-$	-5.1
$FeS(s, trilite) + H^+ = Fe^{2+} + HS^-$	-5.25
$Hg^{2+} + 2HS^- = Hg(SH)_2^0$	37.7
$Hg^{2+} + 2HS^- = HgS_2H^- + H^+$	31.5
$Hg^{2+} + 2HS^- = HgS_2^{2-} + 2H^+$	23.2
$Hg^{2+} + HS^- = HgSH^+$	30.2
$Hg^{2+} + HS^- = HgS_0 + H^+$	26.5
$ROH + HS^- = RSH + OH^-$ solid phase thiol formation	Unknown
$RSH + Hg^{2+} = RSHg^+ + H^+$ sorption to solid	Unknown
$2RSH + Hg^{2+} = (RS)_2Hg + 2H^+$ Sorption to solid	Unknown
$HgS(cinn) = HgS^0$	-9.3
$HgS(cinn) = Hg^{2+} + S^{2-}$	-53.5
$HgS(cinn) + H_2S(aq) = Hg(SH)_2^0$	-5.41
$HgS(cinn) + 2H_2S(aq) = HgH_2S(SH)_2^0$	-3.43
$HgS(cinn) + H_2S(aq) + HS^- = Hg(SH)_3^-$	-2.27
$HgS(cinn) + HS^- = HgS_2^{2-} + H^+$	-13.0
$HgS(cinn) + HS^- = HgS_2H^{-1}$	-4.5
$HgS(cinn) + 2HS^- = HgS_2^{2-} + H_2S$	-6.73
$HgS(cinn) + HS^- + H^+ = Hg(SH)_2$	+1.0
$HgS(cinn) + H^+ = HgSH^+$	-16.81

$HgS(cinn) + (n-1)S(rhom) + HS^- = HgS_n(SH)^{-1}$	-3.8
$HgS(cinn) + (n-1)S(rhom) = HgS_n^0$	-5.9
$HgS(cinn) + (n-1)S(rhom) + HS^- = HgS_nS^{2-} + H^+$	-11.7
$HgS(cinn) + 2(n-1)S(rhom) + HS^- = Hg(S_n)_2^{2-} + H^+$	-11.7
$HgS(cinn) + (n-1)S(rhom) + H_2O = HgS_nOH^- + H^+$	-15.4

Referred to Davison 1991, Benoit, Gilmour et al. 1999, Paquette and Helz 1997, and Jay, Morel et al. 2000.

Appendix B Using FEMLAB to Solve Simulation Models

FEMLAB is a package worked under Matlab. It is powerful, interactive environment for modeling and solving scientific and engineering problems based on partial differential equations (PDEs). The underlying mathematical structure with which FEMLAB operates is a system of PDEs. Finite element method (FEM) is applied to solve the PDEs that describe a model.

B.1 Procedure

1. Chose model. Open a new file and choose physics model/diffusion/time dependent. The 1D model is used;

2. Define geometry. Click the Draw Mode icon and define the geometry by double click on the field. A window Specify Geometry shows up. Input name, start and end values for each sundomain;

3. Define meshes. Clicking the Mesh Mode icon, the nodes and elements are shown on the specified geometry. The geometry can be further refined by click on the Refine Mesh icon. A selected section can be refined by clicking on the Refine Selection icon. Usually it is necessary to refine icon in the area around the interface between two sections.

4. Set subdomain. Click the Subdomain Mode icon. Input coefficient for each sumdomain.

The equation for the selected model is $C' - \nabla \cdot (D\nabla C) = Q$. C in the equation is concentration. D is actually D(eff)/R_f. Q equals zero here. Input values of D and initial concentration C(t_0) for each subdomain.

5. Set boundary conditions. Click the Boundary Mode icon., choose equation for each boundary and input relative coefficients.

The boundary condition for the model at the water-sediment/cap interface is represented by equation $n \cdot (D\nabla C) + qC = g$, here, n = -1, g = 0, D = D(eff)/R_f and q = ka/R_f. Input the value of g and q for this model.

The boundary condition at the bottom of the sediment is represented by the equation $n \cdot (D\nabla C) = 0$. Select q = g = 0.

6. Set up the time scale. Select 'parameter' under the 'solve' in the menu list. Input the output time under 'timestepping' in the pop-up window.

7. Solve. Either click the 'solve' icon in the window Solve Parameters or click the Solve Problem icon.

8. Save. Same it to either Mat-file or M-file.

9. Output. Open the M-file under MATLAB and add the sentences for output of concentration profile and flux. Run the file and notepad file is created for concentration profile and flux respectively. These notepad files can be opened in Excel.

10. Flux calculation. In order to get flux, the output 'flux' should be multiplied by the retardation factor Rf because the input for diffusion coefficient used in FEMLAB model is actually D(eff)/R_f.

B.2 Example M-file for the Capped Case

```
% FEMLAB Model M-file
% Generated 27-Apr-2005 14:23:17 by FEMLAB 2.3.0.153.

flclear fem
% FEMLAB Version
clear vrsn;
vrsn.name='FEMLAB 2.3';
vrsn.major=0;
vrsn.build=153;
fem.version=vrsn;

% Recorded command sequence

% New geometry 1
fem.sdim={'x'};

% Geometry
clear s c p
I1=solid1([0.13 0.14000000000000001],[1 0;0 1]);
I2=solid1([0.14000000000000001 0.14999999999999999],[1 0;0 1]);
objs={I1,I2};
names={'I1','I2'};
s.objs=objs;
s.name=names;

objs={};
names={};
c.objs=objs;
c.name=names;

objs={};
names={};
p.objs=objs;
p.name=names;

drawstruct=struct('s',s,'c',c,'p',p);
fem.draw=drawstruct;
fem.geom=geomcsg(fem);

clear appl
```

```
% Application mode 1
appl{1}.mode=flpdedf1d('dim',{'c'},'sdim',{'x'},'submode','std','tdiff', ...
'on');
appl{1}.dim={'c'};
appl{1}.form='coefficient';
appl{1}.border='off';
appl{1}.name='df';
appl{1}.var={};
appl{1}.assign={'Q';'Q';'flux';'flux'};
appl{1}.elemdefault='Lag2';
appl{1}.shape={'shlag(2,"c")'};
appl{1}.sshape=2;
appl{1}.equ.D={{{'4.07e-15'}},{{'4.5e-14'}}};
appl{1}.equ.Q={'0','0'};
appl{1}.equ.gporder={{4},{4}};
appl{1}.equ.cporder={{2},{2}};
appl{1}.equ.shape={1,1};
appl{1}.equ.init={{{'0.116'}},{{'0'}}};
appl{1}.equ.usage={1,1};
appl{1}.equ.ind=[1 2];
appl{1}.bnd.q={'0','1.6e-11'};
appl{1}.bnd.g={'0','0'};
appl{1}.bnd.c={'0','0'};
appl{1}.bnd.type={'qg0','qg'};
appl{1}.bnd.shape={0,0};
appl{1}.bnd.ind=[1 1 2];

fem.appl=appl;

% Initialize mesh
fem.mesh=meshinit(fem,...
        'Out',    {'mesh'},...
        'Hgrad',  1.3);

% Refine mesh
fem.mesh=meshrefine(fem,...
        'out',    {'mesh'},...
        'rmethod','regular');

% Refine mesh
fem.mesh=meshrefine(fem,...
```

```
        'out',    {'mesh'},...
        'rmethod','regular');

% Refine mesh
fem.mesh=meshrefine(fem,...
        'out',    {'mesh'},...
        'rmethod','regular');

% Refine mesh
fem.mesh=meshrefine(fem,...
        'out',    {'mesh'},...
        'rmethod','regular');

% Refine mesh
fem.mesh=meshrefine(fem,...
        'out',    {'mesh'},...
        'rmethod','regular');

% Differentiation rules
fem.rules={};

% Problem form
fem.outform='coefficient';

% Differentiation
fem.diff={'expr'};

% Differentiation simplification
fem.simplify='on';

% Boundary conditions
clear bnd
bnd.q={'0','1.6e-11'};
bnd.g={'0','0'};
bnd.c={'0','0'};
bnd.type={'qg0','qg'};
bnd.shape={0,0};
bnd.ind=[1 1 2];
fem.appl{1}.bnd=bnd;

% PDE coefficients
clear equ
```

```
equ.D={{{'4.07e-15'}},{{'4.5e-14'}}};
equ.Q={'0','0'};
equ.gporder={{4},{4}};
equ.cporder={{2},{2}};
equ.shape={1,1};
equ.init={{{'0.116'}},{{'0'}}};
equ.usage={1,1};
equ.ind=[1 2];
fem.appl{1}.equ=equ;

% Internal borders
fem.appl{1}.border='off';

% Shape functions
fem.appl{1}.shape={'shlag(2,"c")'};

% Geometry element order
fem.appl{1}.sshape=2;

% Define constants
fem.const={};

% Multiphysics
fem=multiphysics(fem);

% Extend the mesh
fem.xmesh=meshextend(fem,'context','local','cplbndeq','on','cplbndsh','on');

% Evaluate initial condition
init=asseminit(fem,...
        'context','local',...
        'init',   fem.xmesh.eleminit);

% Solve dynamic problem
fem.sol=femtime(fem,...
        'tlist',  0:3154000:315400000,...
        'atol',   0.001,...
        'rtol',   0.01,...
        'jacobian','equ',...
        'mass',   'full',...
        'ode',    'ode15s',...
        'odeopt', struct('InitialStep',{[]},'MaxOrder',{5},'MaxStep',{[]}),...
```

```
        'out',    'sol',...
        'stop',   'on',...
        'init',   init,...
        'report', 'on',...
        'timeind','auto',...
        'context','local',...
        'sd',     'off',...
        'nullfun','flnullorth',...
        'blocksize',5000,...
        'solcomp',{'c'},...
        'linsolver','matlab',...
        'uscale', 'auto');

% Save current fem structure for restart purposes
fem0=fem;

% Plot solution
postplot(fem,...
        'geomnum',1,...
        'context','local',...
        'lindata',{'c','cont','internal'},...
        'linbar', 'on',...
        'linmap', 'jet',...
        'liny',   {'c','cont','internal'},...
        'geom',   'on',...
        'geomcol','bginv',...
        'refine', 3,...
        'contorder',2,...
        'phase',  0,...
        'title',  'Time=315400000  Color Data: concentration (c)  Y Data: concentration (c)  ',...
        'renderer','zbuffer',...
        'solnum', 101)

for A1 = 1:50
   xcoord(A1) = 0.13 + 0.0004 * A1;
end

[flux] = postinterp(fem, 'flux', [0.15], 'solnum', 1:length(fem.sol.tlist));
[conc] = postinterp(fem, 'c', [xcoord], 'solnum', 1:length(fem.sol.tlist));

fid = fopen('conc.txt','w');
for i=1:length(fem.sol.tlist)
```

```
    for j = 1:50
       fprintf(fid,'%d\t', conc(i,j));
   end
       fprintf(fid,'\n');
end
fclose(fid);

fid = fopen('flux.txt','w');
for i=1:length(fem.sol.tlist)
      fprintf(fid,'%d\t', flux(i));
end
fclose(fid);
```

Vita

Jianrong Liu was born in Linyi, Shandong, China, in August, 1970. In September of 1988, she enrolled in University of Petroleum, Dongying, China, for a bachelor's degree program in petrochemical and refinery engineering. Upon completion in June 1992, she joined the Petrochemical Company in Dongying as a process engineer and accepted professional trainings at an ethylene plant in Qilu Petrochemical Company. Because the planned new ethylene plant was suspended due to some reasons, she went back to University of Petroleum in Dongying, studying chemical engineering for a master's degree, which was completed in July 1997.

Upon completing the graduate study, she began to work as a lecturer in the Department of Chemical Engineering, teaching undergraduate courses. In year 2001, after professional trainings and examination, she worked as a registered process safety consultant, and accomplished safety and risk assessments for several units of 4 petrochemical companies in China, besides teaching. In August 2003, she came to the United State to pursue her doctoral degree in the Department of Chemical Engineering, Louisiana State University.

Jianrong competed and won many of women's middle-distance runs held at the university where she studied and worked. Besides running and jogging, she enjoys much kind of exercises, such as playing volleyball, Ping pong, swimming, etc.

Jianrong married Xiaobao Li in the Spring of 1994 and gave birth to Qiuyu Li, on August 8, 1997. Xiaobao is currently a doctoral student in the Department of Civil & Environmental Engineering, Louisiana State University. Qiuyu is a student in fifth grade in East Baton Rouge Parish.